Department of Physics
Indian Institute of Technology Guwahati
Ph.D. Thesis

Effect of perturbation and mixing of different species on the collective behaviour of self-propelled particles

Sagarika Adhikary

Supervisor: Prof. Sitangshu Bikas Santra
October, 2021.

Effect of perturbation and mixing of different species on the collective behaviour of self-propelled particles

A thesis submitted by

Sagarika Adhikary

to

Indian Institute of Technology Guwahati
in partial fulfillment of the requirements
for the award of the degree of
Doctor of Philosophy in Physics

Department of Physics
Indian Institute of Technology Guwahati
Guwahati - 781039, Assam, India

Statement

The work contained in the thesis entitled "*Effect of perturbation and mixing of different species on the collective behaviour of self-propelled particles*" has been carried out by me under the supervision of Prof. S. B. Santra, Professor, Department of Physics, Indian Institute of Technology Guwahati. The thesis is written in the English language. This work has not been submitted elsewhere for the award of any degree.

(Sagarika Adhikary)
Department of Physics
Indian Institute of Technology Guwahati
Guwahati - 781039

March 16, 2022

Certificate

It is certified that the work contained in the thesis entitled "*Effect of perturbation and mixing of different species on the collective behaviour of self-propelled particles*" by Ms. Sagarika Adhikary, a Ph.D. student of the Department of Physics, Indian Institute of Technology Guwahati for the award of Doctor of Philosophy has been carried out under my supervision. This work has not been submitted elsewhere for the award of any degree.

(Prof. S. B. Santra)
Department of Physics
Indian Institute of Technology Guwahati
Guwahati - 781039

March 16, 2022

Dedicated to my beloved parents,
Shree Kashi Kanta Adhikary and Smt. Krishna Adhikary

Acknowledgements

I feel immensely happy and grateful to convey my gratitude to all who have contributed to this thesis in their unique way.

First of all, my sincere gratitude goes to my PhD Supervisor, Prof. Sitangshu Bikas Santra for his patient guidance, continuous encouragement, and careful supervision throughout my PhD thesis work. His insightful advice, critical mentoring and fruitful discussions have helped me to understand the research topic and have been a driving force to better the research skills. I am thankful to him for his assistance to make this thesis possible. The entire process of learning and growing under his mentorship will be a wonderful memory for the rest of my life.

I would like to express my gratitude towards my PhD thesis Doctoral Committee members: Prof. Subhradip Ghosh, Prof. Pankaj Kumar Mishra and Prof. Biplab Bose for their insightful comments, valuable suggestions and constant encouragement during the review seminars and presentations, which have helped to improve many aspects of my research work. I am grateful to other faculty members of the department for being supportive in many regards.

I am grateful to the current and the former Heads of the Department of Physics, Prof. Perumal Alagarsamy, Prof. Subhradip Ghosh, Prof. P. Poulose and Prof. Saurabh Basu, for their various academic help during my PhD. I am thankful to the Department of Physics, IIT Guwahati, to provide the necessary computational facilities. I am grateful to the MHRD, Govt. of India and IIT Guwahati for the financial support and other essential facilities. I also want to thank the technical staff and office members of the department, especially Mr. Basab Bijoy Purkayastha and Mr. Hemanta Medhi, for the assistance in various ways during my research tenure. I am grateful to my senior group members Dr. Sourav Chattapadhyay, Dr. Bappaditya Roy and Dr. Himangshu Bhaumik for their encouragement and helpful

discussions. I want to thank Dr. Sourav Chattapadhyay, especially for numerous help with computational tools and useful discussions during my PhD. I would also like to thank my seniors in the numerical lab, Dr. Debasish das, Dr. Priyadarsini Kapri, Dr. Kartik Sau, Dr. Bijita Sarma, Dr. Sangkha Borah and friends Sheuly, Nawaz, Indu kalpa, Jyoti, Goutam, Gobinda, Jagan, Ghanashyam and other batchmates for various interactions. I am grateful to my friends Sunayana, Sasmita, Monika, Aakansha and Aneeta for their supports and company. I also like to thank Anasua, Ishani, Soumi, Anisha, Cameliadi and Tanushreedi in many regards. I am grateful to have the opportunity for various teaching assistance duties in the experimental physics lab, computational lab, exams, etc. and the experience to work with the M.Sc project students, in which I learn many things. The freedoms in thinking and carrying out my research activities have given me self-confidence and motivation for further life. I am thankful for being on the beautiful campus of IITG. The natural and soothing campus life always nurture my thoughts in solitariness.

Finally, I would like to express my wholehearted gratitude towards my family, whose unconditional love and encouragement inspired me to continue my higher studies. All the blessings, caring words and best supports from my parents always give me the strength to overcome many difficult situations. A special thanks to my brother Jugal K. Adhikary, for all the encouragement and support during my early school life. I want to thank my teachers for their guidance and for drawing my interest in pursuing science as a career. I also want to thank all those inspiring people who have motivated me in one way or another: Smt. Nayan Adhikary, Smt. Suparna Roy, Smt. Uma Adhikary, Avayda, Manasda, Biplab, Tanmay, Lipika, Himani, Victor, Himali, Shreyasi, Arpita, Ananya, Mahika. I want to thank my friends, especially A. N. Arpita, Naurin, Sunanda, Gargi, Manashi, Ratna, Piyali, Debahutidi, Ranjandi and Shilpidi for their encouragement. I am immensely grateful to my best friend, Samit, a friend in all weather, for his continuous encouragement and unwavering support during this timespan. I am thankful to the creation for the necessary energy, nourishment, and blessings in this memorable journey.

– Sagarika

Abstract

Active matter or self-propelled particles (SPPs) are characterised by their inherent ability to consume energy from the environment and eventually drive themselves out of equilibrium. Bacteria swarms, cell clusters, insects, fish schools, birds, human crowd, and even many artificial self-driven systems are all examples of the active matter which exhibits collective motion. In a seminal work, Vicsek *et al.* proposed a model for studying the collective motion of SPPs in two dimensions, famously known as the Vicsek model (VM). In this model, a large number of SPPs move together at a constant speed (v_0), and they align their direction of motion with their neighbours through a short-range alignment interaction. However, the average direction is subject to an angular noise (η). For a given density (ρ_0), an orientational order-disorder transition occurs at a critical noise (η_c). Though the order of transition depends on the values of (ρ_0, v_0), the properties exhibited at the transition point are characterised and understood rigorously.

Perturbations or agitations are common in nature. For example, migration of a herd of animals across forests or steps, traffic flow in busy cities, a microbial colony in natural habitats etc. Hindrance or external disturbances along the path of SPPs can cause a perturbation in the system in the form of disruption of their motion or change in orientation. However, the collective dynamics of SPPs with inherent perturbation in the system is rarely studied. In this thesis, we have studied the collective dynamics of SPPs incorporating a trapping perturbation in the VM under which the SPPs get trapped for a while with a position-dependent trapping probability as they pass through the trapping region and pick up a random velocity direction on release. The study of the VM incorporating such a perturbation reveals several novel properties of the system. It sheds light on the order of transition in the VM, identifies the crossover system size, and clarifies the existence of a tricritical point.

One of the main criteria of VM is that all the SPPs should have the same velocity. However, in natural systems, the velocities of particles need not be the same during

collective motion. For example, fast-moving (active) and slow-moving (dormant) bacteria in a bacterial population or slow-moving vehicles and speedy vehicles in daily traffic. We have studied the collective behaviour of a binary mixture of SPPs with two different motile properties, such as slow-moving SPPs with velocity v_s and fast-moving SPPs with velocity v_f ($v_f \gg v_s$). Both inter and intra-particle interactions are considered in the alignment interaction. The model exhibits many different self-organised pattern formation and phase separation under a short-range interaction without external force or repulsion. The mixing of two different SPPs has a strong non-universal effect on the critical behaviour of the system when the system is studied for higher and higher values of v_f keeping v_s fixed. For high v_f, discontinuous transitions occur not only for the fast-moving SPPs but also for the slow-moving SPPs and the whole system as well.

The effect of orientation adapters on the collective behaviour of SPPs is a crucial aspect to study in the context of VM. In this model, adapter SPPs exist besides the usual SPPs in equal proportion. The adapter SPPs do not interact among themselves but adopt the velocity orientation of the usual SPPs through local interactions. However, the usual SPPs do interact with themselves as well as with the adapters. The adapters move with velocity v_a and induce nontrivial behaviour in the system. The transition nature of the usual SPPs with high velocity v_0 remains as that of the VM. In contrast, the adapters without self-interaction and with $v_a \ll v_0$ synchronise with the usual SPPs and obtain different behaviour. However, interestingly, the adapters with $v_a \gg v_0$ make the transition continuous for both the usual SPPs and the adapters.

The thesis represents many novel results obtained from different models of collective motion of SPPs incorporating perturbation, different species and orientation adapters. The novel results obtained in studying such active systems will be helpful to understanding many related fields, such as swarm robotics, molecular biology, biomedical applications, security systems, traffic and crowd management etc.

Contents

Chapter 1

Introduction

A big flock of starlings can fly in the sky as a coherent travelling group that sometimes produce spectacular aerial displays if collectively they were some giant creatures. Schools of fish display sometimes beautiful, coherent waves like patterns and travels. Getting an attack from a nearby predator, the same fish, can change direction so abruptly and swirl to make some puzzling pattern to avoid the predator. In the insect world, collective motion is also fascinating to observe, such as locust migration can span more than kilometres in search of foods. On the other hand, on a smaller length scale, bacteria and cells interact by chemical signalling and act collectively. These living quantities can be called active matter or self-propelled particles (SPPs). Active matter systems are characterised by their inherent ability to consume energy from the environment and eventually drive themselves far away from the points of equilibria [1–3]. These systems possess directions of motion which is determined by their internal degrees of freedom. Fish schools [4–6], flocking birds [7, 8], mammalian herds [9], human crowd [10, 11], swarms of insects [12–15], herds of wildebeests [16], bacteria swarms [17–19], cell clusters [20], actin filaments inside our cells [21, 22], and many more [1, 23] are all examples of the active matter which exhibits collective behaviour. The collective motion of SPPs is not limited only to living matter. There are many examples of artificial SPPs studied experimentally, including active colloids [24], driven granular matter [25, 26] and others. A wide range of systems exhibiting collective motion strikingly possess many common attributes. Although each of the individual agents may interact at a small scale and possess considerably limited information about the system, form some coherent structure on length scales much larger than the size of each of the constituent particles. These collective behaviour and underlying strategies are important to understand collective decision making and swarm technology [27–30].

Active matter exists at different length scales and timescales, and various models have been proposed to describe and predict its behaviour. Models can be agent-based or with continuum-level descriptions. They can be generic, emphasising universal features, or detailed, capturing specific features. It is challenging to develop a comprehensive theoretical description of living matter because the families or the constitutive systems of active agents are quite diverse, with a wide range of physical attributes and behaviours. The studies and investigations to these systems may be useful to discover new physics ideas or development of new strategies for constructing smart devices and materials. The swarm intelligence of many social insects has far more fascinating implications. During collective motion, each of the independent agents respond to local stimuli without necessitating supervision. This simple fact may have far-flung implications and can be useful to understand and model phenomena such as highway traffic patterns and jamming, controlling collective attack of insect swarms in the farmlands, in order to understand clotting of fluids in living systems and others. In this way, swarm technology is found to be immensely useful in many applications, including robotics, nanotechnology, molecular biology and medicine, traffic and crowd control and security applications [31–35]. In recent years a the significant research effort in this direction to advance further understanding in this field and to use its applications in many different disciplines such as statistical physics [2], biology [36], robotics [37], social transport dynamics [38], soft matter systems [39], and biomedicine [33], among others.

Physically speaking, the collective behaviour of SPPs are highly nontrivial in the sense that they occur in the nonequilibrium systems. Since each of the single constituent particles in such a flock is active; thus, they continuously dissipate energy to execute the systematic non-thermal motion. It is important to note that the collective motion may occur spontaneously in many situations without necessitating any leader, external field, or geometrical consideration in guiding the whole collective dynamics process. The collective motion of a flocking system is an orientation-wise ordered phase of active matter, or SPPs [2]. The ordered motion results from the spontaneous breaking of continuous symmetry. Self-organised pattern formation, spontaneous symmetry breaking, motility-induced phase separation and all such novel properties make these active systems fascinating to explore more and more. The studies pertaining to the active particles have been a topic of active research interest since many years [1, 39–41] not only because of the presence of nonequilibrium phase transitions in these systems. Additionally, phase separation in the active systems also draws considerable research attention. One of the interesting

facts related to these studies are the existence of a motility-induced phase separation of particles [40]. It has been under investigation in several systems, namely, active Brownian spheres [42, 43], active Brownian disks [44, 45, 45–47], polar interactions [48], self-propelled particles [49–52], mixtures of particles having different mobilities [53–55] etc. There are many real-life examples that include cell polarisation [56–61], chemotactically communicating cells [62–64], or even mussels in ecology [65]. The underlying driving processes can be quite different and sometimes self-organised patterns occur in these active systems. We may note that different pattern formation such as stripe, hexagonal, or travelling waves are driven by processes that are also as diverse as the systems where they form [66, 67]. But the the question remains if they share fundamental properties described by a generic model. In most cases, active systems can be classified by the symmetry and the relevance of momentum conservation (wet or dry) [3, 39]. The active matter systems are referred to as wet in cases where they are described by models with momentum conservation in the presence of fluid flow [68, 69]. On the other hand, dry active systems are manifested by the absence of momentum conservation, scenarios in which the agents are in contact with a momentum-absorbing medium. It is worth noting that the absence of momentum conservation may originate due to the existence of other prominent effects, such as volume exclusion, fluctuations, and short-range interactions. In these systems, there is minor relevance of hydrodynamic interactions in systems. Examples in this regard may include various animal flocks on a plane, dense swimming bacterial colonies, or motion of granular beads on frictional surfaces, etc. These systems are known as dry active systems, where the only conserved quantity is the number of particles (neglecting division and death). Where the associated hydrodynamic field is the local density of active units. Over-damped active particles can order in states with polar and nematic symmetries. The former class of particles consists of polar or self-propelled units promoting polar order by aligning the particles head to head or tail to tail, as is evident in the classic Vicsek model [70]. The latter class may consist of both the apolar and polar active particles. For apolar active particles, the activity induces non-directed motion on each cell [71] such as melanocytes cells distributing pigments in the skin. Whereas, for the active polar particles, the interactions aligning the particles regardless of their polarity and the ordered state possessing nematic symmetry, such as self-propelled hard rods [72, 73]. Some other related classes are active Brownian particles [74, 75], chiral active matter [76–79] and so on. In this diverse field, one is to be more precise in specifying the class of systems. More specifically, in this thesis, we focus on dry and polar SPPs. We are

interested in SPPs that display directed flocking motion, akin to the animal groups.

1.1 Literature Review

Initially, the behaviour of self-propelled particles was studied to understand the collective behaviour of animals at the macroscale. In this connection, Reynolds (1987) introduced a Boids model [80] to simulate the motion of flocks of birds, animal herds, and schools of fish within computer graphics applications. In this pioneering work, Reynolds proposed three interaction rules, namely separation, alignment, and cohesion, to efficiently model the collective motion of flocks. Under these three simple rules, the complex movement of the flock can be modelled realistically.

It is expected that the generic features related to the active matter systems can be found in the emergent behaviour observed in simple models. From a statistical viewpoint, simple coarse-grained models should possess universality irrespective of the associated details of the flocking systems. To this aim, Vicsek et al. proposed a flying XY model in 1995, which is called the Vicsek model (VM) [70]. Subsequent theoretical studies and large-scale numerical simulations performed on this model have demonstrated its basic fundamental properties [1, 81]. In most cases, these properties are shared by its other variant models possessing different symmetries [3, 39]. It is precisely for this reason that the VM is considered one of the most basic models describing the physics of collective motion. The model describes the underlying collective behaviours in a simplistic manner, where the agents interact with each other by aligning their direction of movement with neighbouring agents. It was found that the Vicsek model demonstrates the transition from a disordered state (randomized particles distribution) to a state with polar order (a flocking state). The interesting fact is that the transition was exhibited even in two dimensions. On the contrary, the equilibrium systems in two-dimension with local interactions and continuous order parameters do not undergo a true phase transition (the Mermin-Wagner theorem [82]). Whereas the motion of the particles in the flocking systems allows the order to be robust against fluctuations. It is for this reason that the VM was highly effective in the proper description of those behaviours that led to a large number of subsequent developments [83–86]. In statistical physics, many works tried characterizing the dynamical transition, and the other features of the model [1, 87, 88]. The interesting statistical properties of the flocking state include large number fluctuations compared to an equilibrium fluid and instability-mediated formation of travelling waves of high-density [83, 88].

The VM and its different variants are then rigorously studied, and a rich literature exists [1, 3, 85, 89]. Many different patterns such as band formation [90, 91], rotating chains [92], vortices [93, 94] and marching groups [95], etc.; appear in these models. The travelling band formation near the transition is fascinating to observe in many of these systems. Variations on the Vicsek model with different interactions, with local cohesion, and considering the fluid in which the particles move exhibit high-density travelling objects (bands in 2-dimension and sheets in 3-dimension) [91]. In a study of large-scale collective properties of self-propelled rods with nematic alignment [90], density bands are also observed in the system. However, the universality class is found to be different from the Vicsek model. The symmetries of the SPPs and their interaction type are both relevant ingredients for these systems. Different variants of the VM undergo different phase transitions due to several factors that include the type of interactions (metric-free, hardcore, attractive or repulsive) [91, 96–98], the inclusion of noise and disorder in to the system [99, 100], different types of boundary conditions (reflecting, periodic, and with different shapes) [101, 102] etc. For example, the transition nature may critically depend on whether the noise is scalar (which perturbs the final orientation) [70, 103] or vector (which perturbs the individual orientations before averaging)[104]. Moreover, discontinuous and continuous phase transitions are observed if the density of particles below and above the percolation threshold, respectively, for the VM defined on a lattice [96]. Different collective properties have been observed in the study of the VM with topological interactions (which occur between a fixed number of neighbours) [97]. In a network version of VM, the continuous and discontinuous phase transitions are observed for the scalar and vector noises, respectively [105–107]. Selective interaction version of VM is also studied [108], where a particle only aligns to neighbours who have similar directions of their own. In this work, depending on the restriction angle, a change of the order of the phase transition has been observed. In another model [109] with interaction with view angle, where the interaction zone of a particle is a sector of the circle, a transition is observed with the variation of the view angle. There have been a number of nontrivial behaviours observed in some disordered media [23, 110–113] that may include, among others, optimal noise, quasi long-range order, superdiffusive behaviour, phase-separation etc. In addition, it also includes interesting river-like patterns in the presence of some specific disorder in a recent work [114, 115]. Moreover, heterogeneity can exist in the form of variation in behaviour among the constituting agents of the group or can be induced by external perturbation, e.g., some spatial disorder [100]. Systems

with perturbations caused by obstacles [110, 111] or quenched rotator [116] display nontrivial behaviours such as the presence of optimal noise, quasi-long-range order etc. In these active systems, often dense patterns or clusters that form dynamically merge and split. These examples have been observed experimentally in situations as diverse as bacteria swarms [19], actin motility assays [21, 117, 118], animal groups [9], and colloidal particles [119]. The study of geometric properties of the different patterns is also explored using cluster-size analysis in recent works [120, 121].

In addition to the computational models, the theoretical study of SPPs was initiated by Toner and Tu [81, 122]. A hydrodynamic approach is adopted here, where the macroscopic properties of the system are studied as the coupled dynamics of all SPPs cannot be solved at a microscopic level. The large-scale macroscopic behaviour of the system is obtained by looking at the slow and long-wavelength variations of the related physical quantities. These quantities are known as hydrodynamic variables. In the Vicsek model, these are the coarse-grained velocity field and the coarse-grained density field. Then the hydrodynamics is described by these two slowly-varying fields, and the evolution is then derived from conservation laws (particle-number is conserved) and symmetry considerations. It explained the emergence of long-range order in polar phases and the giant density fluctuations which occur in these systems.

Several experiments studied animal populations, either in the wild or in the lab to study their collective motion. Examples may include the work of Couzin et al. that attempts to show how different structures (flocks, swarms, and vortices) may form, and how information related to the external conditions and individual's positions within the group are transmitted through the flock [30, 123]. Besides, there have been experimental studies, such as the STAR FLAG project [7, 8, 124], which showed 3D reconstructions of the paths of every bird in a starling flock. Importantly it was found that the birds align with their neighbours topologically rather than as per metric distance. Other recent examples of experimental systems are bacteria swimming in thin films of liquid [19], microtubule filaments are driven by molecular motors [22] etc. In addition, much effort has been devoted over the past few years to building synthetic SPPs in the lab. They are either extracted from biological materials or purely artificial. Synthetic active matters are then obtained by assembling these self-propelled units. Examples are colloids propelled by self-phoretic effects [24], several physical systems with artificial self-propelled units such as rods or disks [125–127] etc. Over the past years, this multidisciplinary subject has witnessed significant research attention among the researchers from diverse fields of

interests and a large amount of research has bloomed around it with many possible future directions of investigations and explorations.

1.2 Phase transition and its characteristic features

In the case of collective motion of polar SPPs, generally, the phase transition (sometimes known as flocking transition) occurs between an orientationally ordered and orientationally disordered states. The ordered state is often known as the flocking state, where particles move together in a particular direction of motion, whereas a disordered phase represents the random motion of the particles. Since we mainly discuss such transitions in different contexts in the rest of the thesis, we summarise the characteristic features of phase transitions below.

There are many examples of thermal and athermal phase transitions, such as a liquid to gas, paramagnet to a ferromagnet, antiferromagnet to paramagnet, ferrimagnet to paramagnet, para-electric to ferroelectric, normal to a superconductor, normal to a superfluid, liquid to the liquid crystal, order-disorder, percolation and many others. Most phase transitions belong to one of the two types - first-order discontinuous transition or second-order continuous transition. As per Ehrenfest's criteria, nth order phase transition corresponds to the discontinuity or divergence of the nth derivative of the free energy functions at the transition point. Thus, in a first-order transition, the first derivative of the free energy becomes discontinuous, whereas, in the second-order phase transition, the second derivative of the free energy either diverges or becomes discontinuous at the transition point. In order to understand the characteristic features appearing at the transition point, one must study the macroscopic properties of the system around such a point. Since the thermodynamic parameters are different derivatives of the free energy functions, all macroscopic properties can be determined from the non-analyticity of the free energy functions around the transition point. Below we describe the characteristics of discontinuous and continuous transitions briefly in the language of a magnetic system.

Discontinuous transition: The state of a magnetic system is identified by (T, M, H), temperature T, magnetization M and external field H. The Helmholtz free energy $A(T, M)$ and the Gibbs free energy $G(T, H)$ are concave functions of temperature T whereas $A(T, M)$ is a convex function of magnetization M and $G(T, H)$ is a concave function of the external field H [128]. The variations of $G(T, H)$ with H and $A(T, M)$ with M are shown in Fig.1.1(a) and (b) respectively, for $T < T_c$ (where T_c

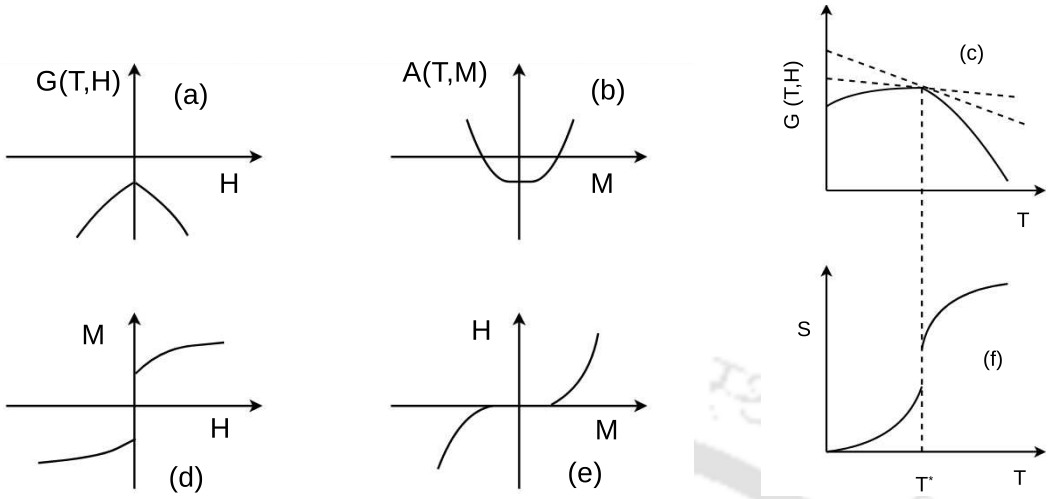

Figure 1.1: Discontinuous transition: Diagram showing variation of (a) Gibbs free energy $G(T,H)$ against H, (b) Helmholtz free energy $A(T,M)$ against M and (c) $G(T,H)$ (or $A(T,M)$) against T. First derivatives (d) $M = -(\partial G/\partial H)_T$ against H, (e) $H = (\partial A/\partial M)_T$ against M and (f) $S = -(\partial G/\partial T)_H$ against T.

is the critical temperature). In Fig.1.1(c), variations of $G(T,H)$ (or $A(T,M)$) with temperature T is shown for $H > 0$. The free energy curves either have differences in slopes or have discontinuities at the transition point. Thermodynamic parameters such as $M = -(\partial G/\partial H)_T$, $H = (\partial A/\partial M)_T$ and entropy $S = -(\partial G/\partial T)_H$ can be obtained from the free energies. For $T < T_c$, the variations of M with H, H with M and S with T are shown in Fig.1.1(d), (e) and (f) respectively. There is a finite discontinuity in M as seen in Fig.1.1(d) and (e). It can also be seen from Fig.1.1(f) there is a discontinuity in entropy at T^*, which corresponds to the latent heat. The transition is called first-order because the first derivatives of $G(T,H)$ and $A(T,M)$ exhibit discontinuities. First-order transitions are generally abrupt and are associated with an emission (or absorption) of the latent heat $L = T^*\Delta S$. Most crystallization and solidification processes are first-order transitions. There is generally a radical change in the structure of the material in a first-order phase transition. In a first-order transition, two (or more) phases of a system co-exist in equilibrium. The first-order or discontinuous transitions can be characterized by a jump in the order parameter, exchange of latent heat, nucleation and growth, the coexistence of two phases and hysteresis.

Continuous transition: For a second-order continuous transition, the two free energy curves meet tangentially at the critical point. The variations of $G(T,H)$ with H and that of $A(T,M)$ with M are shown in Fig.1.2(a) and (b) respectively,

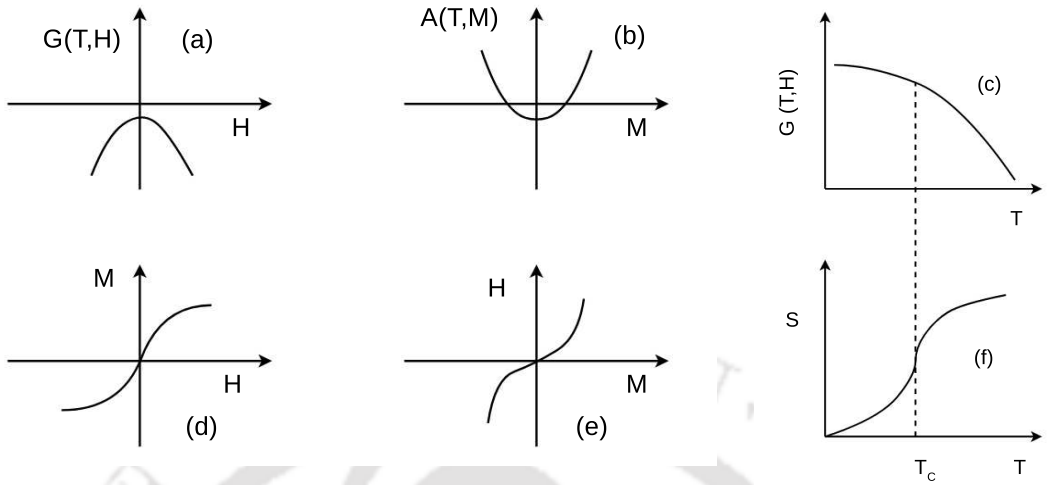

Figure 1.2: Continuous transition: Diagram showing Diagram showing variation of (a) Gibbs free energy $G(T, H)$ against H, (b) Helmholtz free energy $A(T, M)$ against M and (c) $G(T, H)$ (or $A(T, M)$) against T. First derivatives (d) $M = -(\partial G/\partial H)_T$ against H, (e) $H = (\partial A/\partial M)_T$ against M and (f) $S = -(\partial G/\partial T)_H$ against T.

for $T > T_c$ (where T_c is the critical temperature). The variations of $G(T, H)$ (or $A(T, M)$) with temperature T is shown in Fig.1.2(c). The variations of M with H, H with M and S with T are shown in Fig.1.2(d), (e) and (f) respectively. For $T > T_c$, however, no such differences in slopes occur at the transition point. Thus there is no discontinuity either in M or in S. At $T = T_c$, the differences in the slopes vanish for the first time. It is, therefore, a continuous phase transition where the system goes continuously from one phase to another without the supply (or release) of any latent heat. Though the first derivatives are continuous, the second derivatives of the free energy diverge or become singular around the transition point. For example, the susceptibility of a magnetic system $\chi_T = -(\partial^2 G/\partial H^2)_T$ diverge at the critical point. However, though the specific heat $C_H = -T(\partial^2 G/\partial T^2)_H$ diverges in the first-order transition; it has a finite discontinuity or logarithmic divergence at the critical point of a second-order transition. The characteristic features accompanying the second-order continuous phase transitions at a critical point are called critical phenomena. The characteristic features that appear at the critical point where a second-order continuous transition occurs are: order parameter continuously goes to zero, response functions diverge, fluctuations in spin orientation appear at all length scales, long-range order appears in spin-spin correlation, , *i.e.*; correlation length diverges. The singularities in the order parameter M, specific heat C, susceptibility

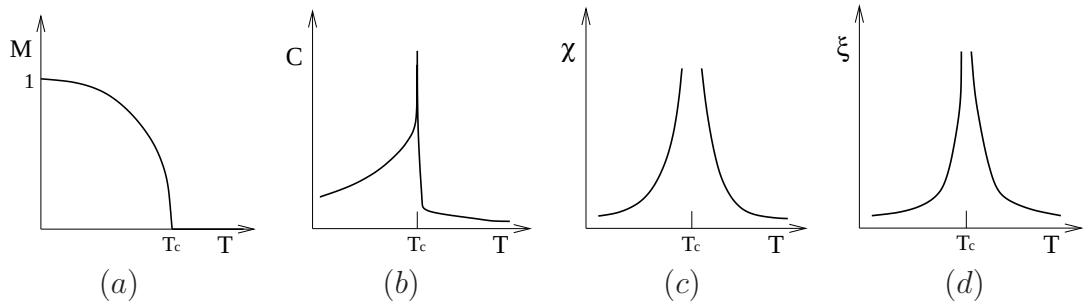

(a) (b) (c) (d)

Figure 1.3: Plot of (a) magnetization M, (b) specific heat C, (c) magnetic susceptibility χ and (d) correlation length ξ versus temperature T.

χ and the correlation length ξ are given by $M \sim (T - T_c)^{\beta}$, $C \sim |T - T_c|^{-\alpha}$, $\chi \sim |T - T_c|^{-\gamma}$, $\xi \sim |T - T_c|^{-\nu}$ where α, β, γ and $\nu$are the respective critical exponents. The variations of these thermodynamic quantities and the correlation length ξ versus temperature around the critical point are shown in Fig.1.3. At $T = T_c$, the scaling of the critical isotherm and the spin-spin correlation function are given by $H \sim M^{\delta}$ and $\Gamma(r) \sim r^{-(d-2+\eta)}$ where δ and η are two exponents. As the thermodynamic quantities are obtained by taking different derivatives of the free energy, the critical exponents describing their singularities then can not be all independent. Assuming that the free energy density $f(t, h)$ be a generalized homogeneous function of reduced temperature t and reduced field h as $T \to T_c$, a set of scaling relations among the critical exponents can be obtained. The usual scaling relations are: $\alpha + 2\beta + \gamma = 2$, $\alpha + \beta(1 + \delta) = 2$, $\beta(\delta - 1) = \gamma$. There are two more hyper-scaling relations: $\nu(2 - \eta) = \gamma$ and $d\nu = 2 - \alpha$ where d is the space dimension.

Tricritical Point: Usually, a line of first-order transitions end at a critical point but not always. A tricritical point is a point where a first-order phase transition line meets a second-order phase transition line. In other words, the triple line ends in a tricritical point where three phases become critical simultaneously. A classic example is the ^{3}He-^{4}He mixture. Since it is a binary mixture, the system has a usual phase separation between a superfluid ^{4}He rich phase and a normal phase with a critical point. The lambda line meets the coexistence curve right at the critical point. However, above the critical point, there is no demixing, but the superfluid-normal lambda transition continues. Hence, it is a tricritical point.

We will be referring to continuous, discontinuous transitions or tricritical points, if any, in the later text whenever they appear.

1.3 Spin Models

We briefly discuss two well-known standard models on the interacting spin systems: Ising and XY model. Knowledge of these systems will be helpful to relate and understand the physics of active systems.

Ising Model: The model is defined on a lattice. Each lattice site is occupied by a classical spin variable s_i, which takes $+1$ or -1 values corresponding to up or down, the direction of quantization introduced by the external field. Usually, the interaction among the spins is limited (however, not restricted) to the nearest neighbour spins only. A term J gives the interaction energy between two spins. The Hamiltonian for such an interacting system is given by

$$\mathcal{H} = -J \sum_{\langle ij \rangle} s_i s_j - \mu H \sum_i s_i \tag{1.1}$$

where H is the external magnetic field, μ is the magnetic moment associated with the spins, and $\langle ij \rangle$ represents the nearest-neighbour interaction. The first term in the Hamiltonian is responsible for cooperative behaviour and the second term corresponds to field energy. The model is exactly solved in 1-dimension, but no phase transition occurs at any finite temperature. A finite critical temperature T_c exits for $d \geq 2$, above which neither long-range order nor spontaneous magnetization exists. However, below T_c, a long-range order develops due to cooperative behaviour, and spontaneous magnetization appears in the system. A second-order continuous phase transition occurs right at $T = T_c$. The model has a spontaneous symmetry breaking (from up-down symmetry to either up or down) as the temperature is reduced from a higher value to a lower one through T_c. The $2d$ model in the absence of an external field is exactly solved, and the exact values of the critical exponents are known. The Ising model can be applied widely for many interacting two states systems.

XY Model: As the Ising spins have only two states, no other orientations than up or down are possible. Because of such restrictions, the Ising model has very restricted application to magnetic systems such as MnF_2. However, fluctuations of the spin orientation away from the axis of quantization must inevitably occur in a spin system. The XY model is also a lattice model in which the spin directions take on continuous values and become aligned with their neighbours' orientation. Consider the XY model on a two-dimensional lattice. On each lattice site, there is a (classical) spin of length $|\mathbf{s}| = 1$, $\mathbf{s}_i = (s_i^x, s_i^y) = (\cos(\theta), \sin(\theta))$ which lies in

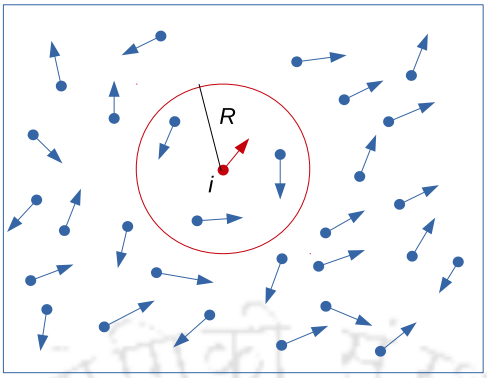

Figure 1.4: Diagram showing the alignment interaction region (circle) of the ith (red) particle. Particle i only interact with the 3 neighbours (blue) present within the circle of radius R centred around the position of the ith particle. The arrow associated with an SPP indicates the direction of velocity.

the XY-plane. The Hamiltonian for such a $2d$ XY model with nearest-neighbour interaction J and no external field is given by

$$\mathcal{H} = -J \sum_{\langle ij \rangle} \mathbf{s}_i . \mathbf{s}_j = -J \sum_{\langle ij \rangle} \cos(\theta_i - \theta_j) \tag{1.2}$$

where the summation is over all the neighbouring lattice sites. The term J represents the strength of the coupling between spins. The XY-model shows conventional phase transition at a finite temperature for $d > 2$. However, in $2d$, the XY-model undergoes a Kosterlitz-Thouless transition in which no long-range order is present in the system.

Below we discuss the Vicsek model extensively and refer to these spin models whenever necessary in the later analogies and discussions.

1.4 Vicsek Model

The simplest two-dimensional agent-based model with discrete-time that displays a flocking transition is the Vicsek model (VM) [70]. The model identifies three minimal ingredients which are sufficient to explain the collective behaviour. They are as follows: (a) the particles have an orientation, similar to the spin, (b) the particles are assumed to align their directions of motion with the neighbours, which is also similar to alignment between neighbouring spins in magnetic systems, and

finally (c) these interactions compete with an angular noise present in the system, which randomises the orientations as the thermal noise play a similar role in the case of magnetic systems. However, in the VM, particles are not static in a lattice; they are self-driven and move with a constant velocity.

We present a brief description of the Vicsek model here. In this model, the collective motion of point-like self-propelled particles (SPPs) is considered in a two-dimensional square box of linear size L for fixed density ρ_0 and speed v_0. The initial positions (x_i, y_i) and the velocity orientations θ_i of all $N = \rho_0 L^2$ particles are randomly distributed where $x_i \in [0, L]$, $y_i \in [0, L]$ and $\theta_i \in [-\pi, +\pi]$. A particle interacts locally with other particles within a region of radius R. It aligns its velocity orientation with that of the average orientation of all the particles within R. The initial random configuration and notion of the interaction region of radius R are shown in Fig.1.4. The final orientation, however, is subject to an external angular noise η that may arise from the fluctuation (or disturbances) in the system. In order to move a particle, the following velocity orientation and poisition update rules are followed:

$$\theta_i(t + \Delta t) = \langle \theta(t) \rangle_R + \Delta\theta \tag{1.3}$$

$$x_i(t + \Delta t) = x_i(t) + v_0 \Delta t \cos\theta_i(t + \Delta t) \tag{1.4}$$

$$y_i(t + \Delta t) = y_i(t) + v_0 \Delta t \sin\theta_i(t + \Delta t) \tag{1.5}$$

where Δt is the time interval and $\Delta\theta$ is randomly chosen with a uniform probability from the interval $[-\eta\pi, +\eta\pi]$. Here $\langle \cdots \rangle_R$ denotes the average of $\theta(t)$ over the particles within the interaction region of radius R. Besides the forward update (FU) rule presented above, there also exists a backward update (BU) rule [70] where the angle of cosine and sine in the position update rule will be given by $\theta_i(t)$ instead of $\theta_i(t + \Delta t)$. Though the model is simple as Eqs.1.3, 1.4 and 1.5 can be easily implemented in a computer algorithm, it is not straightforward to determine the neighbours for each particle at every time step. It quickly becomes computationally expensive as the number of particles grow. Howevere, there exist techniques to find the neighbour list efficiently with less computation time, such as Verlet list [129], linked cell list [130, 131], etc. A methodology using linked cell list algorithm is constructed for the simulation of the thesis work which will be described later.

A flocking transition occurs between orientationally ordered and orientationally disordered states during the collective motion. In the orientationally ordered state, the particles flock together in a particular direction of motion, whereas in

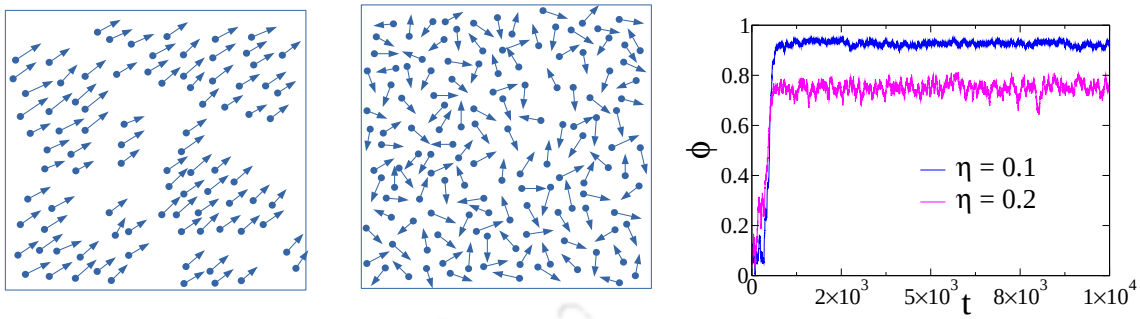

(a) ordered (b) disordered (c) Dynamics of ϕ

Figure 1.5: Diagram showing an orientationally (a) ordered and (b) disordered phase of the Vicsek model. The arrow associated with an SPP indicates the direction of motion. (c) Order parameter ϕ versus time t for different angular noise η.

the orientationally disordered phase, particles move in random directions, as shown in Figure-1.5(a) and (b) respectively. At the onset of the collective behaviour or synchronisation of the orientation of all the SPPs, information should be able to propagate through the entire system. While alignment interactions between particles produce such information, the angular noise present in the system destroys it. Thus there exists a critical noise at which such order-disorder transition occurs. The order parameter in these systems quantifies the degree of alignment between the particles. The order parameter ϕ corresponds to the direction of motion of the centre-of-mass of all the particles. The time evolution of ϕ is shown in Fig.1.5(c). It can be seen that the steady-state value of ϕ decreases as η increases. If the order parameter ϕ is studied against η, ϕ will be vanishingly small at a higher value of η corresponding to the order-disorder transition. Initially, order-disorder phase transition in the VM was believed to be a continuous transition [70, 87, 103, 132, 133]. Vicsek *et al.* [70] and others [103, 132] determined a set of well-defined critical exponents in the low velocity regime. The angular noise term used in the VM is known as "scalar" noise. However, under "vectorial" noise [88, 134], the nature of transition is always discontinuous. Though a continuous transition was observed with scalar noise at low velocities, the transition with similar noise was found to be a discontinuous one with the formation of dense bands in the system at high velocities. It was reported that the presence of periodic boundary conditions (PBCs) enhances the formation of dense band structures [104, 135]. However, later it was established through extensive numerical simulations that there exists a crossover system size $L^*(\rho_0, v_0)$ [104, 136], below which the nature of the transition is contin-

uous and above which the transition is discontinuous. The order-disorder transition in the VM seems to be similar to the transition to order phase in a simple spin system (with zero external fields), leading directly to some homogeneously ordered state. However, the interplay between local order and local density induced by the motion of SPPs can give different results. During movement, SPPs may gather in highly dense structures, increasing the number of interacting neighbours. The local high density of SPPs induces positive feedback on the alignment interaction [137]. Consequently, the dense groups of SPPs may align locally, whereas the rest of the systems do not, and it is entirely different from an equilibrium spin system. Further details will be discussed in the appropriate chapters.

Finally, we would like to emphasise some of the essential features [137] of the VM:

Conservation laws: Since the system is dissipative, there is no conservation of energy. It should also be noted that momentum is not conserved. SPPs are thought to be moving on a dissipative substrate (or in a viscous medium) which acts as a momentum sink [137]. As the momentum is not conserved, therefore, Galileian invariance is broken. There is only one conservation law valid in the VM: the conservation of the total number of particles.

Self-propulsion and local interactions: In the VM, particles are self-propelled and follow the position update rule as discussed earlier. In particular, they change their relative position according to their velocity fluctuations. Thus, the connectivity matrix or the neighbour-list is not static. As the interactions are local $R \ll L$, the connectivity matrix changes in time due to the motion of SPPs in a nontrivial way. As a result, the long-range order emerges in the VM. However, each SPP interacts with an ever-changing set of neighbours, unlike the XY-model with fixed neighbours.

Spontaneous symmetry breaking: It needs to be noted that the equations 1.3,1.4 and 1.5 are isotropic in space, as no preferred direction of motion is given a priori. However, Eq. 1.3 contains an explicit polar alignment term $\langle\theta(t)\rangle_R$. Suppose this alignment term is strong enough to overcome the effect of the angular noise η (when $\eta \ll \eta_c$). In that case, the system develops a global orientational order and thus collective motion, giving rise to a finite polar order parameter ($\phi > 0$). On the other hand, if the angular noise η is much stronger than the alignment term (when $\eta \gg \eta_c$), the SPPs move in all possible directions without any global order ($\phi = 0$). Thus a preferred direction of motion emerges spontaneously from the infinitely many possible directions (continuous symmetry) as the system moves from

the orientationally disordered phase to the ordered phase. Therefore, the system undergoes a spontaneous symmetry breaking at the critical point. This is unlike the spontaneous symmetry breaking in the Ising model, where the high temperature's up-down symmetry gets frozen to either up or down spin orientation at a temperature below T_c.

1.5 Motivation and Plan of thesis

The VM is a minimal model in which the flocking transition is studied, varying the angular noise η alone. Except for a few, most of the theoretical and computational studies on the VM are without any other external influence, internal hindrances, a mixture of different species, or varied motile properties. However, different types of perturbation or heterogeneity can naturally occur in the real world, which eventually leads to interesting novel features in the collective behaviour of a group of active entities. Besides perturbation, in a heterogeneous community, the speed of different species need not be the same. In an active system such as bacterial population or animal swarms, two types of species co-exist with different motile properties. The question is, how would be their collective behaviour? Can such systems be modelled in a simplistic manner? Furthermore, how the nature of interaction among different species would influence collective behaviour? All these questions remain unanswered. In order to explore such areas, we have categorised our investigation in three major parts: (*i*) Effect of perturbation, (*ii*) Collective behaviour of a binary mixture of SPPs and (*iii*) Effect of orientation adapters on the collective behaviour of SPPs.

After this extensive introduction to the subject, we will take up the above-mentioned issues one by one. The upcoming chapters of the thesis are going to be organised in the following manner:

In chapter 2, the effect of the perturbation on the collective motion of SPPs is rigorously studied, incorporating a trapping zone in the VM. It disturbs the motion of a number of particles delaying their motion and randomising orientation. Such trapped particles take some time to get ordered with the rest of the flock. Such randomness at the individual level collectively changes the system dynamics in this model and gives a new set of results. The order of phase transition in the VM was debated over a long time. Our model with perturbation shed light on nature more rigorously. The effect of disturbances is explored over different velocity ranges. The effect of perturbation strength on the system morphologies and dynamical behaviour

is studied thoroughly. Results obtained from finite-size scaling for various system sizes and velocities are reported in this work.

In chapter 3, collective behaviour is studied for a mixture of two different species of SPPs with widely different velocities. The two types of SPPs are mixed randomly with equal proportions. It is intriguing to observe how one type of species can affect the collective behaviour of the other SPPs. Would the time evolution of such a system result in nontrivial collective behaviour in the system as a whole? It appears that the mutual interaction among the two types of SPPs produces a variety of phase segregated patterns in the system such as lanes, clusters, clumps, micro-clumps, etc., at different regions of noise. Furthermore, the system dynamics of the partial system, which contains only one type of species and the whole system considering all the SPPs, are rigorously studied, varying the system size and their relative velocities. Investigation of such a mixed system produces several new features.

In chapter 4, the effect of orientation adapters on the collective behaviour of SPPs is explored. The adapter SPPs do not interact among themselves but adapt the velocity orientation of the usual SPPs through local interactions. However, the usual SPPs do interact with themselves as well as with the adapters. The adapters induce unusual critical behaviour in the system for different velocity ranges. In one part of this chapter, the model is studied, keeping the adapter velocity much smaller than the other SPPs. In another part of this chapter, the model is studied with the adapter velocity higher than the other SPPs. The dynamic behaviour of both models is extensively studied for various velocity ranges. Some novel and counterintuitive results are obtained in both models.

Finally, in chapter 5, a comprehensive summary of the whole thesis is presented. A brief outline of the scope of future studies is also presented, which could emerge based on the research work presented in this thesis.

Chapter 2

Effect of trapping perturbation on the collective dynamics of self-propelled particles

Perturbations or agitations in collective motion are inherent in nature. For example, migration of a herd of animals across forests or steps [138], traffic flow in busy cities [38], a microbial colony in natural habitats [139] etc. Such hindrance or external disturbances along the path of self-propelled particles (SPPs) can cause a perturbation in the system in the form of disruption of their motion or change of orientation. However, the collective dynamics of SPPs with inherent perturbation in the system is rarely studied. In this chapter, we propose a model where constant agitations are implemented on the motion of the SPPs. Such a model is developed incorporating a trapping perturbation in the Vicsek model (VM). Under the perturbation, the particles get trapped for a while with a position-dependent trapping probability as they pass through the trapping region and pick up a random direction of velocity on release. The effect of the perturbation on the VM is studied, varying the scalar noise η and the perturbation strength α. The time evolution of this model sheds light on the long-standing controversy on the nature of orientational order-disorder transitions.

Initially, the nature of phase transition in the VM under the scalar noise was believed to be a continuous transition [70, 87, 106]. A controversy on the nature of transition erupted when it was reported that the continuous order-disorder transition is essentially a discontinuous transition [134] at a high velocity. It was claimed that the discontinuous transition at high velocity is due to an unphysical symmetry breaking induced by the interplay between anisotropic diffusion and the periodic

boundary conditions present in the system [87, 133]. The transition nature of the VM and its different variants are then rigorously studied and references can be found in [1, 3]. However, later it is established through extensive numerical simulations that there exists a crossover system size $L^*(\rho_0, v_0)$ [104, 136] below which the nature of the transition is continuous and above which the transition is discontinuous where dense travelling bands appear in the system. It needs to be noted that $L^*(\rho_0, v_0)$ diverges both for low velocities ($v_0 < 0.05$) and low densities ($\rho_0 < 0.01$) [104]. However, for a given ρ_0, the crossover system size $L^*(\rho_0, v_0)$ at low velocities is quite high to observe the density bands [104]. It was found that the formation of the dense travelling band near the transition region is fluctuation driven and occurs due to the feedback mechanism between local order and local density in which long-wavelength instability appears around the region [137, 140, 141]. It is further noticed that the periodic boundary conditions (PBCs) in the system enhances the formation of these band structures, and they preferably travel parallel or diagonally to one of the boundaries [104, 135]. Several attempts have been made to remove the artefact of PBCs by shifting the re-injection point by a distance ΔL with respect to the specular position on the another side of the boundary [135] or using samples by rotating the frame of observation randomly at every time step [142] and continuous transition has been observed for the system size larger than the crossover.

The order-disorder phase transition in the proposed model is studied via extensive numerical simulations varying the external noise η for different perturbation strength α, particle velocity v_0 and the system size L at a fixed particle density ρ_0. We will explore the effect of the perturbation on the VM, especially on the features like the formation of travelling density bands and nature of phase transition.

2.1 The Model

Collective motion of N number of point-like particles is considered here in a two-dimensional square box of linear size L. Initially, the position $\vec{r}_i$ ($i = 1, 2, 3, \cdots, N$) of all the particles are randomly distributed over the space (off-lattice). A particle at $\vec{r}_i$ has a velocity v_0 in the direction θ_i. Initially, θ_i is randomly distributed over the range $-\pi$ to π. The particles interact locally and align their directions of motion with that of their neighbours in the presence of some external noise. The radius of the neighbourhood region (range of interaction) is set to $R = 1$. Time is incremented as $t = t + \Delta t$, where Δt is the time between two successive updates and it is chosen as $\Delta t = 1$. At time t, the velocity $\vec{v}_i(t)$ of the ith particle is determined

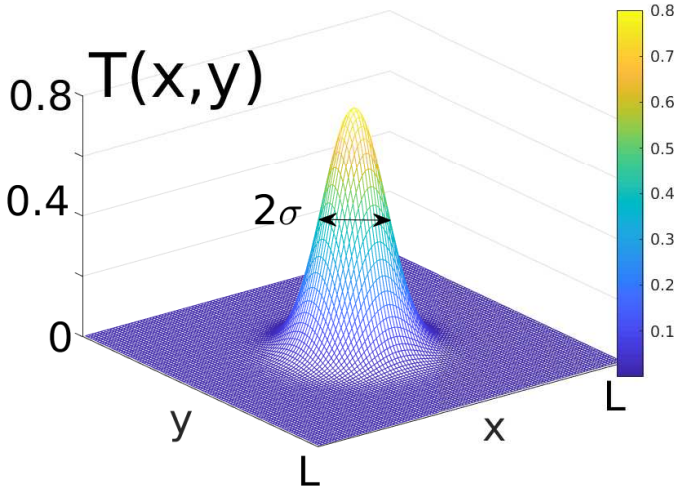

Figure 2.1: Plot of $T(x, y)$ for $\sigma = L/12$ and system of size $L = 10$. The colour bar represents the intensity of $T(x, y)$.

by evaluating the direction $\theta_i(t)$ as

$$\theta_i(t + \Delta t) = \langle \theta(t) \rangle_R + \Delta\theta \tag{2.1}$$

where $\langle \cdots \rangle_R$ denotes the average of $\theta(t)$ over the particles within the interaction region of radius R around the ith particle. The term $\Delta\theta$ is a random orientation chosen with a uniform probability from the interval $[-\eta\pi, +\eta\pi]$. The strength of the angular noise η varies from 0 to 1 and acts as a control parameter in this model. Knowing the velocity $\vec{v}_i(t)$ at every time step, the position of the ith particle $\vec{r}_i$ is updated following the forward update rule as given below

$$\vec{r}_i(t + \Delta t) = \vec{r}_i(t) + \vec{v}_i(t + \Delta t)\Delta t \tag{2.2}$$

The model described above is the VM [70]. Now we introduce a perturbation in the system by imposing a trapping probability distribution $T(x, y)$. The distribution $T(x, y)$ is given by

$$T(x, y) = T_0 \exp\left\{ -\frac{(x - X_0)^2}{2\sigma^2} - \frac{(y - Y_0)^2}{2\sigma^2} \right\} \tag{2.3}$$

where $T_0 = 0.8$, the centre of the distribution is $(X_0 = L/2,\ Y_0 = L/2)$, and σ is the half-width of the distribution.

The strength of perturbation is defined as

$$\alpha = 2\sigma/L \tag{2.4}$$

where 2σ is the width of the effective perturbation region. It should be emphasized that as L changes, the value of σ is changed accordingly to keep α fixed. Note that $\alpha = 0$ corresponds to VM. PBCs are applied in both the x and y directions. A typical trapping probability distribution $T(x, y)$ is shown in Fig.2.1 for $\sigma = L/12$ and system of size $L = 10$. At every time step, a particle positioned at (x, y) is then trapped with a probability $T(x, y)$. The particle remains trapped for a time duration $t_{trap} = n\Delta t$ (n is an integer number), if $z \leq T(x, y)$ where z is a random number uniformly distributed between $[0, 1]$. Otherwise, the particle moves according to the position and orientation update rules given in Eqs.2.2 and 2.1. During the trapping period, the particles do not move ($\vec{v} = 0$), and hence, they do not contribute to the orientation average. At the end of the trapping period, a trapped particle is released with the same v_0 but with a randomly selected orientation between $-\pi$ to π. The trapping perturbation then has two-fold effects on the system. It creates a temporal density fluctuation in the number of the moving particles as well as provides a short impulse on the average orientation besides the angular noise η. It can be noted that the heterogeneous systems of SPPs with static or moving obstacles [110, 111], or quenched rotator [116] which reveal optimal noise, and quasi long-range order are very different from the present model.

As the VM evolves, a transition from a random disordered phase to an ordered phase of collective motion occurs as the noise η is decreased below a critical value η_c. The system undergoes a discontinuous transition, and the ordered phase is characterized by travelling density bands below η_c for the system size $L > L^*(\rho_0, v_0)$, the crossover system size. A homogeneous ordered phase, however, appears for $\eta \ll \eta_c$. It is then intriguing to study the effect of the perturbation on the formation of density bands as well as on the nature phase transition.

2.2 Results and Discussion

Extensive computer simulations are performed in two-dimensional boxes of linear size L ranging from 16 to 256, keeping the particle density fixed at $\rho_0 = N/L^2 = 0.5$ for all simulations. In most of the simulations reported in the literature, the number of particles N and the density ρ_0 is kept fixed. However, in the present model, the

linear size L of the system and the density ρ_0 are kept fixed. The trapping time is taken as $t_{trap} = 2\Delta t$ for the simulation. For a given initial random distribution of particles over the box, the time evolution of the system is studied following Eqs.2.1 and 2.2. One Monte Carlo (MC) time step corresponds to the up-gradation of position and orientation of all the particles. Initial 10^5 MC steps are neglected to achieve the steady state. An ensemble of size 48×10^5 is taken for statistical averages (2×10^5 samples at different times for 24 different initial configurations). Results are obtained for three different velocities $v_0 = 0.1$, $v_0 = 0.5$ and $v_0 = 1.0$.

Though the dynamical update rules are very similar to those of the VM. Such rules can be easily implemented in a computer algorithm. However, it is not straightforward to determine the neighbours for each particle at every time step. It quickly becomes computationally expensive as the number of particles grows. However, there exist techniques to find the neighbour list efficiently with less computation time. We will be following the linked cell list algorithm [130, 131] to identify the dynamic neighbour list.

2.2.1 Methodology and Algorithms

As the particles are moving, the neighbours of a particle change with time. Hence, a particle needs to identify its neighbours within the range of interactions at every time step. The process requires careful consideration of every pair and computing their mutual distance, and it is an $\mathcal{O}(N^2)$ operation for N number of particles. Due to this, it becomes slow even when we consider a system with a thousand particles. Fortunately, there are solutions to this problem based on algorithms originally developed for the study of molecular dynamics. These algorithms are used to find the neighbour list efficiently, such as Verlet list [129], linked cell list algorithm[130, 131] etc. Let us say that the particles only interact with others, which are a maximum distance of R away. In the Verlet list method, a second radius $r_v > R$ is considered. By optimizing the r_v, significant efficiency in the calculations can be ensured. However, the Verlet list scheme becomes computationally expensive when particles exceed a few thousand.

In such cases, the linked cell list algorithm is preferably applied. The idea of this algorithm is rather simple, even if its algorithmic interpretation may not be so straightforward. In this method, the two-dimensional space is divided into smaller cells or boxes of dimension $r_c \times r_c$. Here r_c should be equal to or slightly larger than the cutoff radius R. At each time step, each of the SPPs is assigned a box. Once

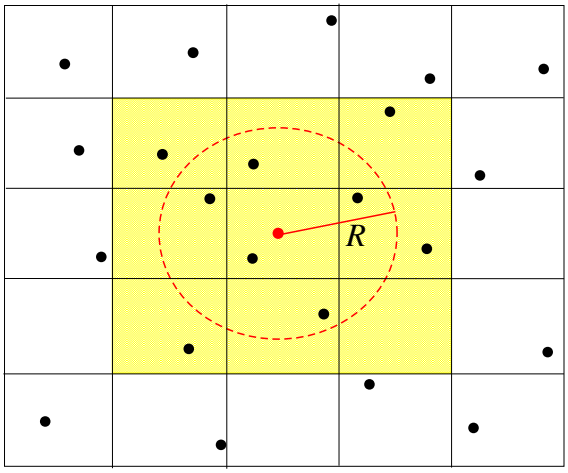

Figure 2.2: Linked cell list algorithm: In this figure the circular region shows the domain of influence on a particle (red) with a cutoff radius R. Hence to calculate the alignment interaction of that particle, one needs to scan all the particles in the neighbouring 8 boxes and the box containing the red one (yellow-shaded).

this is done, it is clear that for any given particle i, all other particles lying outside the box containing i and its next neighbouring boxes cannot be closer than R. Therefore, one immediately and effortlessly reduces its search to a handful of boxes per particle. It is shown in Fig.2.2, where the circular region shows the domain of influence on a particle (red) with a cutoff radius R. Hence to calculate the alignment interaction of that particle, one needs to scan all the particles in the neighbouring 8 boxes and the box containing the red one (yellow-shaded). In this algorithm, a list of the particles in each box is kept. Only those particles that remain in the same box or a neighbouring box are considered for each particle. It is important to keep an array **place**[ ] which will contain its position within the list of the box. As an example, let us say that box 7 possesses the particles 2, 5, 9 and 21: **list**$[7] = 2, 5, 9, 21$. Here, since the particle 9 has array index 3, hence **place**[9]=3. Moreover, we may note that after each time step, the cell list is updated likewise with the new positions of the particles, which is, of course, a $\mathcal{O}(N)$ operation. It is precisely for this reason that the problem is computationally linearized in the cell list method. Such linearization gives rise to an essential improvement if one is interested in asymptotic (i.e., long time and large N) properties. It is worth mentioning that for the boxes situated at the boundaries of the original two-dimensional box (L), the neighbouring boxes are identified applying periodic boundary conditions in both directions. The cell-list

algorithm has also been implemented for simulation purposes in the later chapters.

2.2.2 Finite size scaling

Before we present the results, the finite-size scaling (FSS) relations are presented briefly. Tuning the angular noise η, the system can be taken from a ordered state ($\eta < \eta_c$) to a disordered state ($\eta > \eta_c$). As the system evolved to a steady state starting from a random configuration, the order-parameter $\phi(\eta, L)$ of the system is estimated as

$$\phi(\eta, L) = \frac{1}{Nv_0}\left|\sum_{i=1}^{N}\vec{v}_i\right| \tag{2.5}$$

where $N = \rho_0 L^2$, η is the angular noise and L is the system size. In the ordered state (small η) when all the particles are moving in the same direction, the order parameter ϕ becomes 1 whereas in the disordered state (large η) when all the particles are moving randomly, the order parameter ϕ becomes 0. There exists a critical noise η_c at which the system undergoes a transition from the ordered state to the disordered state. Following equilibrium critical phenomena [143, 144], a finite-size scaling relation for the order parameter is assumed as

$$\phi(\eta, L) = L^{-\beta/\nu}\phi_0[\epsilon L^{1/\nu}] \tag{2.6}$$

where $\epsilon = (\eta - \eta_c)/\eta_c$ the reduced noise, β is the order parameter exponent, ν is the correlation length exponent and ϕ_0 is a scaling function. A probability distribution of the order parameter ϕ is defined as

$$P_L(\phi) = L^{\beta/\nu}\widetilde{P}_L\left[\phi L^{\beta/\nu}\right] \tag{2.7}$$

where $\widetilde{P}_L$ is a scaling function. The susceptibility χ of the system then can be estimated from the fluctuation in order parameter ϕ as

$$\chi = L^2\left[\langle\phi^2\rangle - \langle\phi\rangle^2\right] \tag{2.8}$$

where $\langle\phi^n\rangle = \int \phi^n P_L(\phi)d\phi$. The FSS form of χ is then given by

$$\chi(\eta, L) = L^{\gamma/\nu}\chi_0[\epsilon L^{1/\nu}] \tag{2.9}$$

where χ_0 is a scaling function and $\gamma/\nu = d - 2\beta/\nu$ as both $\langle\phi^2\rangle$ and $\langle\phi\rangle^2$ goes as $L^{-2\beta/\nu}$ and $d = 2$. The susceptibility exponent γ is defined as $\chi \sim \epsilon^{-\gamma}$.

The fourth order Binder cumulant is defined as,

$$U = 1 - \frac{\langle \phi^4 \rangle}{3\langle \phi^2 \rangle^2} \tag{2.10}$$

and its FSS form is given by

$$U(\eta, L) = U_0[\epsilon L^{1/\nu}] \tag{2.11}$$

where U_0 is a scaling functions. At $\eta = \eta_c$ (or $\epsilon = 0$), the cumulant becomes system size L independent. In the case of a continuous phase transition, the plots of U versus η lead to a common intersection point at η_c. However, for a discontinuous phase transition U have a sharp fall towards negative value at transition. This minimum is due to the simultaneous contributions of the two phases coexisting at the transition point. To estimate the critical exponent ν, derivative of $U(\eta, L)$ with respect to the noise η is taken and one obtains the following scaling relation [145],

$$U'(\eta, L) = L^{1/\nu} \frac{U_0'[\epsilon L^{1/\nu}]}{\eta_c} \tag{2.12}$$

where the primes on U and U_0 denote their derivatives. Thus $U'(\eta, L) \sim L^{1/\nu}$ at $\eta = \eta_c$.

In the case of a discontinuous transition, the order parameter exponent β goes to zero. As a consequence, the susceptibility should then scale as $\chi \sim L^d$, where d is the space dimension [146].

2.2.3 Results at $v_0 = 0.1$

It is known that for low velocities, the cross-over system size is quite large, so for the velocity $v_0 = 0.1$, we study the effect of perturbation for system size $L < L^*$. First, we present the morphology of the systems with $\alpha = 0$ (the VM) and with $\alpha = 1/6$ for different angular noise η on a system of size $L = 256$. The snapshots of morphologies of the system with $\alpha = 0$ are shown in the upper panel of Fig.2.3 in (a), (b) and (c) for $\eta = 0.06$, $\eta = 0.20$ and $\eta = 0.40$ respectively. Similarly, the morphologies of the system with $\alpha = 1/6$ are presented in the lower panel of Fig.2.3 in (d) $\eta = 0.06$, (e) $\eta = 0.16$ and (f) $\eta = 0.40$. Particles are represented by the filled circles, and their orientations are represented by their colour. The whole range of angle of orientation 0 to $+\pi$ and 0 to $-\pi$ is subdivided into six regions of width $\pi/3$ each. Colours representing the ranges of orientations are: green for

$\alpha = 0$

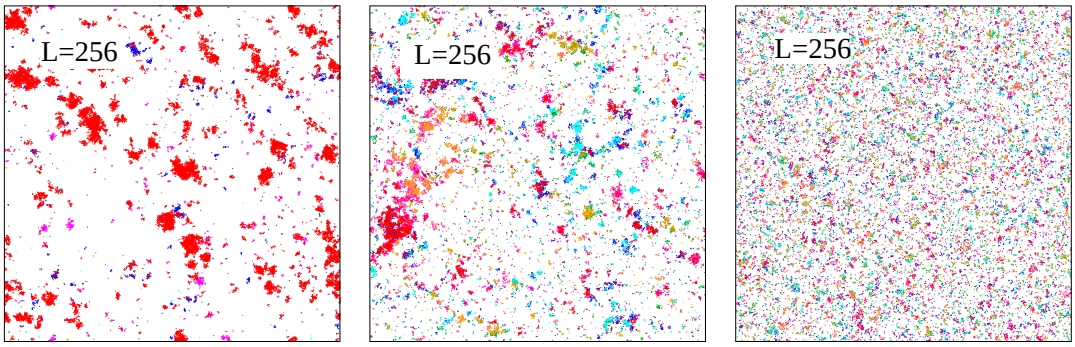

(a) $\eta = 0.06$ (b) $\eta = 0.20$ (c) $\eta = 0.40$

$\alpha = 1/6$

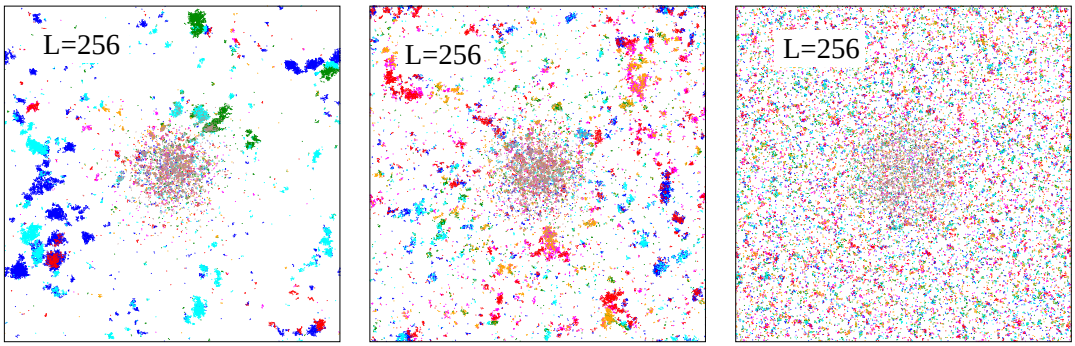

(d) $\eta = 0.06$ (e) $\eta = 0.16$ (f) $\eta = 0.40$

Figure 2.3: For $v_0 = 0.1$: System morphology with $\alpha = 0$ for (a) $\eta = 0.06$, (b) $\eta = 0.20$ and (c) $\eta = 0.40$. Morphology with $\alpha = 1/6$ for (d) $\eta = 0.06$, (e) $\eta = 0.16$ and (f) $\eta = 0.40$. The system size is $L = 256$ and density is $\rho_0 = 0.5$. Colour representation of the orientation range is given as: green for $[0, \pi/3]$, orange for $[\pi/3, 2\pi/3]$, magenta for $[2\pi/3, \pi]$, cyan for $[-\pi/3, 0]$, blue for $[-2\pi/3, -\pi/3]$, red for $[-\pi, -2\pi/3]$. Brown points are the trapped particles.

$[0, \pi/3]$, orange for $[\pi/3, 2\pi/3]$, magenta for $[2\pi/3, \pi]$, cyan for $[-\pi/3, 0]$, blue for $[-2\pi/3, -\pi/3]$ and red for $[-\pi, -2\pi/3]$. The trapped particles are represented by brown colour. In the case of $\alpha = 0$, the ordered phase ($\eta < \eta_c$) of the system has dense clusters of particles that are moving with a global direction within the range of orientation $[-\pi, -2\pi/3]$ represented in red (Fig.2.3(a)). A few small clusters of particles with different colours are scattered in the system. However, for $\alpha = 1/6$ apart from the trapped particles (in brown), dense clusters of particles are also formed in the ordered phase (Fig.2.3(d)). Though most of the clusters are moving in a particular direction indicated by the colour cyan, also there are a number of clusters moving in different directions. Some excess heterogeneity in the colour

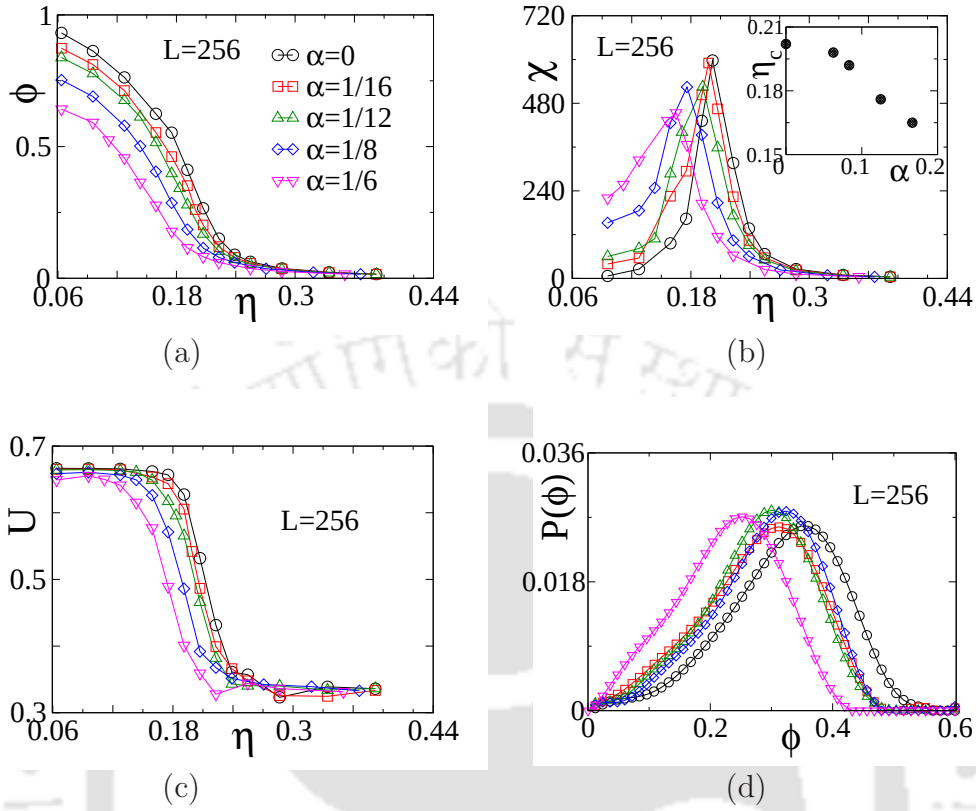

Figure 2.4: For $v_0 = 0.1$: Plot of (a) ϕ, (b) χ and (c) U versus η for several values of α on a system of size $L = 256$. Different symbols and colours used for different values of α are given in the legend of plot (a). Plot of η_c versus α is given in the inset of plot (b). The order parameter distribution $P(\phi)$ for different α at their respective η_cs are plotted in (d). Same symbol and colour set is used for all the plots.

(orientation) distribution in the case of $\alpha = 1/6$ has occurred in comparison to the situation of $\alpha = 0$. Such heterogeneity in the orientation distribution must have caused due to the local fluctuation imparted by the perturbation. Near the phase transition $\eta \approx \eta_c$ (Fig.2.3(b) and Fig.2.3(e)), fluctuations in orientation (colour) as well as in the size of the clusters appear throughout the system for both $\alpha = 0$ and $\alpha = 1/6$. In the disordered phase of $\alpha = 0$ in Fig.2.3(c) and that of $\alpha = 1/6$ in Fig.2.3(f), however, clusters have broken down into individual particles or into tiny clusters which are moving randomly in all possible directions as expected in a disordered phase.

The effect of the perturbation on the order parameter ϕ, susceptibility χ, and Binder cumulant U is now presented. In Fig.2.4(a), ϕ is plotted against η for several values of α. At small values of η (ordered phase), the value of the order parameter ϕ decreases significantly with increasing α, the perturbation strength. However,

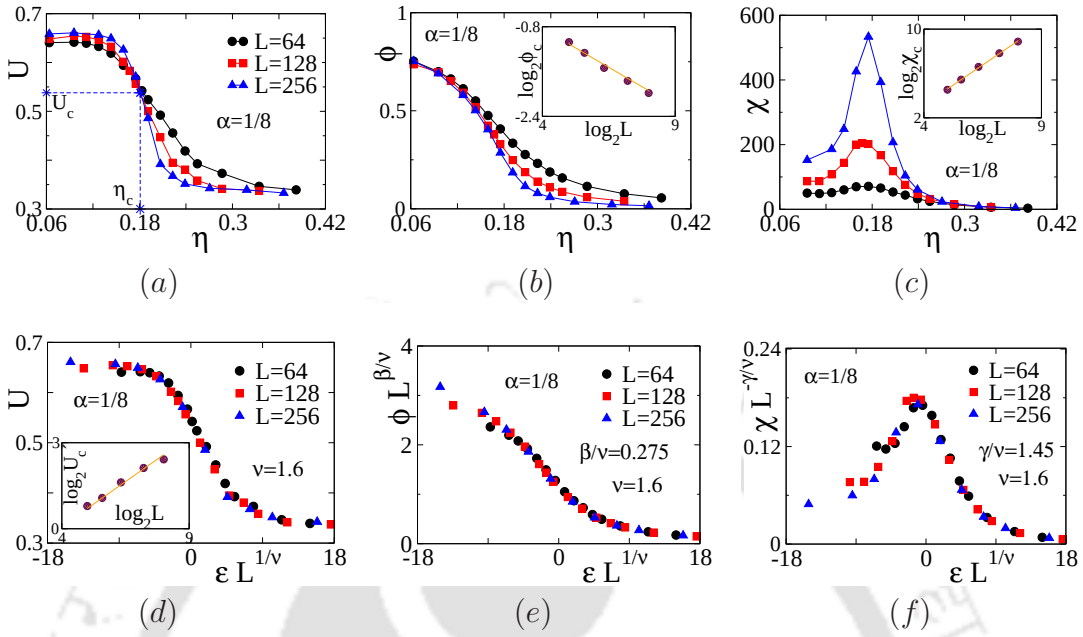

Figure 2.5: For $v_0 = 0.1$ and $\alpha = 1/8$: (a) Plot of U versus η and different system sizes L. (b) Plot of ϕ versus η for different L. In the inset, $log_2(\phi_c)$ is plotted against $log_2(L)$. (c) Plot of χ versus η for different L. In the inset, $log_2(\chi_c)$ is plotted against $log_2(L)$. (d) Plot of U versus the scaled noise $\epsilon L^{1/\nu}$. In the inset, $log_2(U_c')$ is plotted against $log_2(L)$ at η_c. (e) Plot of $\phi L^{\beta/\nu}$ against $\epsilon L^{1/\nu}$. (f) Plot of $\chi L^{-\gamma/\nu}$ against $\epsilon L^{1/\nu}$. Values of the exponents taken as $\beta/\nu = 0.275$, $\gamma/\nu = 1.45$ and $\nu = 1.6$.

irrespective of the value of α, the system undergoes an order-disorder transition at a critical noise that depends on α. In Fig.2.4(b), χ is plotted against η for the same set of α values. It can be seen that χ diverges at the critical noise η_c. The values of the critical noise η_c are noted from the positions of the peaks in χ and the variation of the critical noise η_c with α is shown in the inset of Fig.2.4(b). The location of the peak in χ depends weakly on α. The Binder cumulant U is plotted against η in Fig.2.4(c) for the same set of α values. It can be seen that U remains positive in the whole range of η irrespective of the perturbation strength α, which indicates a continuous phase transition for all these values of α. The order parameter distribution $P(\phi)$ at η_c is shown in Fig.2.4(d). Unimodal distribution of $P(\phi)$ is found to occur for all values of α as expected in a continuous phase transition.

Now we confirm the nature of transition at $v = 0.1$ for $\alpha = 1/8$ performing a finite-size scaling (FSS) analysis. The Binder cumulant U is plotted against the angular noise η in Fig.2.5(a) for different system sizes L. In a continuous phase

transition, the Binder cumulant becomes independent of the system size L at the criticality. Hence, the plots of U versus η for different L are expected to intersect at η_c, the L independent critical point. The values of η_c and corresponding U_c are identified from Fig.2.5(a) as $\eta_c = 0.180$ and $U_c = 0.54$ for the systems with $\alpha = 1/8$. In Fig.2.5(b), order parameter ϕ is plotted against η for different L using the same symbol set of the Fig.2.5(a). In the inset of Fig.2.5(b), the values of ϕ_c (ϕ at $\eta = \eta_c$) are plotted against L in double logarithmic scale as $\phi(\eta_c, L) \sim L^{-\beta/\nu}$ (Eq.2.6). The value of β/ν for the VM is reported as ≈ 0.275 [103]. A straight line with slope $\beta/\nu = 0.275$ is also found to fit well through the data points of the systems with $\alpha = 1/8$. Susceptibility χ is plotted against η in Fig.2.5(c) for different L using the same symbol set of the Fig.2.5(a). In the inset of Fig.2.5(c), the values of χ_c (χ at $\eta = \eta_c$) are plotted against L in double logarithmic scale as $\chi(\eta_c, L) \sim L^{\gamma/\nu}$ (Eq.2.9). For the VM, the value of γ/ν is ≈ 1.45 as reported in the literature [103]. The data points for the systems with $\alpha = 1/8$ are also found to fit well through a straight line with slope $\gamma/\nu = 1.45$. As $U'(\eta_c, L) \sim L^{1/\nu}$ (Eq.2.12), the values of $U'(\eta_c, L)$ are plotted against L in double logarithmic scale in the inset of Fig.2.5(d) in order to extract the exponent ν. A straight line with slope $1/\nu = 0.625$ (guide to eye), $\nu = 1.6$ that of the VM [103], seems representing well the data points. Taking $\nu = 1.6$ and $\eta_c = 0.18$, U for different L are plotted against the scaled variable $\epsilon L^{1/\nu}$ where $\epsilon = (\eta - \eta_c)/\eta_c$ in Fig.2.5(d) and a reasonable collapse of data is obtained. Taking $\beta/\nu = 0.275$ and $\eta_c = 0.18$, the scaled order parameters $\phi L^{\beta/\nu}$ are plotted against the scaled variable $\epsilon L^{1/\nu}$ in Fig.2.5(e) and a reasonable collapse of data is obtained. Taking $\gamma/\nu = 1.45$ and $\eta_c = 0.18$, $\chi L^{-\gamma/\nu}$ for different L are plotted against the scaled variable $\epsilon L^{1/\nu}$ in Fig.2.5(f) and a reasonable collapse of data is obtained.

The order parameter distributions $P(\phi)$ at $\eta = \eta_c$ for the systems with $\alpha = 1/8$ is plotted in Fig.2.6(a) for $L = 64$, 128 and 256. It can be seen that as L increases, the width of the distribution decreases, and the height of the distribution increases as expected in a continuous transition. To verify the scaling form of $P(\phi)$ given in Eq.2.7, the scaled distribution $P(\phi)L^{-\beta/\nu}$ is plotted against the scaled order parameter $\phi L^{\beta/\nu}$ in Fig.2.6(b) taking $\beta/\nu = 0.275$. Though there is not a good collapse of data, the plots come over each other reasonably. Thus, the FSS analysis for the systems with $\alpha = 1/8$ at a low velocity $v_0 = 0.1$ shows a continuous phase transition. The nature of the transition is found to be independent in the wide range of the perturbation strength α. Moreover, the values of the critical exponents remain unchanged in the presence of perturbation, and the universality class of the

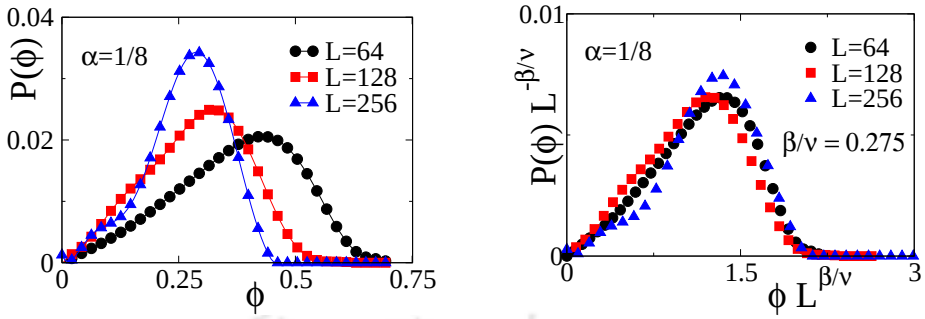

Figure 2.6: For $v_0 = 0.1$ and $\alpha = 1/8$: (a) Plot of $P(\phi)$ against ϕ at $\eta_c = 0.180$ for different system size L. (b) Plot of scaled distribution $P(\phi)L^{-\beta/\nu}$ against $\phi L^{\beta/\nu}$.

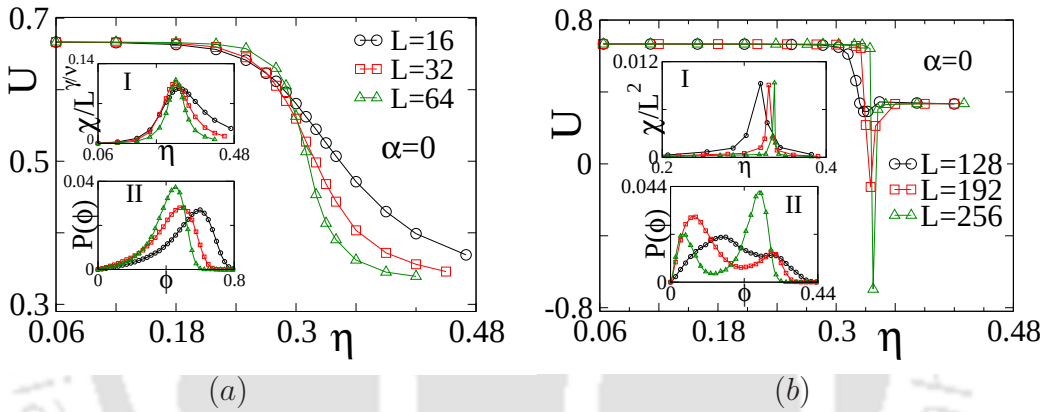

Figure 2.7: Results of VM ($\alpha = 0$) at $v_0 = 0.5$: (a) Plot of U against η for small system sizes $L = 16$, 32 and 64. Inset I, plot of $\chi/L^{\gamma/\nu}$ against η and inset II, plot of $P(\phi)$ at η_c. (b) Plot of U against η for large system size $L = 128$, 192 and 256. Plot of χ/L^2 against η in inset I and plot of $P(\phi)$ at η_c in inset II.

VM remains preserved at the low-velocity regime.

2.2.4 Results at $v_0 = 0.5$

It has already been reported in the literature that at high velocities, the continuous order-disorder transition in the VM becomes a discontinuous one as the system size increases [134, 136]. We have performed MC simulation for systems with $\alpha = 0$ (the VM) on a wide range of system sizes starting from $L = 16$ up to $L = 256$. Evidence for continuous transitions in smaller systems, $L = 16$, 32 and 64, are given in Fig.2.7(a). In this figure, Binder cumulant U is plotted against η and found to be positive across the transition point. The plots also pass through a

common intersection point at $\eta_c \approx 0.29$. In the inset I of Fig.2.7(a), the plots of $\chi/L^{\gamma/\nu}$ versus η are given. It can be seen that all the peaks are at the same height for $\gamma/\nu = 1.45$ [103]. Thus the values of the susceptibility at $\eta = \eta_c$ scale as $\chi \sim L^{\gamma/\nu}$. The distributions $P(\phi)$ of all three system sizes are found to be unimodal at the transition point, as shown in the inset II of Fig.2.7(a). All these are characteristics of a continuous transition. On the other hand, characteristic behaviour of U, χ, and $P(\phi)$ for higher system sizes $L = 128, 192$ and 256 are given in Fig.2.7(b). It can be seen that for $L = 256$ and $L = 192$, U becomes negative and for $L = 128$ a dip appears in U near the transition point. The plots of χ/L^2 versus η in the inset I of Fig.2.7(b) show that the peak values of χ/L^2 are L independent. The distributions $P(\phi)$ at $\eta = \eta_c$ are found bimodal distributions as shown in the inset II of Fig.2.7(b). These are the characteristic of a discontinuous transition. The discontinuous nature is usually accompanied by the emergence of density band structures and can be described in terms of feedback mechanism [137]. There exists an interplay between local order and local density induced by their collective motion. During movement, particles may gather in highly dense structures, increasing the number of interacting neighbours. Locally high density induces positive feedback on the alignment interaction. Consequently, the dense groups of SPPs may align locally, whereas the rest of the systems are random. It leads to a phase-separated ordered phase where dense band structures occur in the system up to the transition noise value in the ordered phase. It is, therefore, important to explore the effect of trapping perturbation on the order-disorder transition in higher system sizes at a high velocity.

The snapshots of system morphology at $v_0 = 0.5$ for a system of size $L = 256$ with $\alpha = 0$ (the VM) and with $\alpha = 1/6$ are shown in Fig.2.8(a) and (b) respectively. Snapshots are taken at their respective transition points. The orientations are represented by different colours, as described in Fig.2.3. For the system with $\alpha = 0$, a dense band of particles is found to appear with clusters of different colours, mostly orange, magenta and red as shown in Fig.2.8(a). These colours represent the range of orientations $[\pi/3, 2\pi/3]$, $[2\pi/3, \pi]$ and $[-\pi, -2\pi/3]$ respectively. However, the particles lying outside the band are randomly oriented and do not form any dense cluster. As the clusters in the band are moving in different directions, the band is expected to disappear over a number of MC steps. The corresponding steady-state dynamics of the order parameter of the system with $\alpha = 0$ is given in Fig.2.8(c) at $\eta \approx \eta_c$. The plot of ϕ versus the MC step, t in Fig.2.8(c) displays abrupt changes in the value of the order parameter ϕ from a higher value to a smaller value with time t.

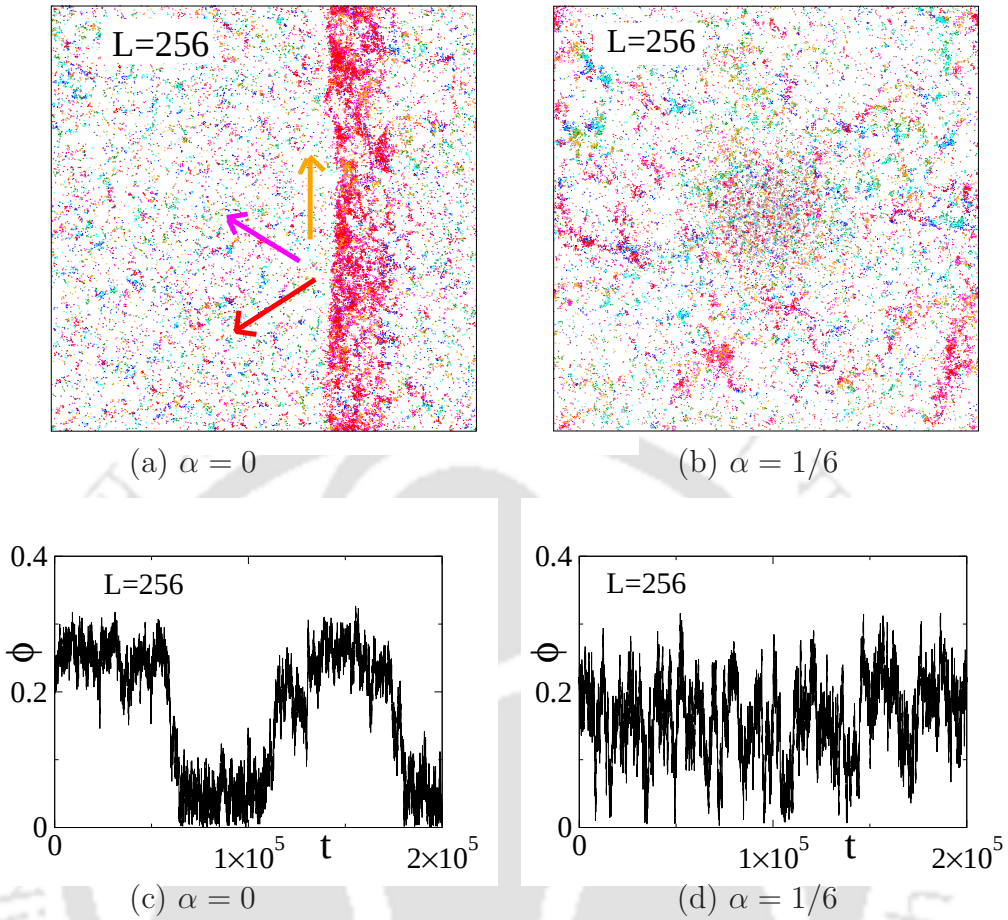

Figure 2.8: For $v_0 = 0.5$: System morphology with (a) $\alpha = 0$ for $\eta_c \approx 0.337$ and with (b) $\alpha = 1/6$ for $\eta_c \approx 0.278$. The system size is $L = 256$ and density is $\rho_0 = 0.5$. Colour representation of orientation range is given as per Fig.2.3. Brown points are the trapped particles. Order parameter dynamics at their respective transition points for (c) $\alpha = 0$ and (d) $\alpha = 1/6$.

The higher value of ϕ corresponds to an ordered phase with the band and the lower value of ϕ corresponds to a random or disordered phase. Thus at the criticality, two phases co-exist, and the system oscillates between them as time progresses. The appearance and disappearance of travelling bands and the co-existence of two phases are the characteristic features of a discontinuous transition. In the snapshot of a system of size $L = 256$ with $\alpha = 1/6$, given in Fig.2.8(b), no such dense band of particles is formed. Instead of that, fluctuations in orientation (colour) as well as in the size of the clusters appear throughout the system (Fig.2.8(b)). The steady-state dynamics of the order parameter of the system with $\alpha = 1/6$ is shown in Fig.2.8(d) at $\eta \approx \eta_c$. The order parameter dynamics of the system with $\alpha = 1/6$ shows a fluctuation around a mean value of ϕ, and no evidence of the existence of

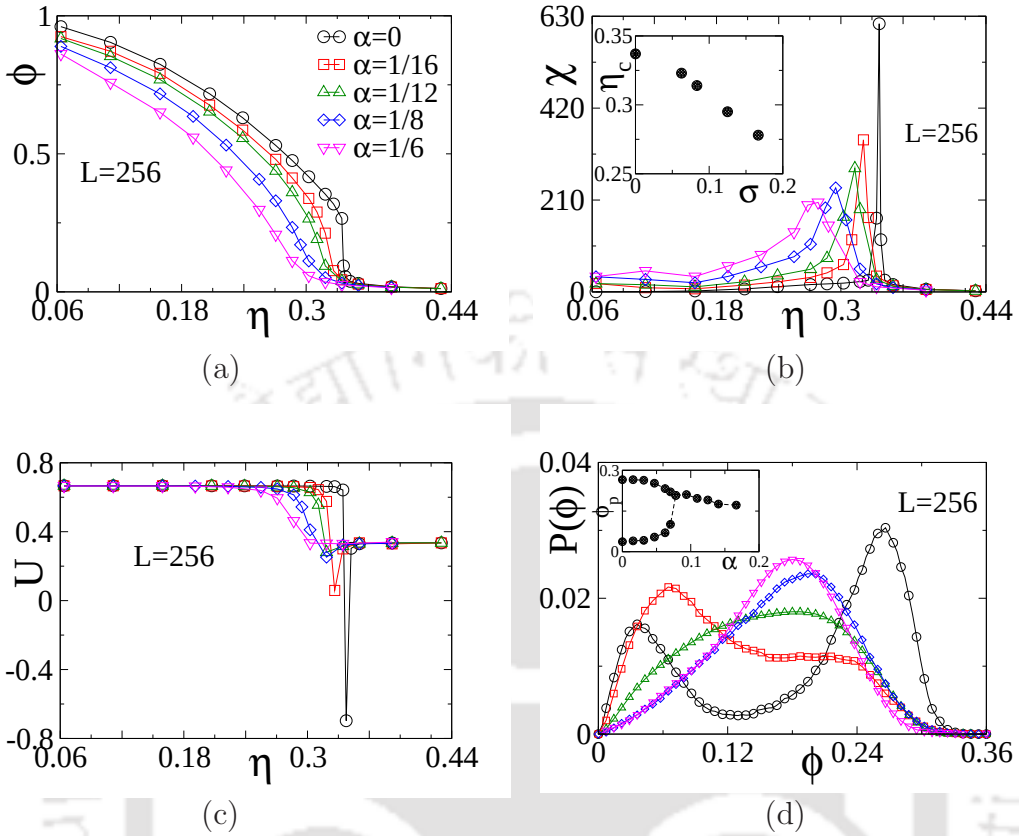

Figure 2.9: For $v_0 = 0.5$: Plot of (a) ϕ, (b) χ and (c) U versus η for several values of α on a system of size $L = 256$. Different symbols and colours used for different values of α are given in the legend of plot (a). Plot of η_c versus σ is given in the inset of plot (b). (d) Plot of $P(\phi)$ for different α at their respective η_c. In the inset of (d), ϕ_P is plotted against α.

two phases is observed. Such fluctuation at all length scales is expected to occur in the system at the critical point of a continuous phase transition. Thus at $v_0 = 0.5$, the system with perturbation is distinctly different from that of a system without perturbation.

We now present the effect of perturbation strength α at $v_0 = 0.5$ on order parameter ϕ, susceptibility χ and Binder cumulant U on a system of size $L = 256$ in Fig.2.9(a), (b) and (c) respectively. It can be seen that α has a strong influence on the behaviour of these dynamical quantities. The discontinuous transition with a drastic jump in the value of ϕ for $\alpha = 0$ seems to smoothen out, and ϕ continuously goes to zero as α increases to 1/6 (Fig.2.9(a)). A plot of χ versus η is given in Fig.2.9(b) for different α values. The sharp jump in χ for $\alpha = 0$ decreases as α increases. In the inset of Fig.2.9(b), the values of the critical noise η_c are given

against α, which are obtained from the susceptibility (χ) peak. The values of η_c are noted as 0.337, 0.322, 0.314, 0.295, 0.278 for $\alpha = 0$, 1/16, 1/12, 1/8 and 1/6 respectively. The binder cumulant U is plotted in Fig.2.9(c) for the same values of α. The negative dip in U reduces and becomes positive as α increases. In Fig.2.9(d), the distribution of order parameter $P(\phi)$ is plotted for different values of α at their respective η_c for the system of size $L = 256$. As the perturbation strength, α, is increased, the $P(\phi)$ changes from a bimodal distribution that of a discontinuous transition to a unimodal distribution that of a continuous transition. The distributions $P(\phi)$ are also obtained at several intermediate values of α between 0 and 1/6 than those displayed in Fig.2.9(d). The peak positions ϕ_p are plotted against α in the inset of Fig.2.9(d). It can be seen that the order parameter distribution $P(\phi)$ is bimodal below a critical strength of perturbation, and it is unimodal above such a strength $\alpha^* \approx 1/12$. A line of continuous transitions is found to bifurcate at $\alpha^* \approx 1/12$ into two lines of discontinuous transitions. It acts as a tricritical point. Below the perturbation strength α^*, insufficient perturbation or agitation in the system can not destroy the formation of the travelling density band or the occurrence of discontinuous transition. The critical strength α^*, however, depends on the density ρ_0, velocity v_0 and the system size L.

As the order-disorder transition at $v_0 = 0.5$ for systems with higher values of α seems to be continuous, we confirm the nature of transition performing FSS analysis involving systems of both smaller and higher sizes with $\alpha = 1/6$. In Fig.2.10(a), the Binder cumulant U is plotted against the angular noise η for $L = 64$, 128, and 256. The plots are found to intercept at a common point ($\eta_c = 0.283, U_c = 0.47$) as expected for a continuous transition. In Fig.2.10(b) and (c), the order parameter ϕ and susceptibility χ is plotted against the angular noise η for the system of sizes $L = 64$, 128, and 256. In Fig.2.10(d), U for different L are plotted against the scaled variable $\epsilon L^{1/\nu}$ ($\epsilon = (\eta - \eta_c)/\eta_c$) taking $\nu = 1.6$ and $\eta_c = 0.283$, and a reasonable collapse of data is obtained. In Fig.2.10(e), the scaling of the order parameter ϕ is presented by plotting $\phi L^{\beta/\nu}$ against $\epsilon L^{1/\nu}$ taking $\beta/\nu = 0.275$. A reasonable collapse of data is obtained. The scaled susceptibility $\chi L^{-\gamma/\nu}$ is plotted against the scaled variable $\epsilon L^{1/\nu}$ in Fig.2.10(f) and a reasonable collapse of data is obtained taking $\gamma/\nu = 1.45$. The probability distribution $P(\phi)$ is shown in Fig.2.11(a) at the transition point $\eta_c = 0.283$ for different system size L with $\alpha = 1/6$. The scaled distribution $P(\phi)L^{-\beta/\nu}$ is plotted against the scaled order parameter $\phi L^{\beta/\nu}$ in Fig.2.11(b). With $\beta/\nu = 0.275$, a reasonable data collapse is observed. At $v_0 = 0.5$, the systems with a reasonable perturbation strength α then exhibits FSS

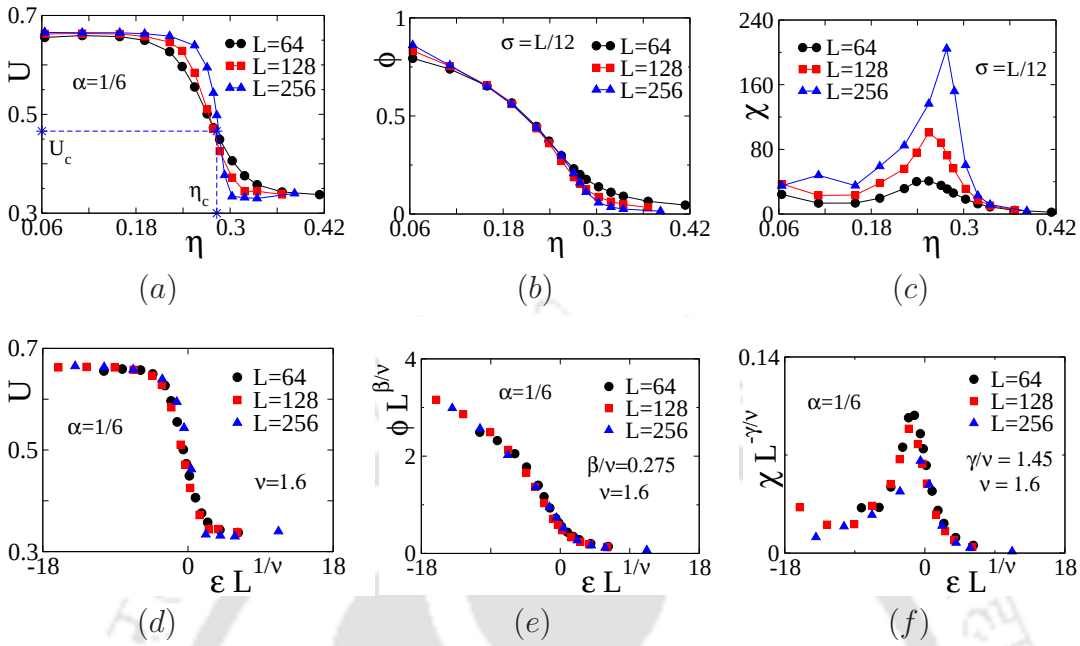

Figure 2.10: $v_0 = 0.5$ and $\alpha = 1/6$: (a) Plot of U, (b) ϕ and (c) χ versus η for different L. (d) Plot of U versus the scaled noise $\epsilon L^{1/\nu}$. (e) Plot of $\phi L^{\beta/\nu}$ against $\epsilon L^{1/\nu}$. (f) Plot of $\chi L^{-\gamma/\nu}$ against $\epsilon L^{1/\nu}$. Values of the exponents taken as $\beta/\nu = 0.275$, $\gamma/\nu = 1.45$ and $\nu = 1.6$.

with the critical exponents as that of the VM [103]. At $v_0 = 0.5$, the systems with a reasonable perturbation strength α then exhibits FSS with the critical exponents as that of the VM and the transition belongs to that of the same universality class of the VM. The continuous transition in the VM is also observed by rotating the frame of observation randomly at every time step for a system of $N = 131072$ particles with velocity $v_0 = 0.5$ [142]. By removing the artefact of PBCs by shifting the re-injection point by a distance ΔL with respect to the specular position on the other side of the boundary, it was also shown that the VM undergoes continuous transition [135].

It should be noted here that the density of active particles is less than the total density ρ_0 at a given time due to the trapping of SPPs under the trapping perturbation. For a system of size $L = 256$, the average number of trapped particles N_{tr} per MC step is shown in Fig.2.12(a) for different values of α where error bars indicate the deviations. For a perturbation strength $\alpha = 1/6$, N_{tr} is nearly 3045 out of the total number of particles $N = 32768$. Thus the reduced density of the system is given by $\rho_r = (N - N_{tr})/L^2 \approx 0.45$. It is important to emphasize here that the continuous transition observed for this system ($L = 256$, $\alpha = 1/6$) is not

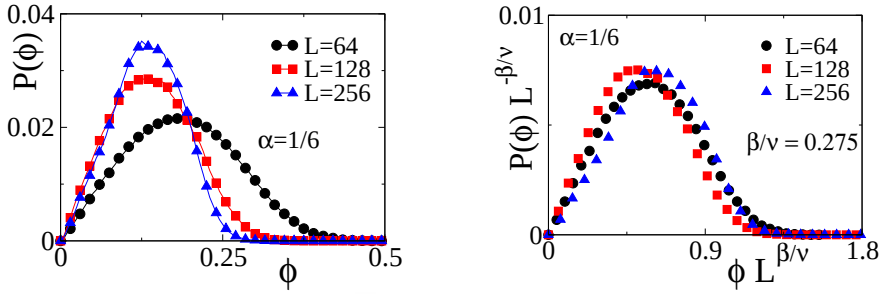

Figure 2.11: $v_0 = 0.5$ and $\alpha = 1/6$: (a) Plot of $P(\phi)$ against ϕ at $\eta_c = 0.283$ for different system size L. (b) Plot of scaled distribution $P(\phi)L^{-\beta/\nu}$ against $\phi L^{\beta/\nu}$.

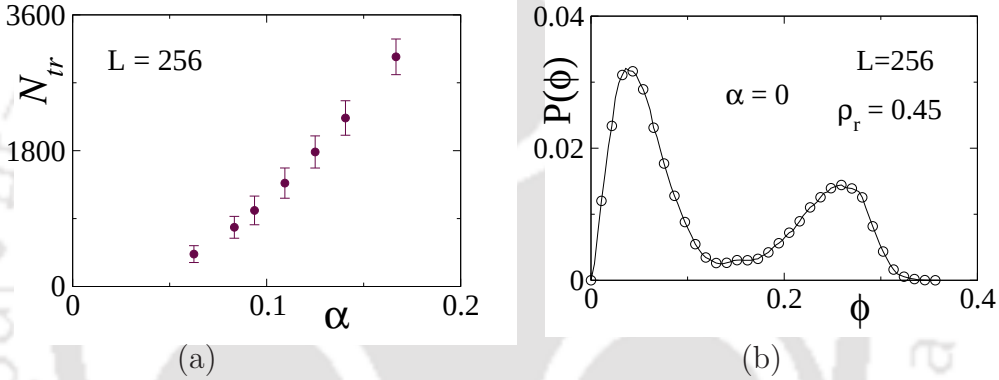

Figure 2.12: For $v_0 = 0.5$: (a) Plot of N_{tr} against α for the system size $L = 256$, $\rho_0 = 0.5$ ($N = 32768$). (b) Plot of $P(\phi)$ at the respective transition with the reduced density $\rho_r \approx 0.45$ ($N = 29723$) for $\alpha = 0$.

due to the reduced density of particles in the VM rather, it is due to the non-trivial effect of perturbation in the system. In order to establish the statement, we perform a simulation for $\alpha = 0$, the VM, taking reduced density $\rho_r = 0.45$ and obtain the distribution of order-parameter $P(\phi)$ at the transition point $\eta_c \approx 0.325$. $P(\phi)$ is plotted in Fig.2.12(b) against the order parameter ϕ and it shows a bimodal distribution as it was for $\rho_0 = 0.5$. Such an observation implies that it is not the reduced density. Rather the interplay between density fluctuation and randomization of the orientations are responsible for destroying the density bands and making the transition continuous.

As the VM undergoes discontinuous transition above a crossover system size $L^*(\rho_0, v_0)$ [104], it is now important to verify whether the effect of perturbation is independent of system size and the asymptotic behaviour of the VM is going to be continuous or not. Simulations are performed on a larger system size $L = 512$, for

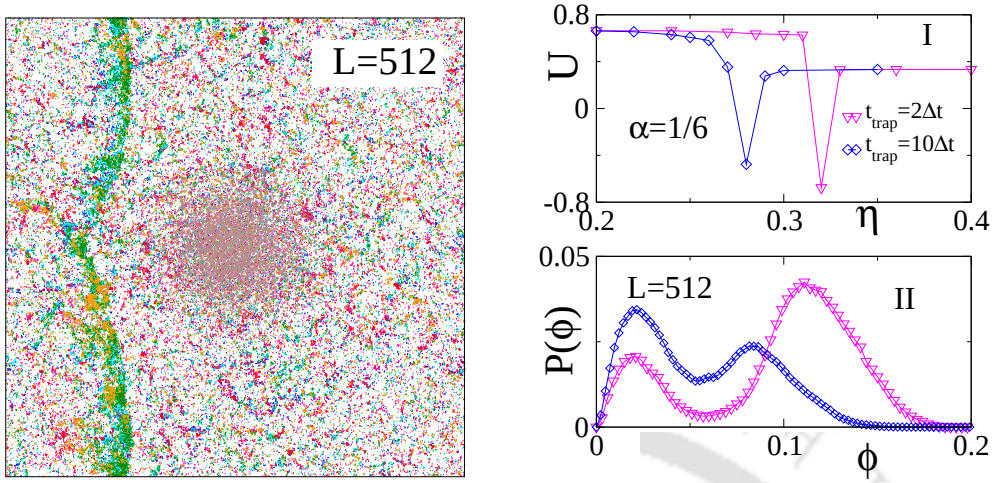

(a) (b)

Figure 2.13: For $v_0 = 0.5$: (a) System morphology for $\alpha = 1/6$ at $\eta_c \approx 0.315$, $L = 512$, $\rho_0 = 0.5$ ($N = 131072$). Colour representation of orientation ranges in the configuration are as per Fig.2.3. (b) Plot of U against η in I and plot of $P(\phi)$ at η_c in II for $\alpha = 1/6$. Pink for $t_{trap} = 2\Delta t$ and blue for $t_{trap} = 10\Delta t$ in both I and II.

the perturbation strength $\alpha = 1/6$ keeping $\rho_0 = 0.5$. The total number of particles in the system is now $N = 131072$. The steady-state configuration of such a system near the transition point $\eta_c \approx 0.315$ is shown in Fig.2.13(a). It can be seen that a dense travelling band persists in the system. The trapping perturbation is not enough to destroy the formation of the travelling band in the system. The variation of Binder-cumulant U and the distribution of order parameter $P(\phi)$ at the transition point are shown in Fig.2.13(b)I and II respectively. At the transition point, the Binder-cumulant U becomes negative, and $P(\phi)$ exhibits a bimodal distribution. Thus, the system now undergoes a discontinuous transition. The nature of transition in this system is further verified for an extended trapping time $t_{trap} = 10\Delta t$. It is observed that the dense band of particles still appears in the system. U and $P(\phi)$ for this case are shown in blue in Fig.2.13(b)I and II respectively. It can be seen that the Binder cumulant still remains negative, and the order parameter distribution is bimodal. Though the transition occurs at a lower η_c, the nature of transition remains unchanged for $t_{trap} = 10\Delta t$. However, it should be noted that the crossover system size $L^*(\rho_0, v_0)$ now depends on α. The crossover system size of the VM with perturbation $L^*_\alpha(\rho_0, v_0)$ is always greater than $L^*(\rho_0, v_0)$, that of the VM without perturbation. The perturbation is able to increase the crossover system size of the VM from $L^*(\rho_0, v_0) \approx 100$ to a larger system size $256 < L^*_\alpha(\rho_0, v_0) < 512$ for $\rho_0 = 0.5$, $v_0 = 0.5$ and $\alpha = 1/6$. Thus there is more than a two-fold increase in the

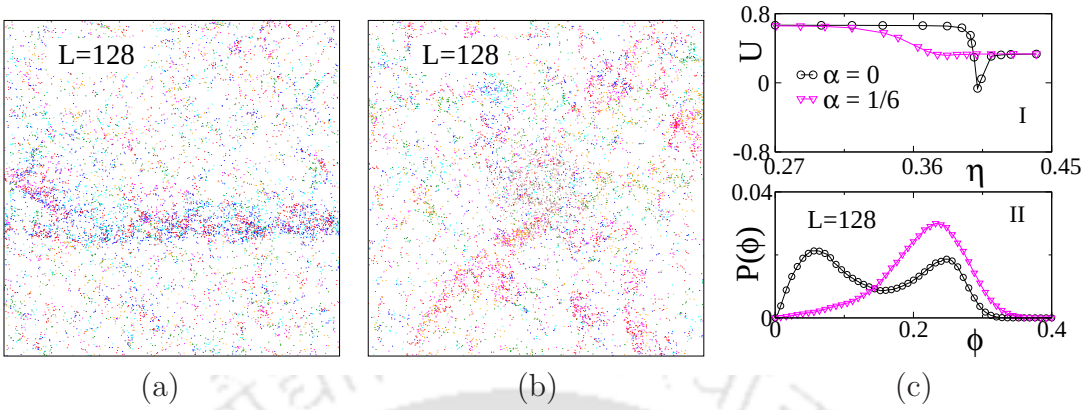

(a) (b) (c)

Figure 2.14: For $v_0 = 1.0$: System morphology with (a) $\alpha = 0$ and (b) $\alpha = 1/6$ at the respective η_c, system size is $L = 128$, $\rho_0 = 0.5$ ($N = 8192$). (c) Plot of U against η in I and plot of the distribution $P(\phi)$ of ϕ in II. Colour representation of the orientation ranges in the configuration are as per Fig.2.3.

crossover size. The situation is going to be more drastic at higher velocities. Below we present a few results for $v_0 = 1.0$.

2.2.5 Results at $v_0 = 1.0$

At high velocity such as $v_0 = 1.0$, the density band appears in a system of size as low as $L = 80$, with density $\rho_0 = 0.5$ ($N = 3200$). To study the effect perturbation at such a higher velocity ($v_0 = 1.0$), we considered two system sizes, $L = 128$ and $L = 256$, keeping the density $\rho_0 = 0.5$ same (the number of particles is kept as $N = 8192$ and $N = 32768$ respectively). For the system of size $L = 128$, the snapshot of system morphology for $\alpha = 0$ and $\alpha = 1/6$ is shown in Fig.2.14(a) and (b) respectively. The prominent density band that was formed in the VM ($\alpha = 0$) on $L = 128$ disappeared when the perturbation of strength $\alpha = 1/6$ is applied. Decrease of band density and optimal noise are also observed in a different model for a ring-shaped perturbation with different trapping rules [147]. The variation of the Binder cumulant U against η in plotted in Fig.2.14(c)I. It is also compared with the case of $\alpha = 0$. It can be seen that the negative dip in U for $\alpha = 0$ has disappeared, and it becomes positive for $\alpha = 1/6$. The distribution $P(\phi)$ of ϕ for $\alpha = 0$ and $1/6$ are shown in Fig.2.14(c)II. The bimodal distribution of ϕ for $\alpha = 0$ becomes unimodal for $\alpha = 1/6$. Thus application perturbation in the VM at $v_0 = 1.0$ makes the discontinuous transition a continuous transition for a system of size $L = 128$ with density $\rho_0 = 0.5$.

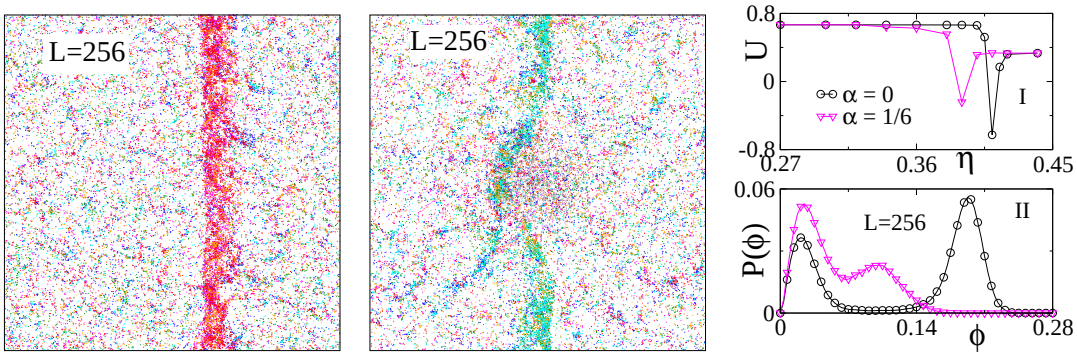

(a) (b) (c)

Figure 2.15: For $v_0 = 1.0$: System morphology with (a) $\alpha = 0$ and (b) $\alpha = 1/6$ at the respective η_c, system size is fixed as $L = 256$, $\rho_0 = 0.5$ ($N = 32768$). (c) Plot of U against η in I and plot of $P(\phi)$ of ϕ in II. Colour representation of the orientation ranges in the configuration are as per Fig.2.3.

Now the effect of perturbation is checked for a higher system size $L = 256$, $\rho_0 = 0.5$ ($N = 32768$). The snapshot of system morphology for $\alpha = 0$ and $\alpha = 1/6$ is shown in Fig.2.15(a) and (b) respectively. Even with a perturbation strength $\alpha = 1/6$, the travelling band persists in the system with a slight distortion around the central zone of the trapping perturbation. The variation of U against η is presented in Fig. 2.15(c)I for $\alpha = 0$ and $\alpha = 1/6$. The Binder cumulant U still remains negative at the transition for $\alpha = 1/6$. The distribution $P(\phi)$ of ϕ are bimodal for both $\alpha = 0$ and $\alpha = 1/6$ as shown in Fig.2.15(c)II. Characteristics of U and that of the $P(\phi)$ both indicate that the transition is discontinuous at $\alpha = 1/6$. Though the further increase of α to $1/4$ shows disappearance of the travelling band, positive U at η_c with a small dip and a unimodal distribution $P(\phi)$, no critical transition in the system is observed. Rather a smooth crossover from order to disorder phase without any peak in susceptibility χ is found to occur. Again the crossover system size $L^*_\alpha(\rho_0, v_0)$ has increased upon application of perturbation and for $v_0 = 1.0$ it somewhere between $L = 128$ and 256 for the particle density $\rho_0 = 0.5$.

2.3 Summary and Discussion

In this chapter, a new model is constructed by imposing trapping perturbation on the VM. The model is then studied varying the scalar noise η for different perturbation strength α and velocities v_0. Simulations are performed for different system of sizes L at three different velocities $v_0 = 0.1$, $v_0 = 0.5$ and $v_0 = 1.0$ respectively. De-

pending on the system size L, velocity v_0 and perturbation strength α, continuous and discontinuous order-disorder transitions occur in the system. The continuous transitions are characterized by positive Binder cumulant U and unimodal distribution of the order parameter $P(\phi)$. Whereas a negative dip in the Binder cumulant U and bimodal distribution $P(\phi)$ of the order parameter ϕ characterizes the discontinuous transition. FSS analysis is performed for all situations. For low velocity like $v_0 = 0.1$, the crossover system size is expected to be very large, and no travelling band is observed for the system size $L = 256$. In this case, the effect of perturbation enhances the transition point to a low noise value. It is found that the transition type of the perturbed system is continuous, and the critical exponents are found to be the same as the VM. Then for the higher velocities, the effect of perturbation is studied for system size greater than the crossover size. There exists a crossover system size $L^*(\rho_0, v_0) \approx 100$ for the VM without perturbation ($\alpha = 0$) for $v_0 = 0.5$ and $\rho_0 = 0.5$ below which the model exhibits continuous transition and above which it exhibits discontinuous transition with dense travelling bands in the system. In the presence of trapping perturbation, the value of crossover system size $L^*_\alpha(\rho_0, v_0)$ increases and becomes greater than $L^*(\rho_0, v_0)$, that of without perturbation. Further, there exists a tricritical point α^* for a given system of size L, $L^*(\rho_0, v_0) < L < L^*_\alpha(\rho_0, v_0)$, below which the transition is discontinuous and above which the transition is continuous. As the velocity v_0 increases, the value of $L^*_\alpha(\rho_0, v_0)$ decreases but remains greater than the corresponding $L^*(\rho_0, v_0)$. The continuous transition in the VM under perturbation for a system of size $L < L^*_\alpha(\rho_0, v_0)$ is not due to the system's reduced density because of trapping; rather, it is because of the density fluctuation and randomization of orientation. Furthermore, the continuous transitions observed in the VM with perturbation is characterized by the same critical exponents of the VM without perturbation for $L < L^*(\rho_0, v_0)$. On the other hand, in the VM with perturbation, for $L > L^*_\alpha(\rho_0, v_0)$, the effect of the positive feedback mechanism becomes stronger than the perturbation. As a result, dense travelling bands reappear in the system, and the transition becomes discontinuous. Thus the perturbation in the form of fluctuations in local density and orientation can destroy the dense travelling band in the system up to a certain system size $L^*_\alpha(\rho_0, v_0)$ for a given ρ_0, v_0 and α. For the systems of size beyond $L^*_\alpha(\rho_0, v_0)$, the transition remains discontinuous even in the presence of perturbation.

Chapter 3

Pattern formation and phase transition in the collective dynamics of a binary mixture of polar self-propelled particles

Collective pattern formation and self-organization of active or self-propelled particles (SPPs) spontaneously occur in nature at different length scales. For example, actin filaments can form different structures as microclusters, stripes, and traveling waves [21, 117], bacterial swarms growing in the lab can self-organize into high-density coherent patterns [18, 19, 148–150], army ants [151], insect swarms [14, 15], spiny lobsters [152, 153], fish schools [154], flocking birds [7, 8], pedestrian flow [155, 156], artificial systems of SPPs [25, 26], etc. Some of these systems also exhibit motility-induced phase separation. Phase separation strategies of active particles are studied in various branches of science [40, 157]. Different examples of phase separation in active systems include: a mixture of active Brownian particles with different diffusion constant [54, 158], a mixture of active and passive particles [55, 159–161], binary active particles with different alignment interactions [162], oppositely driven binary mixture of particles [163–165], chiral active matter [77, 166], a mixture of polar and apolar SPPs [167] and many others. However, the study of phase separation and dynamic transition in a binary mixture of polar SPPs with different motile properties is a new area of research.

Collective behaviour of polar SPPs of common motile properties is extensively studied following the seminal Vicsek Model (VM) [70]. In this model, a large number of polar SPPs move together at a constant speed, and they align their direction of

motion with their neighbours through a short-range alignment interaction. However, the average direction is subject to an angular noise (η). For a given density (ρ), an orientational order-disorder transition occurs at a critical noise (η_c). One of the main criteria of VM is that all the polar SPPs should have the same velocity. However, in natural systems, the velocities of particles need not be the same during collective motion. For example, fast-moving (active) and slow-moving (dormant) bacteria in a bacterial population or slow-moving vehicles and speedy vehicles in daily traffic. We propose a model with two types of polar SPPs having two widely different velocities. It is intriguing to observe whether self-organized pattern formation and phase separation occur under a short-range interaction without any external force or repulsion in this binary model (BM). Furthermore, will there be any criticality in the system? Should the system undergo any order-disorder transition at a critical point? What would be the nature of such transition? In this study, we explore answers to all these questions. The collective dynamics and the underlying mechanism could also explain the similar pattern formation and dynamical behaviour observed in other systems.

In the next section, we present the model. The pattern formation and order-disorder phase transition are then presented. Finally, we discuss different velocity regimes and conclude. In the rest of the paper, we denote the polar SPPs as SPPs only.

3.1 Binary Model

Collective motion of a mixture of SPPs with two different motility is modelled over a two-dimensional square box of linear size L. The different motilities of SPPs are modelled, assigning widely different velocities to them. The fast-moving SPPs move with a velocity v_f and the slow-moving SPPs move with a velocity v_s where $v_f \gg v_s$. The two types of SPPs are taken in equal proportion. If N_f is the number of fast-moving SPPs and N_s is the number of slow-moving SPPs, then $N_f = N_s = N/2$ where N is the total number of SPPs in the system. Initially, the position $\vec{r}_{p,i}$, $i = 1, 2, 3, \cdots, N/2$ of all the SPPs are randomly distributed over the space (off-lattice) where $p \in \{s, f\}$. The initial orientation θ_i of an SPP is randomly selected in the range $-\pi$ to π, irrespective of their type. The SPPs of both types interact within a local neighbourhood $R = 1$ and determine their average orientation. Both inter-particle and intra-particle interactions are considered in estimating the average orientation. The distribution of randomly oriented 25 fast-moving SPPs (in orange)

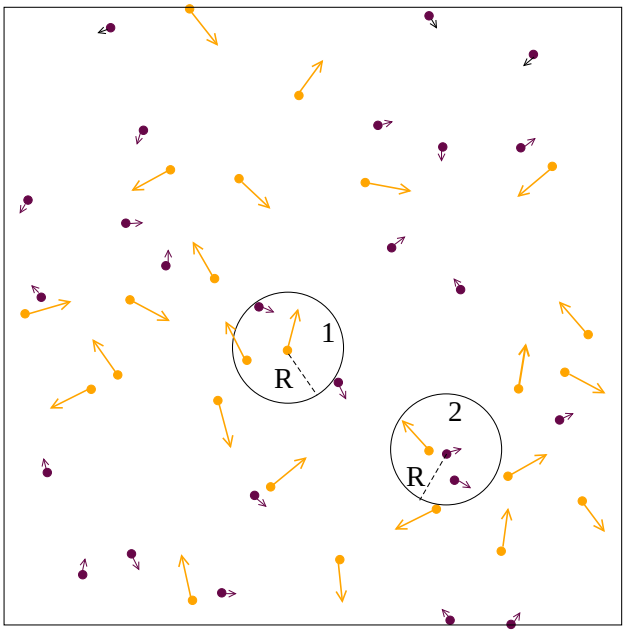

Figure 3.1: The distribution of binary SPPs is shown on a system of size $L = 10$ where $N_f = N_s = 25$. The Orange colour represents the fast-moving SPPs, and the maroon colour represents the slow-moving SPPs. The arrow associated with an SPP indicates the direction of velocity. A fast-moving SPP at the centre of circle-1 and a slow-moving SPP at the centre of circle-2 interact with both slow and fast-moving SPPs present within the radius R.

and 25 slow-moving SPPs (in maroon) are shown in Fig.3.1. Longer and shorter arrows show the velocities v_f and v_s, respectively.

The time evolution of the orientation θ_i of the ith SPP is determined by

$$\theta_i(t + \Delta t) = \langle \theta(t) \rangle_R + \Delta\theta \tag{3.1}$$

where $\Delta\theta$ is a random orientation chosen with a uniform probability from the interval $[-\eta\pi, +\eta\pi]$. The strength of the angular noise η varies from 0 to 1. The term $\langle \cdots \rangle_R$ is defined as

$$\langle \theta(t) \rangle_R = \arctan\left[\frac{\langle \sin\theta \rangle}{\langle \cos\theta \rangle}\right];$$
$$\langle \sin\theta \rangle = \frac{1}{n}\sum_{j\in\{R\}} \sin\theta_j; \quad \langle \cos\theta \rangle = \frac{1}{n}\sum_{j\in\{R\}} \cos\theta_j$$

where n is the number of SPPs in the neighbourhood region R that includes both the slow and fast-moving SPPs. It should be noted that the magnitude of velocity

of individual SPPs are igonred and only the orientations are teken into account in estimating $\langle\theta(t)\rangle_R$. After averaging, an SPP of type-p ($p \in \{s, f\}$) at the position $\vec{r}_{p,i}$ is thus moving with a speed v_p in the direction θ_i. Knowing the velocity $\vec{v}_{p,i}(t)$ at every time step, the position of the ith SPP $\vec{r}_{p,i}$ is updated following the forward update rule as given below

$$\vec{r}_{p,i}(t + \Delta t) = \vec{r}_{p,i}(t) + \vec{v}_{p,i}(t)\Delta t \tag{3.2}$$

where Δt is the time between two successive updates, and it is chosen as $\Delta t = 1$. The linked cell-list algorithm as discussed in chapter-2 is used to keep track of time varying neighbour list. Periodic boundary conditions (PBCs) in the horizontal and vertical directions are applied in case the position vector crosses the boundary of the square box. Eq.3.1 and Eq.3.2 are then evolved with time and the dynamical properties are studied varying the angular noise η for different velocity ranges.

In a special situation if $v_s = v_f = v_0$, the BM will boil down to the VM with velocity v_0 for all SPPs [70].

3.2 Results and Discussion

For a given initial random distribution of SPPs over a square box of size L, the system's time evolution is studied following Eq.3.1 and Eq.3.2 by performing Monte Carlo simulations. One Monte Carlo time step corresponds to the up-gradation of position and orientation of all the SPPs. Initial 7×10^5 Monte Carlo steps are neglected to achieve the steady-state. An ensemble of size 48×10^5 is taken for statistical averages (2×10^5 time samples for each 24 different initial configurations). Simulations are performed for different velocities of the fast-moving SPPs: $v_f = 30v_s$, $v_f = 50v_s$, $v_f = 100v_s$ and $v_f = 150v_s$ keeping the velocity of the slow-moving SPPs fixed at $v_s = 0.01$. The two SPPs are taken in equal proportions. The overall density of SPPs, $\rho_0 = N/L^2$, is kept fixed as $\rho_0 = 0.5$ for all the observations. First, we will discuss the formation of the collective patterns in this model. The phase transition will be discussed later.

3.2.1 Collective Patterns

First, we present the morphologies of the system of binary SPPs with $v_f = 30v_s$ and $v_s = 0.01$ at different angular noise η on a system of size $L = 128$ in Fig.3.2. SPPs are represented by circles with two different colors: orange for the fast-moving SPPs

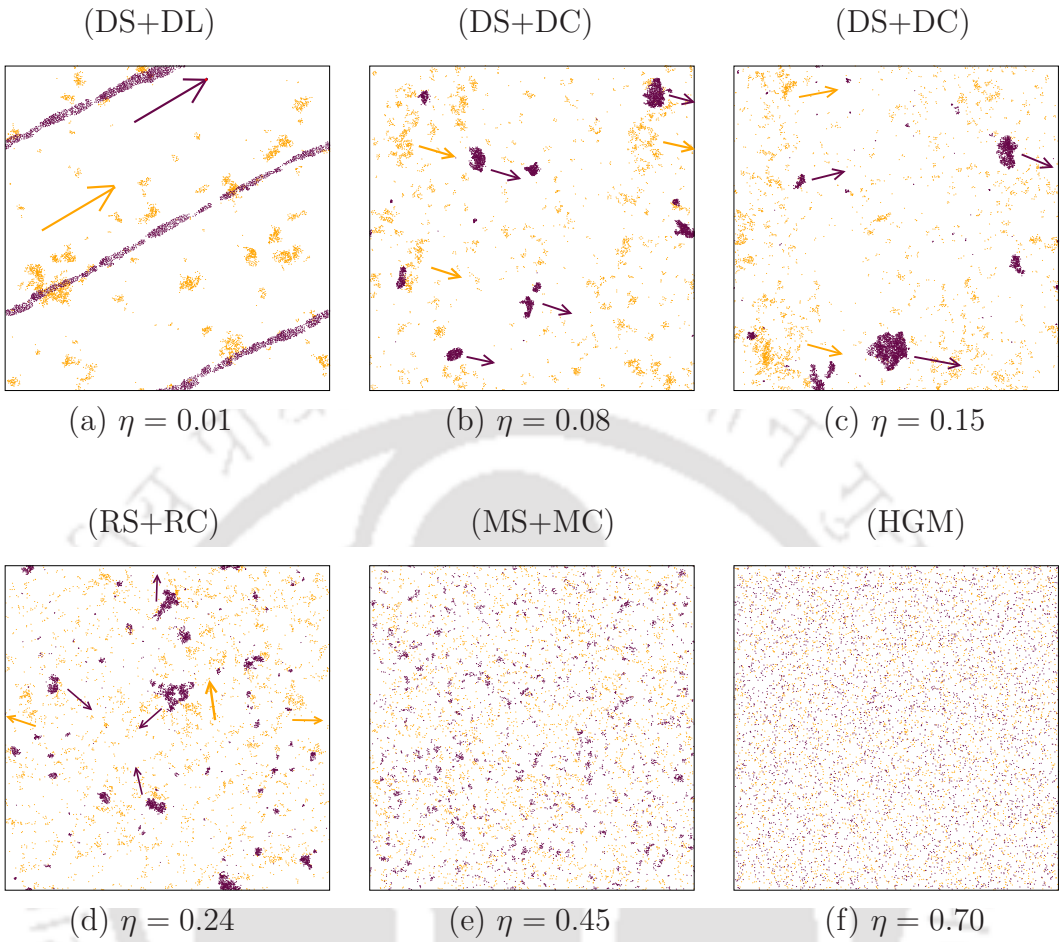

Figure 3.2: Morphologies of the system of SPPs with $v_f = 30v_s$ and $v_s = 0.01$ for different angular noise (a) $\eta = 0.01$, (b) $\eta = 0.08$, (c) $\eta = 0.15$, (d) $\eta = 0.24$, (e) $\eta = 0.45$ and (f) $\eta = 0.70$ for a system of size $L = 128$. The orange colour represents the fast-moving SPPs, and the maroon colour represents slow-moving SPPs.

($v_f = 30v_s$) and maroon for the slow-moving SPPs ($v_s = 0.01$). A variety of patterns appear as the angular noise η varies. For a low angular noise $\eta = 0.01$, it is observed in Fig.3.2(a) that the fast-moving SPPs form clusters and they move in a particular direction (indicated by the orange arrow). On the other hand, the slow-moving SPPs are moving on a narrow lane in the same direction (indicated by the maroon arrow) as the clusters of fast-moving SPPs. The narrow lanes formed by the slow-moving SPPs are called directed lanes (DL), and the clusters of fast-moving SPPs are called directed clusters (DS). It seems that the motion of the fast-moving SPPs guides the motion of the slow-moving SPPs. At each time step, the fast-moving SPPs travel a much larger distance than the slow-moving SPPs, and consequently, they influence the ordering of the distant flocks of both types. For a given initial configuration,

the direction of motion of DS (or DL) is spontaneously selected toward an arbitrary direction. Such lane formation was not observed in the VM with monodispersed SPPs. With the increase of η, the directed clusters of fast-moving SPPs look a little scattered, whereas the slow-moving SPPs form clumps (or compact clusters) that still move in the same direction of DS of the fast-moving SPPs. We call these clumps of slow-moving SPPs as directed clumps (DC). The system morphology of this phase is shown in Fig.3.2(b) and (c) for $\eta = 0.08$ and $\eta = 0.15$ respectively. The morphologies are given in Fig.3.2(a),(b) and (c) correspond to the orientationally ordered phases. In these phases, the patterns are phase-separated according to the velocities of the SPPs, and the flocks of different types of SPPs move in the same direction. The phase separation is due to the difference in velocities of the two types of SPPs, and the same direction of motion of different flocks is due to the mutual alignment interaction of all the SPPs. Further increase of noise to $\eta = 0.24$ induces random motion to both the clusters of fast-moving SPPs and the clumps of slow-moving SPPs. We call the randomly moving clusters of fast-moving SPPs by random clusters (RS) and the randomly moving clumps of the slow-moving SPPs by random clumps (RC). The morphology at $\eta = 0.24$ is shown in Fig.3.2(d). Thus, DS and DC become RS and RC as the noise changes from $\eta = 0.15$ to $\eta = 0.24$. Usually, the orientational order-disorder transition (as in the VM) occurs between a directed phase and a random phase. In this binary model, such a transition occurs at $\eta_c \approx 0.19$ when DS+DC goes to RS+RC. As η is increased beyond 0.24, the RS and RC begin to dissolve into a larger number of micro-clusters (MS) of fast-moving SPPs and micro-clumps (MC) of slow-moving SPPs, respectively. The situation is shown in Fig.3.2(e) for $\eta = 0.45$. For relatively high η, a homogeneous gas-like mixture (HGM) of slow and fast-moving SPPs is observed. It is shown for $\eta = 0.70$ in Fig.3.2(f). However, the formation of lanes, clumps, etc., were observed in a model of SPPs with density-dependent motility [168]. Particle aggregations, thick lanes, etc., were also observed due to crowding and jamming in a lattice model of SPPs [96]. Stripes, similar to lane pattern, is observed in a model of self-propelled agents with both velocity alignment and aggregation at a low noise [95]. The aggregation interaction, which characterizes the tendency of the agents to gather during movement, plays a nontrivial role in the collective dynamics in this model. Whereas, in the BM, in the presence of only alignment interaction, lane pattern by the slow-moving SPPs occurs for very low noise. It seems that movement of slow-moving SPPs in a significantly smaller length scale induces such aggregation. Except for the lane formation by the slow-moving SPPs at very low

noise, the patterns that appeared at different values of η are similar to those obtained in the VM with mono-dispersed SPPs of specific velocities. Similar ordered phase (at low noise) patterns also appear in the cases of higher velocities of the fast-moving SPPs such as $v_f = 50v_s$ and $v_f = 150v_s$ with $v_s = 0.01$.

To characterize these different patterns, we measure a few quantities for the BM with velocities $v_f = 30v_s$ and $v_s = 0.01$ on a system of size $L = 256$ ($N = 32768$). The patterns described above consists of numerous flocks of different shapes and sizes. A flock is a collection of interacting SPPs. Two SPPs are in the same flock if their separation $r \leq R$ (within the interaction zone). A flock could be in the form of lane, cluster, clump, or micro-clump. First, we analyze the size of the largest flock M_p of the p-type ($p \in \{s, f\}$) SPPs. The value of M_p is given by the number of SPPs that belong to the largest flock. The value of M_p is expected to decrease with increasing η. In Fig.3.3(a), the variations of M_s and M_f against η are shown. For the lowest value of η (0.01), the largest flock size of the slow-moving SPPs is $M_s \approx 7490$ and that of the fast-moving SPPs is $M_f \approx 1360$. The value of M_s is larger than that of M_f as the slow-moving SPPs are densely packed along the lanes. As η increases, the value of M_s decreases sharply, whereas M_f decreases relatively slowly. Near the transition region, there is a slight increase in M_s as a few larger clumps appear in the system. The increase in M_f in this region, however, is relatively small in comparison to M_s. At the transition point ($\eta_c \approx 0.19$), the largest flock sizes of the two SPPs are $M_f \approx 386$ and $M_s \approx 2162$. With a further increase of η, the largest flock breaks down to smaller flocks. For high η, the size of the largest flock not only becomes small but also the values of M_s and M_f become comparable, $M_s \approx 15$ and $M_f \approx 14$ at $\eta = 0.70$.

It is important to count the number of flocks $N_{C,p}$ ($p \in \{s, f\}$) at different values of η. The number of flocks is expected to increase as η increases. The variation of $N_{C,p}$ is shown in Fig.3.3(b). For $\eta = 0.01$, the number of flocks of slow-moving SPPs is $N_{C,s} \approx 54$ and that of the fast-moving SPPs is $N_{C,f} \approx 483$. There are more DS than DL. Though the lane looks continuous, it is actually fragmented into 54 parts and all are aligned in the same direction. In this region, both $N_{C,f}$ and $N_{C,s}$ are small. As η increases, $N_{C,f}$ grows faster than $N_{C,s}$ and it is found that $N_{C,f} > N_{C,s}$ for all η. Near the transition point ($\eta_c \approx 0.19$), the number of flocks are $N_{C,f} \approx 3862$ and $N_{C,s} \approx 340$. However, $N_{C,s}$ increase slowly with η, and then there is a rapid increase near $\eta \approx 0.40$ where MS and MC phase occurs. Whereas, $N_{C,f}$ increases gradually with η. For $\eta = 0.70$, the number of flocks of slow-moving SPPs becomes $N_{C,s} \approx 10068$, whereas, $N_{C,f} \approx 10318$. As the total number of SPPs

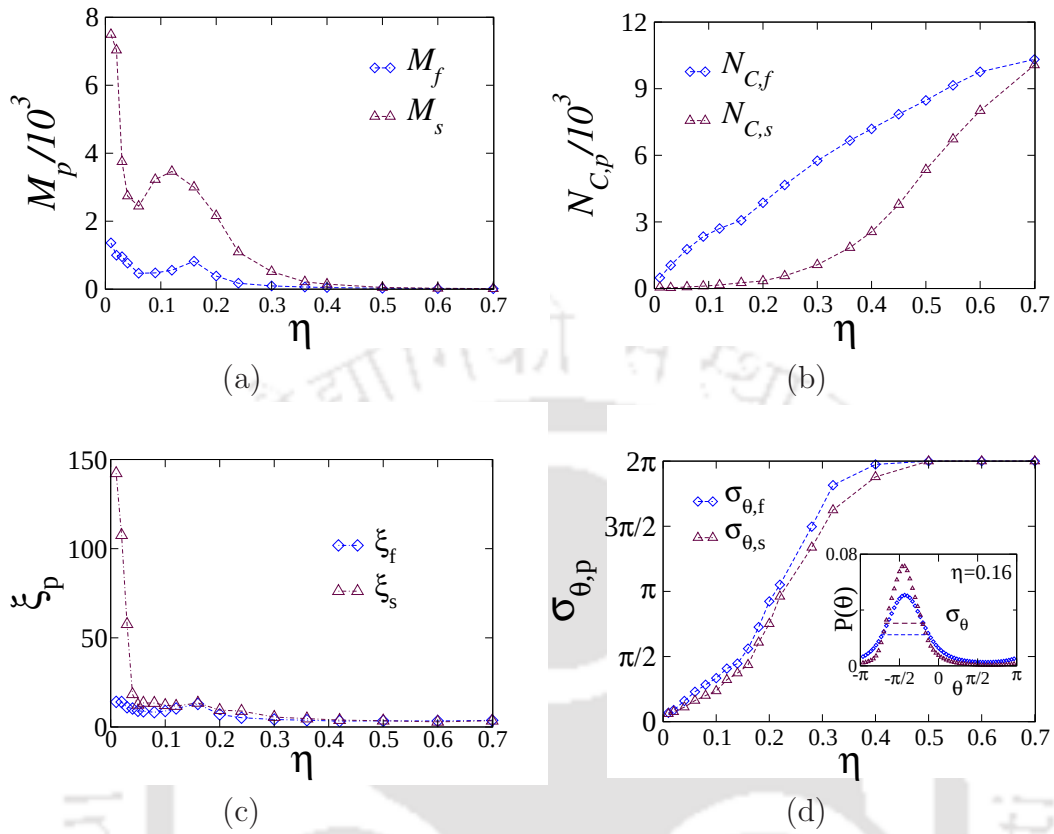

Figure 3.3: $v_f = 30v_s, v_s = 0.01$: (a) Plot of M_p against η. (b) Plot of $N_{C,p}$ against η. (c) Plot of ξ_p against η. (d) Plot of $\sigma_{\theta,p}$ versus η. In the inset of (d), $P(\theta)$ is plotted for $\eta = 0.16$ with the same symbols and colours for the fast and slow-moving SPPs. System size is $L = 256$.

in the system is 32768, the number of SPPs per flock is less than 2. The system of SPPs at this high η thus becomes a spatially homogeneously mixed gas.

In order to determine the extension of a flock, the correlation-length is determined separately for both type of particle flocks. The correlation length ξ is defined [169] as

$$\xi^2 = \frac{2\sum_m R_m^2(m)m^2 n_m}{\sum_m m^2 n_m} \tag{3.3}$$

where R_m is the radius of gyration of a flock of size m. The variation of the correlation lengths ξ_p ($p \in \{s, f\}$) are shown in Fig.3.3(c). For $\eta = 0.01$, the value of ξ_s is ≈ 140 whereas ξ_f is ≈ 14. This is because the slow-moving SPPs form elongated DL with large number of SPPs but the fast-moving SPPs form almost isotropic DS with relatively lesser number of SPPs in each cluster. The correlation length ξ_s decreases sharply as η is increased slightly. The value of ξ_f is relatively

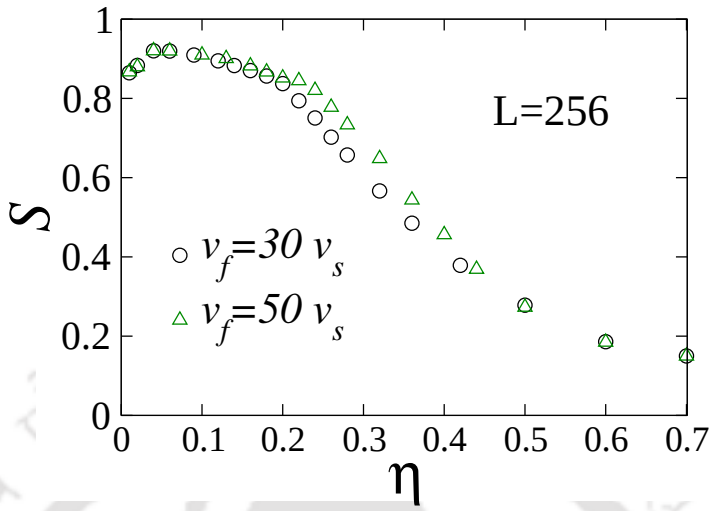

Figure 3.4: Plot of the segregation coefficient S versus η for $v_f = 30v_s$ and $v_f = 50v_s$ with $v_s = 0.01$ for a system of size $L = 256$.

less in this region and changes slowly with increasing η. Note that in determining ξ_p, flocks of size $m < 4$ are negleted.

The orientations of SPPs change from a particular direction (ordered state) to random directions (disordered state) as η varies from a small to a large value. The orientation distribution $P(\theta)$ of the SPPs is expected to be highly peaked in the ordered state and to be a flat one in the disordered state. To characterize the change in orientation, the full width at half maximum (σ_θ) is determined from the distributions $P(\theta)$ at every η. In determining σ_θ, a steady-state time average is considered for a given initial configuration only. The value of $\sigma_{\theta,p}$ for p-type ($p \in \{s, f\}$) SPPs is expected to increase from 0 to 2π as η changes from zero to a high value. In Fig.3.3(d), the variation of $\sigma_{\theta,p}$ against η is shown. The distribution of orientations $P(\theta)$ for both the SPPs are given in the inset of Fig.3.3(d) for $\eta = 0.16$. It is observed that the distributions are peaked at a particular angle. Though $\sigma_{\theta,f}$ slightly wider than $\sigma_{\theta,s}$, $\sigma_{\theta,p} \approx \pi/2$ for both the SPPs at $\eta = 0.16$. At the lowest $\eta = 0.01$, the values of $\sigma_{\theta,f}$ and $\sigma_{\theta,s}$ are very small approximately 0.2 radian. Near the transition region, $\sigma_{\theta,p}$ is approximately π for both the SPPs. With further increase of η, as the $P(\theta)$ becomes flat, $\sigma_{\theta,p}$ becomes 2π for higher angular noise ($\eta > 0.40$).

The segregation coefficient is calculated to study phase-separation or demixing between the two types of SPPs. The square box of area L^2 is divided into Q square sub-regions of linear size l and area L^2/Q each. The segregation coefficient [77, 170]

is defined as

$$S = \frac{1}{N}\sum_{j=1}^{Q} |n_{fj} - n_{sj}| \tag{3.4}$$

where j is the index for the sub-regions, n_f and n_s are the number of the fast and slow-moving SPPs respectively in the sub-region area. The coefficient S is determined for the patterns described above, taking $l = 8$, similar to the length scale of the average flock size near the transition. The value $S = 1$ represents a fully demixed or phase-separated pattern, whereas it is low for mixed structures. The variation of the coefficient S for $v_f = 30v_s$ and $v_f = 50v_s$ (with $v_s = 0.01$) at different η values are shown in Fig.3.4. It can be seen that the coefficient S is high at smaller η, where phase-separated patterns appear in the system. The slight decrease in S at very small $\eta(\approx 0.01)$ may have arisen from the empty sub-regions. Whereas, at higher η, S decreases with η as they mix uniformly, and phase separation disappears. Such phase separation was also observed in a binary mixture of active Brownian particles with wide differences in the diffusion constant [54].

Finally we investigate the spatio-temporal correlations in the directed clusters and clumps around the transition point. The temporal correlation is measured by the velocity time autocorrelation function $C(t)$ and the spatial correlation is measured by the two-point velocity correlation function $g(r)$ [171] and are given by

$$C(t) = \left\langle \frac{\vec{v}_i(0)\cdot\vec{v}_i(t)}{|\vec{v}_i(0)||\vec{v}_i(t)|} \right\rangle, g(r) = \left\langle \frac{\vec{v}_i(0)\cdot\vec{v}_j(r)}{|\vec{v}_i(0)||\vec{v}_j(r)|} \right\rangle \tag{3.5}$$

where i and j are particle indices and $\langle\cdots\rangle$ stands for an ensemble average over $1000N$. The estimates of $C(t)$ versus t and $g(r)$ versus r for three different noise values as $\eta = 0.15$, $0.19(\eta_c)$ and 0.24 for the system of size $L = 256$ are plotted in Fig.3.5(a) and (b) respectively. The system is highly correlated over time in the DS+DC ($\eta = 0.15$) phase. The correlation is less and decays significantly around $t = 100$ for $\eta_c = 0.19$. Furthermore, $C(t)$ decays sharply for $\eta = 0.24$, implying that the correaltion is less in the RS+RC phase. The value of $g(r)$ is also found high for smaller r for $\eta = 0.15$. As r increases, the correlation decreases and become almost constant to a moderately high value ($g(r) \approx 0.6$). For $\eta_c = 0.19$, $g(r)$ decays faster than that with $\eta = 0.15$. Whereas in the random phase with $\eta = 0.24$, $g(r) \approx 0$ for $r = 32$.

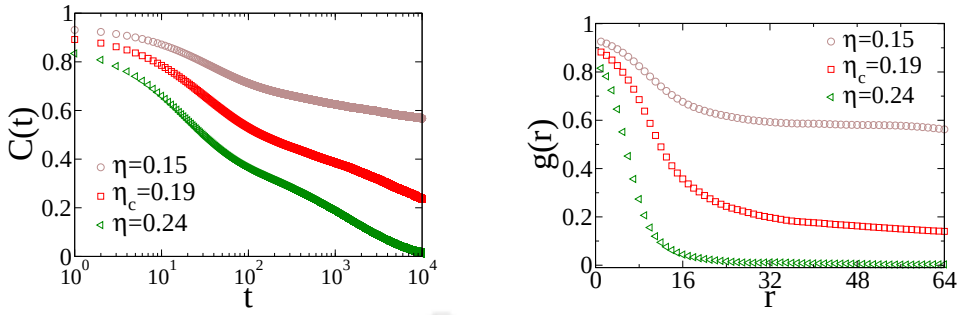

(a) (b)

Figure 3.5: $v_f = 30v_s, v_s = 0.01$: (a) Plot of $C(t)$ against t. (b) Plot of $g(r)$ against r. System size is fixed at $L = 256$.

3.2.2 Phase transition

As the angular noise η changes from 0 to a higher value, the system undergoes a transition from an orientational ordered state to an orientational disordered state. Such a transition occurs when the directed clusters and directed clumps (DS+DC) phase (Fig.3.2(c)) changes to random clusters and random clumps (RS+RC) phase (Fig.3.2(d)) in the binary system around the critical noise $\eta = \eta_c$. We analyze the data for phase transition for the whole system, considering both the slow-moving and fast-moving SPPs together as well as the partial systems involving only one type of SPPs. The order parameter of the transition ϕ for the whole system is defined as

$$\phi(\eta, L) = \frac{1}{N}\left|\sum_{p}\sum_{i=1}^{N_p}\frac{\vec{v}_{p,i}}{|\vec{v}_{p,i}|}\right| \tag{3.6}$$

where N is the total number of SPPs. The partial order-parameter of the transition ϕ_p for the p-type SPPs is defined as

$$\phi_p(\eta, L) = \frac{1}{N_p}\left|\sum_{i=1}^{N_p}\frac{\vec{v}_{p,i}}{|\vec{v}_{p,i}|}\right| \tag{3.7}$$

where N_p is the number of p-type ($p \in \{s, f\}$) SPPs. The susceptibility χ for the whole system and that of the partial systems χ_p can be estimated from the fluctuation in their respective order parameters ϕ and ϕ_p as

$$\chi = L^2\left[\langle\phi^2\rangle - \langle\phi\rangle^2\right], \quad \chi_p = L^2\left[\langle\phi_p^2\rangle - \langle\phi_p\rangle^2\right] \tag{3.8}$$

where $\langle\phi^n\rangle = \int \phi^n P(\phi)d\phi$, $\langle\phi_p^n\rangle = \int \phi_p^n P(\phi_p)d\phi_p$, $P(\phi)$ and $P(\phi_p)$ are the distribution functions of ϕ and ϕ_p respectively, L is the linear dimension of the system.

Similarly, the fourth order Binder cumulant for the whole system U and that of the partial systems U_p are defined as,

$$U = 1 - \frac{\langle \phi^4 \rangle}{3\langle \phi^2 \rangle^2}, \quad U_p = 1 - \frac{\langle \phi_p^4 \rangle}{3\langle \phi_p^2 \rangle^2} \tag{3.9}$$

where the higher order averages are obtained following the definitions of $\langle \phi^n \rangle$ and $\langle \phi_p^n \rangle$ given above.

If the orientational order-disorder transition is continuous, the finite size scaling (FSS) relations of the above parameters can be given following the equilibrium thermal critical phenomena [143, 144], as

$$\phi(\eta, L) = L^{-\beta/\nu} \phi_0[\epsilon L^{1/\nu}] \tag{3.10}$$

where $\epsilon = (\eta - \eta_c)/\eta_c$ the reduced noise, β is the order parameter exponent, ν is the correlation length exponent and ϕ_0 is a scaling function. At the criticality $\eta = \eta_c$, $\phi(\eta_c, L) \sim L^{-\beta/\nu}$. The order parameter distribution $P_L(\phi)$ for a given system of size L is defined as

$$P_L(\phi) = L^{\beta/\nu} \widetilde{P}_L \left[\phi L^{\beta/\nu}\right] \tag{3.11}$$

where $\widetilde{P}_L$ is a scaling function. At the criticality, the distribution $P_L(\phi)$ is unimodal for a continuous transition. The FSS form of the susceptibility is given by

$$\chi(\eta, L) = L^{\gamma/\nu} \chi_0[\epsilon L^{1/\nu}] \tag{3.12}$$

where χ_0 is a scaling function, $\gamma/\nu = d - 2\beta/\nu$ and d $(= 2)$ is the space-dimension. At $\eta = \eta_c$, $\chi(\eta_c, L) \sim L^{\gamma/\nu}$. The FSS form of the fourth order Binder cumulant is given by

$$U(\eta, L) = U_0[\epsilon L^{1/\nu}] \tag{3.13}$$

where U_0 is a scaling function. The derivative of $U(\eta, L)$ with respect to η follows a scaling relation [145],

$$U'(\eta, L) = L^{1/\nu} \frac{U_0'[\epsilon L^{1/\nu}]}{\eta_c} \tag{3.14}$$

where the primes on U and U_0 denote their derivatives with respect to η. For a continuous transition, the cumulant U always remain positive. At $\eta = \eta_c$, the cumulants of different systems of size L become independent of L. Whereas, $U'(\eta_c, L) \sim L^{1/\nu}$ at the transition.

In case the orientational order-disorder transition is discontinuous, the order

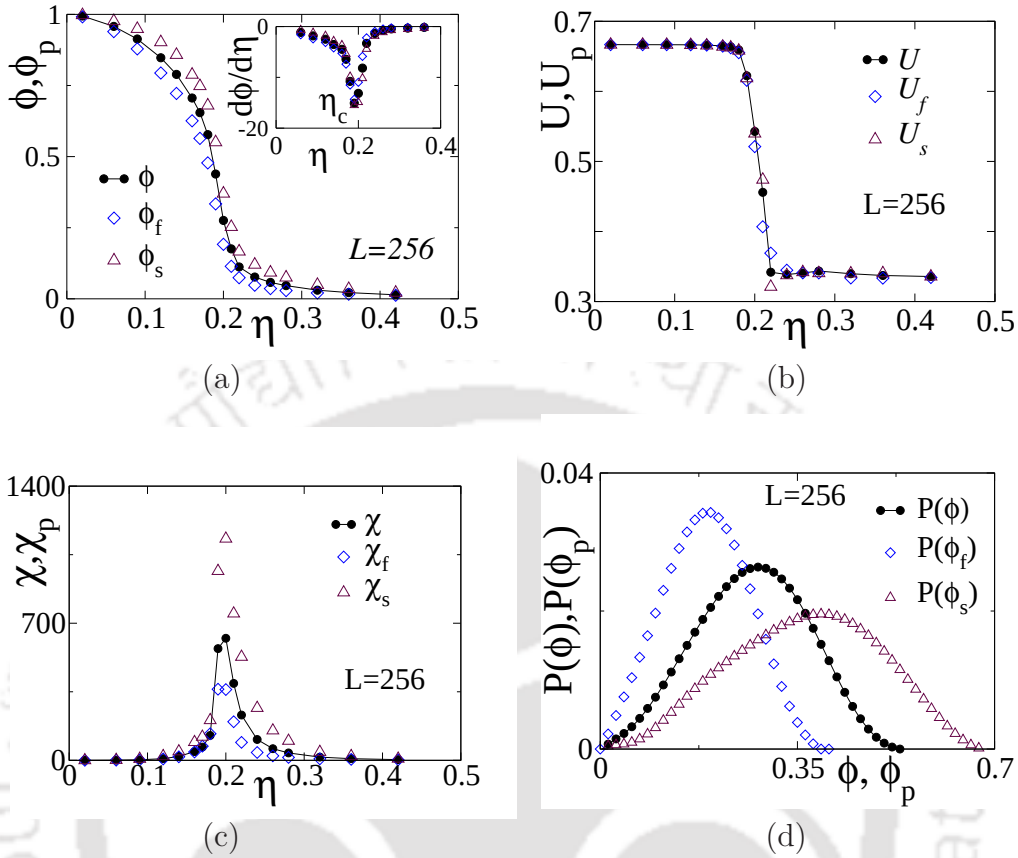

Figure 3.6: $v_f = 30v_s, v_s = 0.01$: (a) Plot of ϕ and ϕ_p versus η. Derivatives of ϕ and ϕ_p with respect to η are shown in the inset. (b) Plot of χ and χ_p versus η. (c) Plot of U and U_p versus η. (d) Plot of $P(\phi)$ and $P(\phi_p)$ at $\eta = \eta_c$. System size is $L = 256$.

parameter exponent β should go to zero. As a consequence, the susceptibility should then scale as $\chi \sim L^d$, where d is the space dimension. The Binder cumulant U would exhibit a sharp fall towards a negative value at the transition point. As the system exhibits the coexistence of two phases, the order parameter distribution $P(\phi)$ would be a bimodal distribution for a discontinuous transition.

3.2.3 Results with $v_f = 30v_s$ and $v_s = 0.01$

Variations of order parameter ϕ, Binder cumulant U, susceptibility χ and order parameter distribution $P(\phi)$ are studied varying the angular noise η on systems of different sizes L. In Fig.3.6, we present data for ϕ, U, χ and $P(\phi)$ for $v_f = 30v_s$ and $v_s = 0.01$ on a system of size $L = 256$. The order parameter ϕ of the whole system and ϕ_p, that of the partial systems, are plotted against η in Fig.3.6(a). The

values of ϕ and ϕ_p decrease continuously and smoothly from a positive value to zero as η changes from a smaller value to a higher value. The derivatives of ϕ and ϕ_p with respect to η are plotted in the inset of Fig.3.6(a). A phase transition occurs at $\eta_c \approx 0.19$, corresponding to the dips in the derivatives. The whole system, as well as the partial systems, undergo a phase transition at the same critical noise $\eta_c \approx 0.19$. It is evident from the configurations given in Fig.3.2(c) and (d) that the system is going from an orientationally ordered phase DS+DC to an orientationally disordered phase RS+RC around $\eta_c \approx 0.19$. It is interesting to note that the value of the order parameter of the fast-moving SPPs ϕ_f is less than the value of the order parameter of the slow-moving SPPs ϕ_s at all values of η. However, in a monodispersed system like VM, the SPPs always have more polar order at a higher velocity than at a lower velocity [145]. At a high velocity, the interaction between distant flocks is higher due to the fast movement of SPPs, which results in a much stronger order which is not achievable at low velocities in the VM of monodispersed SPPs. Thus, the order parameter of a particular type of SPPs is highly influenced by the motion of other types of SPPs in the BM. The fluctuations in order parameters χ and χ_p are plotted against η in Fig.3.6(b) for $L = 256$. The fluctuations for all the order parameters diverge at $\eta_c \approx 0.19$. The fluctuation for the slow-moving SPPs at η_c is much higher than that of the fast-moving SPPs. It is similar to the observations in the VM with monodispersed SPPs.

The Binder cumulants, U and U_p are plotted against η in Fig.3.6(c) for $L = 256$. It can be seen that the values of U, U_f and U_s are all positive over the whole range of η. The distributions of order parameters $P(\phi)$ and $P(\phi_p)$ obtained at $\eta = \eta_c$ are presented in Fig.3.6(d). All three distributions are found to be unimodal. The positive value of the Binder cumulant and unimodal distribution of the order parameter indicates a continuous transition from the DS+DC phase to the RS+RC phase. Not only the system as a whole but also the partial systems undergo continuous transitions under the influence of mutual interactions of both the SPPs in this velocity regime. It is important to note that in the VM with monodispersed SPPs, there exists a crossover system size $L^*(\rho_0, v_0)$ [104, 136, 172], above which the transition is discontinuous. Such discontinuous transitions are characterized by the appearance of dense travelling bands in the system. Neither travelling density band is observed in the system configuration (Fig.3.2) nor any other features of discontinuous transition are observed in these velocities. It seems for the given ρ and v_f the crossover system size L^* is far beyond $L = 256$.

Now we will extract the critical exponents for the whole system with velocities

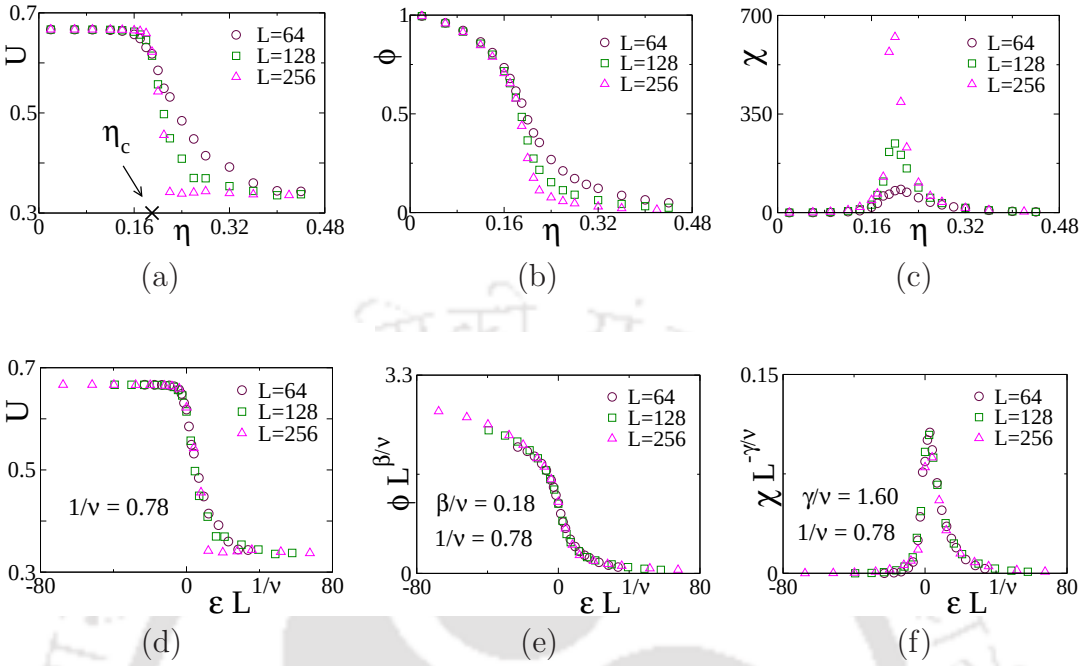

Figure 3.7: $v_f = 30v_s, v_s = 0.01$: (a) Plot of U versus η, (b) plot of ϕ versus η and (c) plot of χ versus η for $L = 64$, 128 and 256. The cross on the η-axis indicates η_c. (d) Plot of U versus the scaled noise $\epsilon L^{1/\nu}$. (e) Plot of $\phi L^{\beta/\nu}$ against $\epsilon L^{1/\nu}$. (f) Plot of $\chi L^{-\gamma/\nu}$ against $\epsilon L^{1/\nu}$. The values of the exponents are taken as $\beta/\nu = 0.18$, $\gamma/\nu = 1.60$ and $1/\nu = 0.78$.

of SPPs as $v_f = 30v_s$ and $v_s = 0.01$ performing FSS analysis. Binder cumulant U, order parameter ϕ and susceptibility χ are plotted against the angular noise η for three different systems of sizes $L = 64$, 128 and 256 in Fig.3.7(a),(b) and (c) respectively. The plots of U versus η (Fig.3.7(a)) for different L intersect at $\eta_c \approx 0.19$, the L independent critical point as expected in a continuous transition. It is marked by a cross on the η-axis. The corresponding U_c is identified as $U_c \approx 0.61$. As mentioned in the beginning of this section, $U'(\eta_c, L) \sim L^{1/\nu}$, $\phi(\eta_c, L) \sim L^{-\beta/\nu}$ and $\chi(\eta_c, L) \sim L^{\gamma/\nu}$ at the criticality. Following these scaling relations, rough estimates of the exponents $1/\nu$, β/ν and γ/ν are obtained. The best possible FSS form of the scaled parameters against the scaled noise $\epsilon L^{1/\nu}$ are obtained tuning these exponents further. U, $\phi L^{\beta/\nu}$, and $\chi L^{-\gamma/\nu}$ are plotted against $\epsilon L^{1/\nu}$ in Fig.3.7(d), (e) and (f) respectively. A reasonable collapse of data in all three cases are obtained taking $1/\nu = 0.78$, $\beta/\nu = 0.18$ and $\gamma/\nu = 1.60$ at $\eta_c = 0.19$. The critical exponents satisfy the scaling relation $\gamma/\nu + 2\beta/\nu = 2$ within error bars.

It should be emphasized here that the FSS forms of U_p, ϕ_p and χ_p for the partial systems are also verified, and the scaling relations are satisfied with the same critical

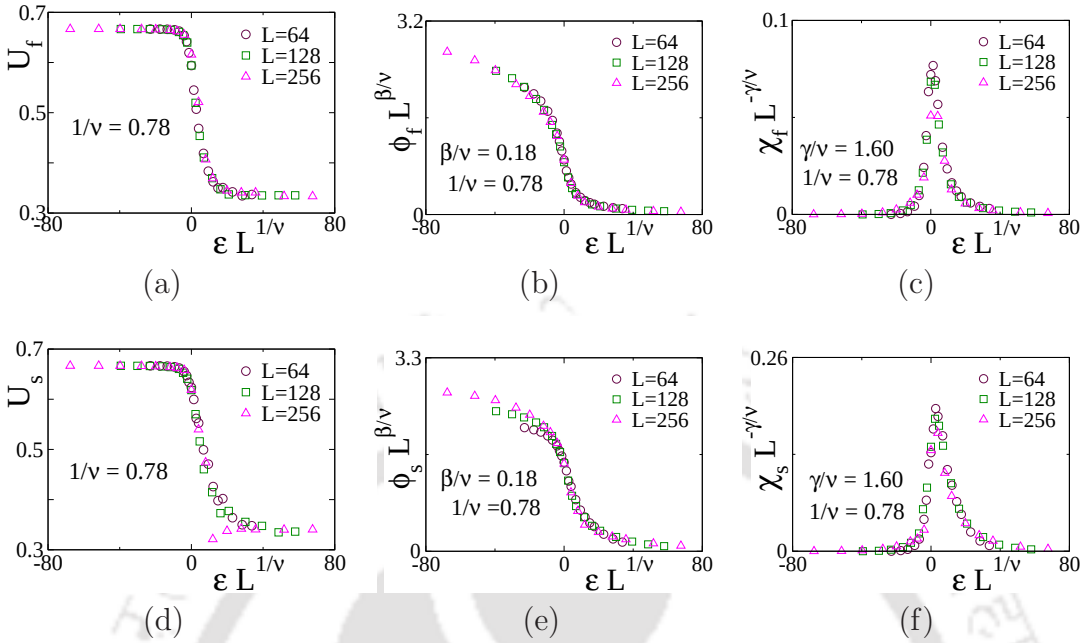

Figure 3.8: $v_f = 30v_s, v_s = 0.01$: Plot of (a) U_f, (b) $\phi_f L^{\beta/\nu}$ and (c) $\chi_f L^{-\gamma/\nu}$ versus the scaled noise $\epsilon L^{1/\nu}$ for fast SPPs. Plot of (d) U_s, (e) $\phi_s L^{\beta/\nu}$ and (f) $\chi_s L^{-\gamma/\nu}$ versus $\epsilon L^{1/\nu}$ for slow SPPs. Critical exponents are same as the Fig. 3.7.

exponents within error bars. In Fig.3.8(a),(b) and (c), U_f, $\phi_f L^{\beta/\nu}$ and $\chi_f L^{-\gamma/\nu}$ are plotted respectively against $\epsilon L^{1/\nu}$. Whereas, in Fig.3.8(e),(f) and (g), U_s, $\phi_s L^{\beta/\nu}$ and $\chi_s L^{-\gamma/\nu}$ are plotted respectively against $\epsilon L^{1/\nu}$. The values of the critical exponents are implemented as $1/\nu = 0.78$, $\beta/\nu = 0.18$ and $\gamma = 1.60$ the same as the whole system. Though there is not a good collapse of data, the plots come over each other reasonably.

The values of these critical exponents are reported in Table.3.1 and compared with those of the VM of monodispersed SPPs with velocity $v = 0.1$. The values of the exponents ($1/\nu = 0.62(12)$, $\beta/\nu = 0.275(5)$, and $\gamma/\nu = 1.45(2)$) for the VM with velocity $v = 0.1$ and density regime $\rho = 1/8$ to $3/4$ are taken from the Ref.[103]. The values of the critical exponents are very different from those of the VM. Though the nature of transition in the whole system as well as in the partial systems remains the same as that of the VM at low velocity, the critical exponents are different. The BM belongs to a new universality class.

Exponents	VM $v_0 = 0.1$	BM: $v_f = 30v_s$, $v_s = 0.01$	BM: $v_f = 50v_s$, $v_s = 0.01$
$1/\nu$	0.62(12)	0.78(9)	1.01(5)
β/ν	0.275(5)	0.18(1)	0.18(2)
γ/ν	1.45(2)	1.60(4)	1.60(8)
$\gamma/\nu + 2\beta/\nu$	2.00(3)	1.96(4)	1.96(8)

Table 3.1: Values of the critical exponents obtained for the BM at different velocities of fast-moving SPPs $v_f = 30v_s$ and $50v_s$ keeping $v_s = 0.01$. The exponents for the VM with $v_0 = 0.1$ (taken from Ref.[103]) are presented for comparison.

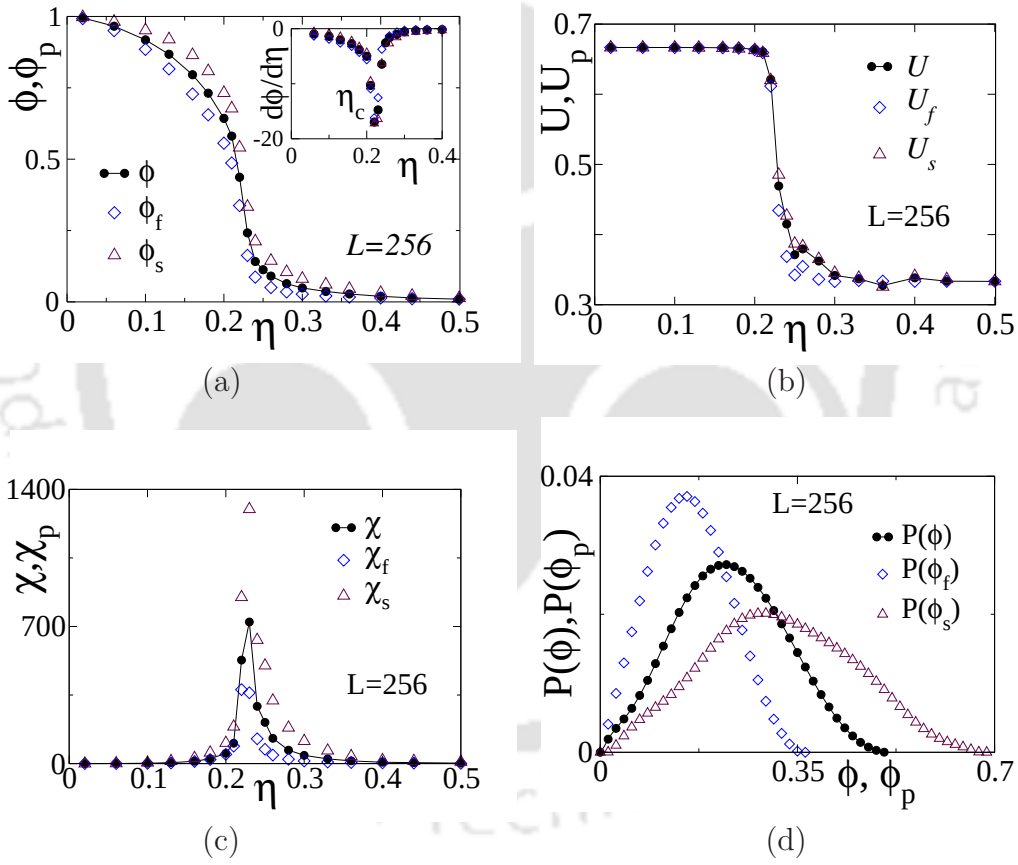

Figure 3.9: $v_f = 50v_s, v_s = 0.01$: (a) Plot of ϕ and ϕ_p versus η. Derivatives of ϕ and ϕ_p with respect to η are shown in the inset. (b) Plot of χ and χ_p versus η. (c) Plot of U and U_p versus η. (d) Plot of $P(\phi)$ and $P(\phi_p)$ at η_c. System size is $L = 256$.

3.2.4 Results with $v_f = 50v_s$ and $v_s = 0.01$

Variations of order parameter ϕ, Binder cumulant U, susceptibility χ and order parameter distribution $P(\phi)$ are presented in Fig.3.9 for velocities $v_f = 50v_s$ and

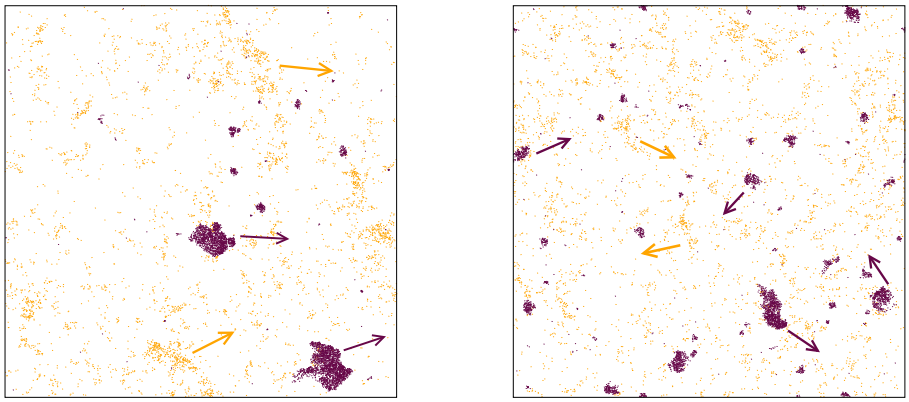

(a) (b)

Figure 3.10: $v_f = 50v_s, v_s = 0.01$: Morphology of the system of size $L = 128$ for (a) $\eta = 0.18$ and (b) $\eta = 0.26$. Orange and maroon colors represent the fast and slow-moving SPPs. The arrows represent the directions of motion.

$v_s = 0.01$ of the SPPs. The order parameter ϕ of the whole system and that of the partial systems ϕ_p are plotted against η in Fig.3.9(a). The values of ϕ and ϕ_p are decreasing smoothly to zero as η increases. The derivatives of ϕ and ϕ_p with respect to η are plotted in the inset of Fig.3.9(a) and minima of the plots at the transition noise $\eta_c \approx 0.22$ (same for the whole and partial systems) are observed. It can be noted that ϕ_f is also less than ϕ_s similar to that of $v_f = 30v_s$ situation. The respective fluctuations in order parameter, χ and χ_p are plotted against η in Fig.3.9(b). They diverge at $\eta_c \approx 0.22$ for all the SPPs. In this case also, the fluctuation at η_c is much higher for the slow-moving SPPs than the fast-moving SPPs. In Fig.3.9(c), U and U_p are plotted against η. Both U and U_p remain positive over the whole range of η. In Fig.3.9(d), the distribution of order parameters $P(\phi)$ and $P(\phi_p)$ are plotted at $\eta = \eta_c$. The distributions are unimodal. The positive Binder cumulants and unimodal distributions of order parameters indicate a continuous transition in the whole system as well as in the partial systems for the case of $v_f = 50v_s$ and $v_s = 0.01$. The phase transition occurs at η_c between the DS+DC phase and the RS+RC phase. The morphology of the DS+DC phase at $\eta = 0.18$ is shown in Fig.3.10(a) and that of the RS+RC phase at $\eta = 0.26$ is shown in Fig.3.10(b). It can be seen that the directed clusters of fast-moving SPPs and directed clumps of slow-moving SPPs are moving in the same direction in the ordered phase and the clusters of fast-moving SPPs and clumps of slow-moving SPPs are in random directions of motion in the disordered phase.

In the case of VM, it is known that the crossover system size $L^*(\rho_0, v_0)$ diverges

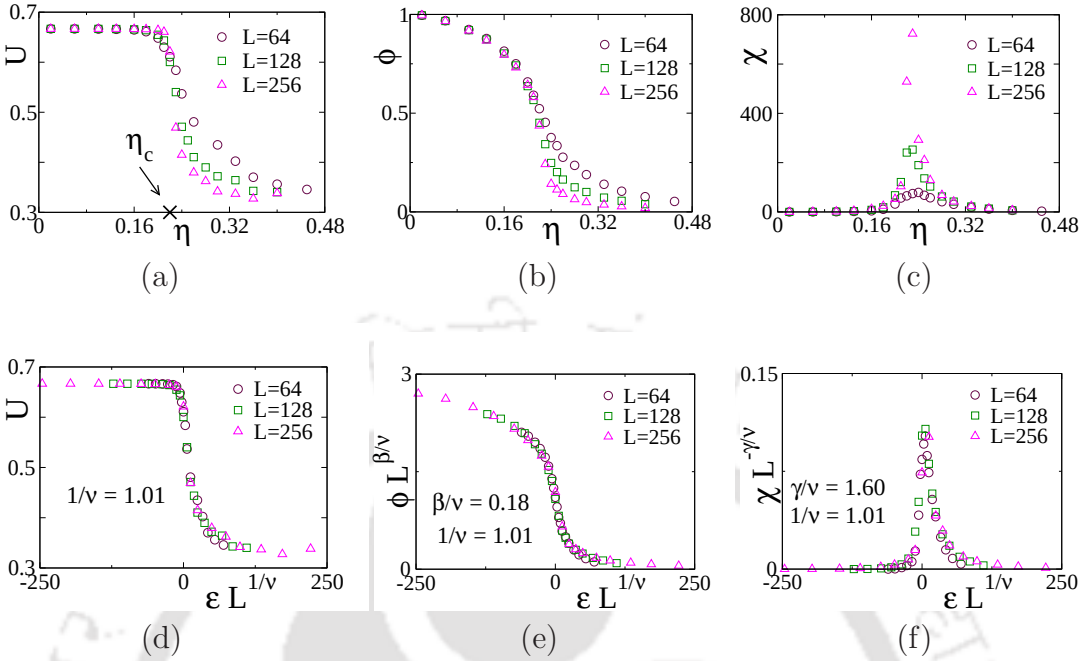

Figure 3.11: $v_f = 50v_s, v_s = 0.01$: (a) Plot of U versus η, (b) plot of ϕ versus η and (c) plot of χ versus η for $L = 64$, 128 and 256. The cross on the η-axis indicates η_c. (d) Plot of U versus the scaled noise $\epsilon L^{1/\nu}$. (e) Plot of $\phi L^{\beta/\nu}$ against $\epsilon L^{1/\nu}$. (f) Plot of $\chi L^{-\gamma/\nu}$ against $\epsilon L^{1/\nu}$. The values of the exponents are taken as $\beta/\nu = 0.18$, $\gamma/\nu = 1.60$ and $1/\nu = 1.01$.

for low velocities ($v_0 < 0.05$) and low density $\rho_0 (< 0.01)$. For the velocity $v_0 = 0.5$ and density $\rho_0 = 0.25$, it is known that $L^*(\rho_0, v_0) \approx 150$ [104]. However, in the BM, no such density bands of fast-moving SPPs with $v_f = 50v_s = 0.5$ occur when mixed with the slow-moving SPPs ($v_s = 0.01$) even at a system size $L = 256$ much higher than the crossover size L^*. It seems that slow-moving SPPs have a significant influence on the non-formation of travelling bands by the fast-moving SPPs as well as on the nature of the phase transition. It is interesting to observe that both types of SPPs maintain the same nature of phase transition in the BM.

Now we perform the FSS analysis in this case to extract the values of the critical exponents. The Binder cumulant U, the order parameter ϕ and the susceptibility χ are plotted against the angular noise η in Fig.3.11(a), (b) and (c) respectively for different system sizes $L = 64$, 128 and 256. The plots of U versus η in Fig.3.11(a) for different L intersect at $\eta_c \approx 0.22$, marked by a cross on the η-axis. The corresponding critical value of the cumulant is $U_c \approx 0.61$. As followed in the case of $v_f = 30v_s$, rough estimates of the exponents $1/\nu$, β/ν and γ/ν are obtained from the critical scaling relations $U'(\eta_c, L) \sim L^{1/\nu}$, $\phi(\eta_c, L) \sim L^{-\beta/\nu}$ and $\chi(\eta_c, L) \sim L^{\gamma/\nu}$.

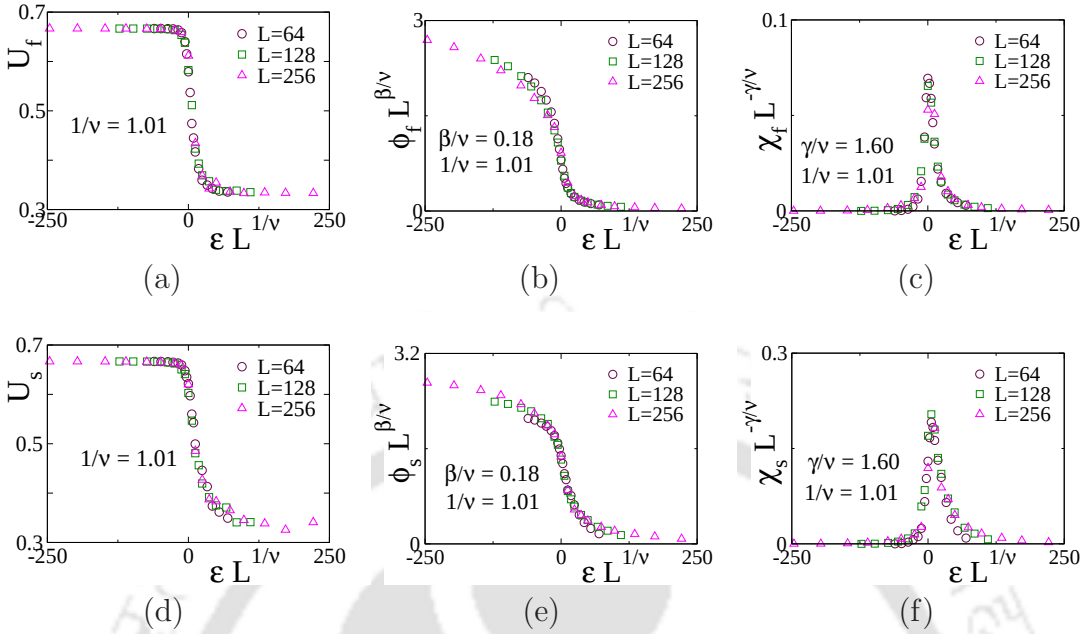

Figure 3.12: $v_f = 50v_s, v_s = 0.01$: Plot of (a) U_f, (b) $\phi_f L^{\beta/\nu}$ and (c) $\chi_f L^{-\gamma/\nu}$ versus the scaled noise $\epsilon L^{1/\nu}$ for fast SPPs. Plot of (d) U_s, (e) $\phi_s L^{\beta/\nu}$ and (f) $\chi_s L^{-\gamma/\nu}$ versus $\epsilon L^{1/\nu}$ for slow SPPs. Critical exponents are kept same as the Fig.3.11.

The best possible FSS form of the scaled parameters against the scaled noise $\epsilon L^{1/\nu}$ are obtained tuning these exponents further. The Binder cumulant U, the scaled order parameter $\phi L^{\beta/\nu}$, and the scaled susceptibility $\chi L^{-\gamma/\nu}$ are plotted against $\epsilon L^{1/\nu}$ in Fig.3.11(d), (e) and (f) respectively. A reasonable collapse of data in all three cases are obtained tuning the rough estimates of exponents further to $1/\nu = 1.01$, $\beta/\nu = 0.18$ and $\gamma/\nu = 1.60$. The exponents satisfy the scaling relation $\gamma/\nu + 2\beta/\nu = 2$ within error bars.

Similarly, in Fig.3.12(a),(b) and (c), U_f, $\phi_f L^{\beta/\nu}$ and $\chi_f L^{-\gamma/\nu}$ are plotted respectively against $\epsilon L^{1/\nu}$. Whereas, in Fig.3.12(e),(f) and (g), U_s, $\phi_s L^{\beta/\nu}$ and $\chi_s L^{-\gamma/\nu}$ are plotted respectively against $\epsilon L^{1/\nu}$. The values of the critical exponents are implemented as $1/\nu = 1.01$, $\beta/\nu = 0.18$ and $\gamma = 1.60$ same as the whole system. Though there is not a good collapse of data, the plots come over each other reasonably.

The values of the critical exponents are reported in Table.3.1 and compared with the others. Though the ratio of exponents β/ν and γ/ν are the same for $v_f = 30v_s$ and $v_f = 50v_s$ situations, the absolute values of β and γ are different as the correlation length exponent is different for these two situations. The value of ν has decreased as the value of v_f is increased. As a consequence, the values of the exponents β and γ are also decreasing. The critical exponents for the BM are very

different from that of the VM. The BM, therefore, belongs to a new universality class than the VM. Moreover, as the critical exponents for $v_f = 50v_s$ case are different from the $v_f = 30v_s$ case, the universality class of BM is v_f dependent for a fixed v_s. Hence, the binary model is non-universal.

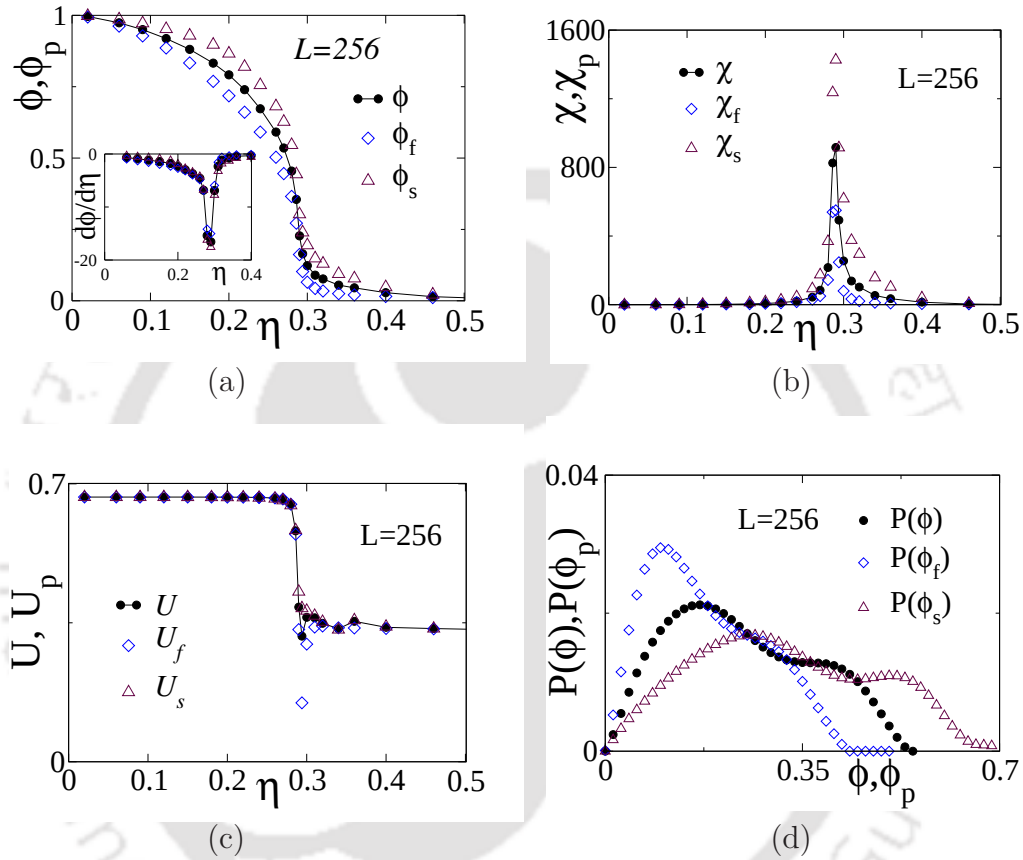

Figure 3.13: $v_f = 100v_s, v_s = 0.01$: (a) Plot of ϕ and ϕ_p versus η. Derivatives of ϕ and ϕ_p with respect to η are shown in the inset. (b) Plot of χ and χ_p versus η. (c) Plot of U and U_p versus η. (d) Plot of $P(\phi)$ and $P(\phi_p)$ at η_c. System size is $L = 256$.

3.2.5 Results with $v_f = 100v_s$ and $v_s = 0.01$

Variations of order parameter ϕ, Binder cumulant U, susceptibility χ and order parameter distribution $P(\phi)$ are presented in Fig.3.13(a), (b), (c) and (d) respectively for velocities $v_f = 100v_s$ and $v_s = 0.01$. ϕ and ϕ_s against angular noise η are also shown in Fig.3.13(a) and from the dip in the derivatives (inset) $\eta_c \approx 0.29$. From the peak of χ and chi_p, same η_c is also observed. The Binder cumulants U and U_p versus η plots is shown in Fig.3.13(c). U_f and U has a dip at the transition (still not negative), whereas U_s has no such minimum for the slow SPPs at the transition re-

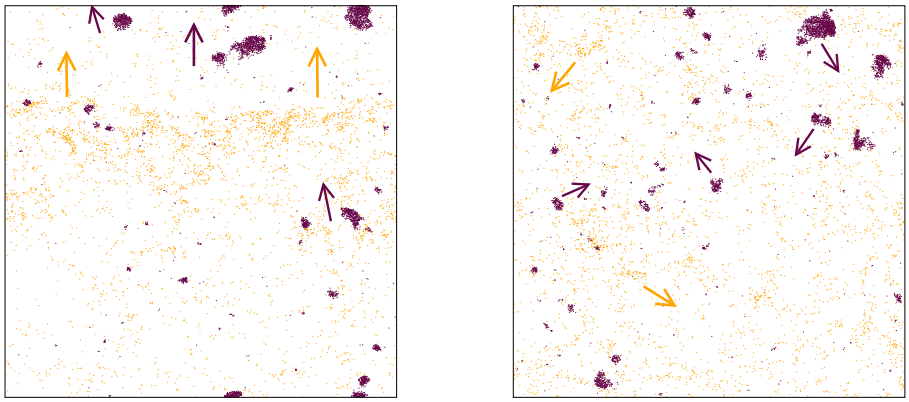

(a) (b)

Figure 3.14: $v_f = 100v_s, v_s = 0.01$: Morphology plot for (a) $\eta = 0.26$ and (b) $\eta = 0.32$ with system size $L = 128$. Orange and maroon colours represent the fast and slow-moving SPPs.

gion. The distribution of order parameter at η_c is also shown in Fig.3.13(d). In this case, $P(\phi)$ and $P(\phi_p)$ does not show unimodal distribution. It seems that, in case of $v_f = 100v_s$ ($v_s = 0.01$), the order parameter distribution deviates from the unimodal distribution. The system morphology is shown for $\eta = 0.26$ and $\eta = 0.32$ on a system of size $L = 128$ in Fig.3.14(a) and (b). In this case, a dense travelling band of fast-moving SPPs start appearing in the system near the transition $\eta \leq \eta_c$ with the directed clusters (DC) of slow-moving SPPs (Fig.3.14(a)). Whereas, for $\eta > \eta_c$, random clusters of fast-moving and random clumps of slow-moving SPPs, RS+RC phase occurs in the system. These are indications for a crossover to discontinuous transition from a continuous transition regime.

3.2.6 Results with $v_f = 150v_s$ and $v_s = 0.01$

The situation will be more dramatic if the value of v_f is increased further. We now present simulation results obtained for much higher velocity of the fast-moving SPPs $v_f = 150v_s$ keping the velocity of the slow-moving SPPs as $v_s = 0.01$. The order parameter of the whole system and the partial systems, ϕ and ϕ_p are plotted against η in Fig.3.15(a). There are jumps in the values of ϕ and ϕ_p near the transition. The derivatives of ϕ and ϕ_p with respect to η are plotted in the inset of Fig.3.15(a) and sharp minima are observed at $\eta_c \approx 0.33$ (same for the whole and the partial systems). The respective fluctuations in order parameter, χ and χ_p are plotted against η in Fig.3.15(b). There is a sharp peak in the fluctuations at $\eta_c \approx 0.33$ for all the order parameters. In the inset of Fig.3.15(b), the scaled

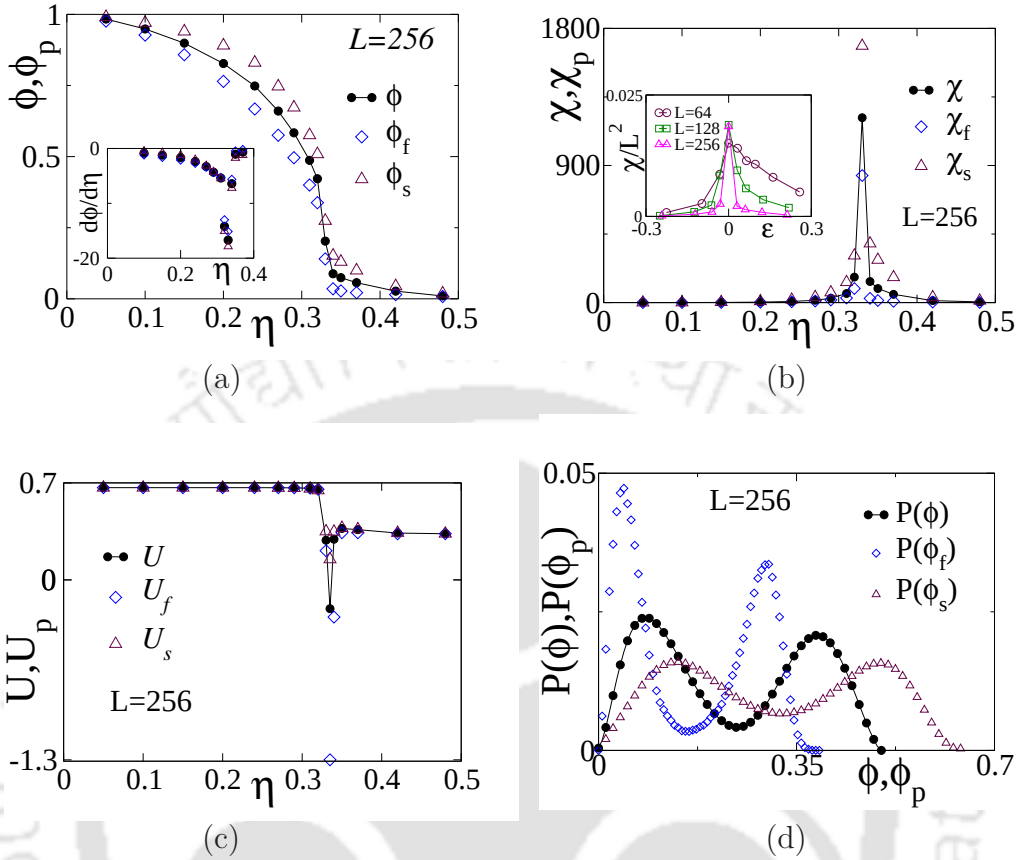

Figure 3.15: $v_f = 150v_s, v_s = 0.01$: (a) Plot of ϕ and ϕ_p versus η. Derivatives of ϕ and ϕ_p with respect to η are shown in the inset. (b) Plot of χ and χ_p versus η. In the inset, χL^{-2} is plotted against ϵ for $L = 64$, $L = 128$ and $L = 256$. (c) Plot of U and U_p versus η. (d) Plot of $P(\phi)$ and $P(\phi_p)$ at η_c.

fluctuations χL^{-2} are plotted against ϵ for different systems of sizes $L = 64$, 128 and 256. The critical values (or pick values) of scaled χ become almost L independent. Hence, $\chi \sim L^2$, as in the case of a discontinuous transition. The Binder cumulants U and U_p versus η plots are shown in Fig.3.15(c). The cumulant for the fast-moving SPPs, U_f and that of the whole system U have sharp negative dips at the transition. However, the cumulant of the slow-moving SPPs (U_s) has a dip at the transition point but has yet to achieve a negative value. The distributions of order parameters $P(\phi)$ and $P(\phi_p)$ at $\eta = \eta_c$ are shown in Fig.3.15(d). In this case, all three distributions $P(\phi)$, $P(\phi_f)$ and $P(\phi_s)$ exhibit bimodal distributions which implies the two-phase co-existence in the system. These are characteristic features of a discontinuous transition. Discontinuous transition is known to occur in the VM with monodispersed SPPs at high velocities [104]. At the transition region of the

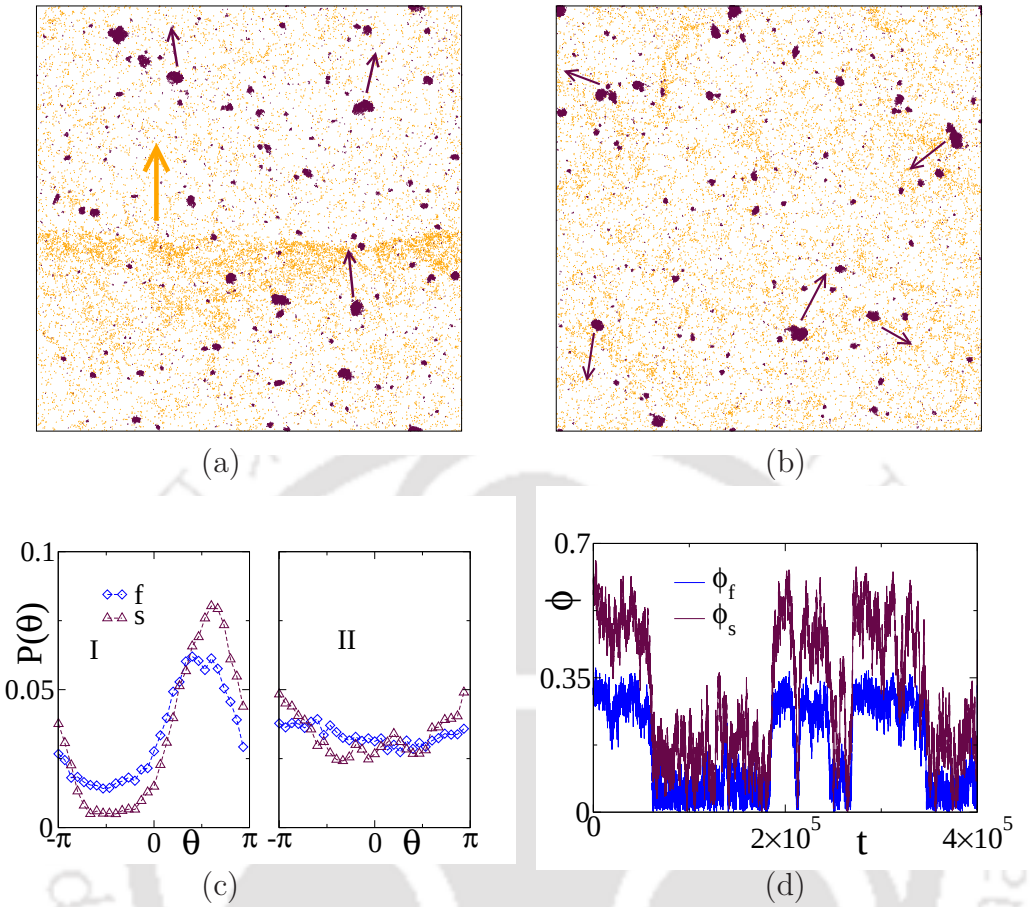

Figure 3.16: $v_f = 150v_s, v_s = 0.01$: Morphology at (a) $t = 3 \times 10^5$ and (b) $t = 4 \times 10^5$ for $\eta_c = 0.33$ on a system of size $L = 256$. Orange and maroon colors represent the fast and slow-moving SPPs. (c) $P(\theta)$ of the morphology (a) and (b) are plotted in I and II. (d) Order-parameter dynamics at η_c.

VM, dense travelling bands of SPPs form and disappear, resulting in the coexistence of two phases in the system. It is then important to verify whether this is the case for the fast-moving SPPs here or not. More interestingly, what are the two phases going to be for the slow-moving SPPs? Below we explain the situation by studying the time evolution of the system morphology at the transition region.

The morphology of a system of size $L = 256$ at two different time instants 3×10^5 and 4×10^5 are shown in Fig.3.16(a) and Fig.3.16(b) respectively for $\eta = \eta_c$. In Fig.3.16(a), a dense travelling band of the fast-moving SPPs and clumps of slow-moving SPPs are seen. Interestingly, the band and clumps are moving in the same direction, as indicated by the orange and maroon arrows, respectively. However, in Fig.3.16(b), the dense travelling band of fast-moving SPPs disappears, and the clumps of slow-moving SPPs start moving randomly in the system. It seems as soon

as the fast-moving SPPs form the dense travelling band, they take over the whole system and force the clumps of the slow-moving SPPs to follow their direction of motion. The corresponding orientation distributions $P(\theta)$ for both the SPPs are shown in Fig.3.16(c)-I and Fig.3.16(c)-II respectively. In Fig.3.16(c)-I, $P(\theta)$ of both the SPPs are peaked at a particular θ. Thus, the slow-moving SPPs follow the direction of motion of the travelling band of the fast-moving SPPs. Whereas, in Fig.3.16(c)-II, the distributions $P(\theta)$ for both the SPPs are flat. Hence, the clumps of slow-moving SPPs and the clusters of fast-moving SPPs move randomly. The steady-state dynamics at $\eta = \eta_c$ of the order parameters are given in Fig.3.16(d) where the values of both ϕ_f (blue) and ϕ_s (maroon) oscillate between two phases in a synchronized manner. The higher value of ϕ_f corresponds to the presence of the travelling band (an ordered phase) and the lower value of ϕ_f corresponds to the disappearance of the travelling band (a random or disordered phase). On the other hand, the higher value of ϕ_s corresponds to the ordered phase of directed clumps (DC) of slow-moving SPPs, and the lower value of ϕ_s corresponds to a disordered phase of randomly moving clumps (RC) of slow-moving SPPs. This is very different from the scenarios in the previous cases with $v_f = 30v_s$ and $v_f = 50v_s$. In those cases, a smooth continuous transition from the DS+DC phase to the RS+RC phase used to occur. The presence of a dense travelling band of fast-moving SPPs at much higher v_f does not allow the slow-moving SPPs to undergo a continuous transition from DC to RC. Rather, the change of phase of the slow-moving SPPs from DC to RC is in synchronization with the appearance and disappearance of the density band of fast-moving SPPs.

It is intriguing that in a binary system, both the fast-moving and slow-moving SPPs undergo continuous transition at low-velocity ratios, whereas they both undergo discontinuous transition at high-velocity ratios. A crossover from continuous to discontinuous transition is expected at an intermediate velocity ratio. It has been observed that the order parameter distribution starts deviating from the unimodal distribution and the dense travelling band of fast-moving SPPs starts appearing in the system in the case of $v_f = 100v_s$ ($v_s = 0.01$). It is interesting to note that for a given velocity ratio, the two different SPPs are not able to undergo two different types of transitions, continuous or discontinuous, simultaneously in this binary system because of the local inter-particle interaction.

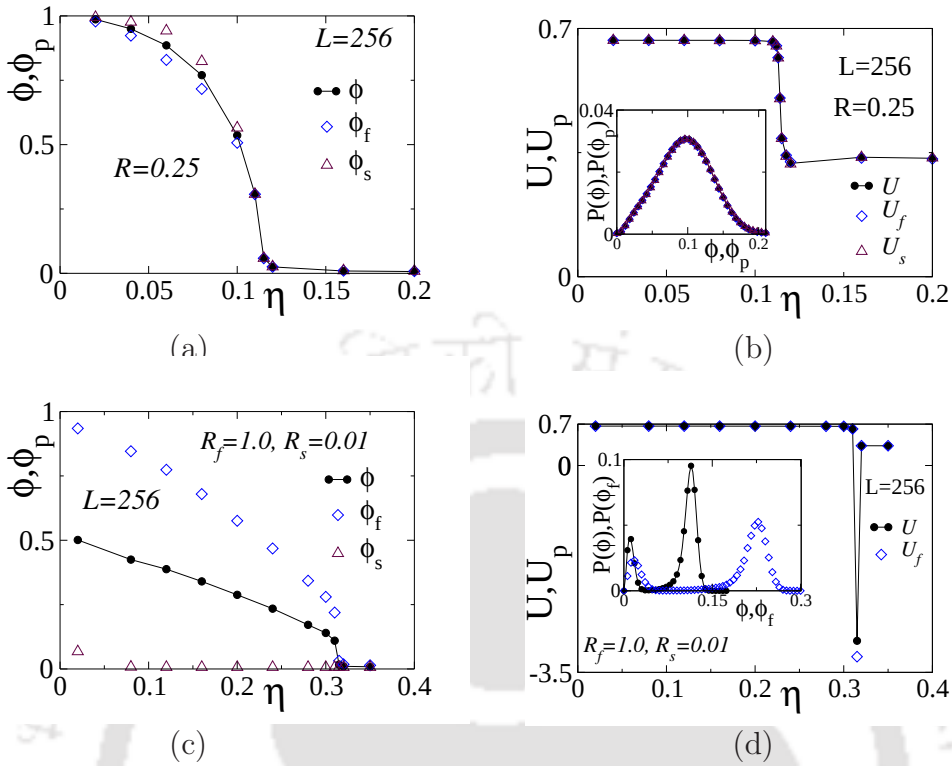

Figure 3.17: $v_f = 150v_s, v_s = 0.01$: Plot of (a) ϕ and ϕ_p, (b) U and U_p versus η for $R = 0.25$. In the inset of (b), $P(\phi)$ and $P(\phi_p)$ at η_c are plotted. Plot of (c) ϕ and ϕ_p, (d) U and U_f versus η for $R_f = 1.0$ and $R_s = 0.01$. In the inset of (d), $P(\phi)$ and $P(\phi_f)$ at η_c are plotted. System size is $L = 256$.

3.2.6.1 Effect of interaction radius R

The value of R essentially determines the number of neighbours (n) to interact for an SPP at every move. So n increases as R increases and vice versa. So far, the interaction radius R for both the SPPs was set to 1. It is important to know the effect of interaction radius R on the system with high velocity ratio $v_f = 150v_s$ among two SPPs. First, we investigate reducing the interaction radius to $R = 0.25$ for both the SPPs. The order parameters (ϕ and ϕ_p) and the Binder cumulants (U and U_p) are plotted against η in Fig.3.17(a) and Fig.3.17(b) respectively. It can be seen that all the order parameters continuously go to zero at a critical noise $\eta_c \approx 0.11$, which is much less than the $\eta_c = 0.33$ with $R = 1.0$. Such a behaviour is also observed in the monodispersed case [145]. Moreover, the Binder cumulants U, U_f, and U_s are all found to be positive. In the inset of Fig.3.17(b), $P(\phi)$ and $P(\phi_p)$ are plotted at η_c and all the three distributions are unimodal. Thus the discontinuous transition for $R = 1.0$ becomes continuous for $R = 0.25$ for both the SPPs with $v_f = 150v_s$. Because of the reduced interaction region, very few SPPs participate in providing

a global orientation to a particular SPP. The feedback provided by the fast-moving SPPs to a distant point also becomes weak. As a result, the density band could not form in the system, and the external noise is able to break the ordering in a continuous fashion for both the SPPs.

As a second case, we study the same system with different interaction radii for two types of SPPs. Two different radii are taken as $R_f = 1.0$ and $R_s = 0.01$ for the fast and slow-moving SPPs respectively. The order parameter ϕ and ϕ_p are plotted against η in Fig.3.17(c). The order parameter ϕ_f is suddenly going to zero at $\eta_c \approx 0.32$, almost at the same η_c with $R_f = R_s = 1.0$. Due to the extremely small interaction radius, the slow-moving SPPs have almost no one to interact with and could not form any order state ($\phi_s \approx 0$) even at low noise. Hence, no transition is observed in ϕ_s. The total order parameter ϕ, however, shows a transition. In Fig.3.17(d), the Binder cumulants, U and U_f are plotted against η. It can be seen that the values of U_f and U both have sharp negative dips at the transition. In the inset of Fig.3.17(d), $P(\phi)$ and $P(\phi_f)$ at η_c are plotted, and both are found bimodal. Thus the fast-moving SPPs retain their characteristics of discontinuous transition with $R = 1$ at high velocity $v_f = 150v_s$.

Density ρ can also be a parameter to study this system. The results presented above are for a fixed density $\rho = 0.5$. However, at higher densities, the traveling density bands may appear at lower velocities. Thus, one expects discontinuous transitions to occur for lower velocity regimes at higher densities. Such systems are computationally expensive as it involves a large number of interacting particles.

3.3 Summary and Discussion

The collective behaviour of the BM has revealed a number of interesting properties. A variety of phase-separated collective patterns such as directed lanes, clusters, clumps, micro-cluster, micro-clumps, etc., appeared in the system. Such phase segregation and cluster formations occur due to the huge difference in velocities as well as in diffusivity of the two SPPs in the system. The system exhibits a continuous order-disorder transition from DS+DC to RS+RC at a critical noise η_c for $v_f = 30v_s$ and $50v_s$ with $v_s = 0.01$ with a new set of critical exponents. The critical exponents are not only different from those of the VM but also depend on v_f. Though the continuous transition of the slow-moving SPPs is expected, it was quite unexpected for the fast-moving SPPs with $v_f = 50v_s = 0.5$ as the VM exhibits a discontinuous transition at $v_0 = 0.5$ on a system of size $L = 256$. Thus the slow-moving SPPs

induce the moderately fast-moving SPPs to manifest a similar behaviour. At a high velocity ratio ($v_f = 150v_s$), interestingly both the SPPs exhibit discontinuous order-disorder transitions. In this discontinuous transition, the fast-moving SPPs coexist between the phase with a travelling band and no travelling band, while the slow-moving SPPs coexist between the DC and RC phases. The travelling bands and DCs appear simultaneously and move in the same direction. It seems that the presence of the inter-particle interaction causes such phase synchronization. Both continuous and discontinuous transitions do not occur simultaneously for two types of SPPs in the system. It seems crossover from continuous to discontinuous transition will occur at velocity ratio $v_f \approx 100v_s$ for $v_s = 0.01$. The nature of transitions and the value of critical noise is expected to vary with the interaction radius and density.

Chapter 4

Effect of orientation adapters on the collective dynamics of self-propelled particles

The effect of orientation adapters on the collective behaviour of SPPs is a crucial aspect to study in the context of the Vicsek Model (VM). The orientation adapters are the species that adapt their direction of motion from other SPPs. In this model, adapter SPPs exist besides the usual SPPs in equal proportion. The adapter SPPs do not interact among themselves but adopt the velocity orientation of the usual SPPs through local interactions. However, the usual SPPs do interact with themselves as well as with the adapters. A mixture of SPPs with different properties and their collective behaviour is studied in different systems such as a mixture of active and passive particles [55, 161], a mixture of SPPs with opposite rotation [77, 166], mixture of SPPs with different sizes [159] and others [164, 165, 173]. Various self-organised coherent patterns, phase segregation, and other nontrivial behaviours have been observed in such mixed systems [40, 157]. However, the study mixture of species with different interaction properties in the polar SPPs is a relatively new area of research.

This chapter implements a model where the two types SPPs are different by their alignment interaction rules. Moreover, their velocities will be dissimilar. The adapters induce nontrivial collective behaviour in the system. The orientational order-disorder phase transition will be studied by performing extensive computer simulations. This chapter has two parts. In part-I, the adapters' velocity is much smaller than the velocity of usual SPPs. The collective behaviour is studied by constructing an appropriate model. In part-II, the adapters move with higher velocity

than the usual SPPs. The previous model is suitably modified for this situation and studied extensively.

Part-I

4.1 The Model

A mixture of usual SPPs with adapter SPPs is modelled over a two-dimensional square box of linear size L with periodic boundary conditions. The usual SPPs move with a velocity v_0, and the adapter SPPs move with velocity v_a. In this case, they have widely different velocities as $v_0 \gg v_a$ where the velocity of the adapters v_a is fixed to a low value. They are taken in equal proportion. If N_0 is the number of usual SPPs and N_a is the number of adapters, then $N_0 = N_a = N/2$ where N is the total number of SPPs in the system. Initially, the position $\vec{r}_{p,i}$, $i = 1, 2, 3, \cdots, N/2$ of all the SPPs are randomly distributed over the space where $p \in \{0, a\}$. The initial orientation $\theta_{p,i}$ of an SPP is randomly selected in the range $-\pi$ to π, irrespective of their type. The usual SPPs interact within a local neighbourhood $R = 1$ and determine their average orientation. Whereas an adapter only interacts with usual SPPs within the local neighbourhood $R = 1$ and determine their average orientation. The distribution of randomly oriented 25 usual SPPs (in orange) and 25 adapters (in indigo) are shown in Fig.4.1. Longer and shorter arrows show the velocities v_0 and v_a, respectively.

The time evolution of the orientation $\theta_{0,i}$ of an usual SPP is determined by

$$\theta_{0,i}(t + \Delta t) = \langle \theta(t) \rangle_{R \in \{0,a\}} + \Delta\theta \tag{4.1}$$

Where, The interaction term $\langle \cdots \rangle_{R \in \{0,a\}}$ for usual SPPs includes both the usual SPPs (0) and the adapters (a) within the radius R. Whereas, time evolution of the orientation $\theta_{a,i}$ of an adapter SPP is determined by

$$\theta_{a,i}(t + \Delta t) = \langle \theta(t) \rangle_{R \in \{0\}} + \Delta\theta \tag{4.2}$$

where, the interaction term $\langle \cdots \rangle_{R \in \{0\}}$ for adapters only includes the usual SPPs within the radius R. It should be noted that the magnitude of velocity of individual SPPs are igonred and only the orientations are taken into account in estimating $\langle \theta(t) \rangle_R$ for both the usual SPPs and the adapters. Here, $\Delta\theta$ is a random orientation

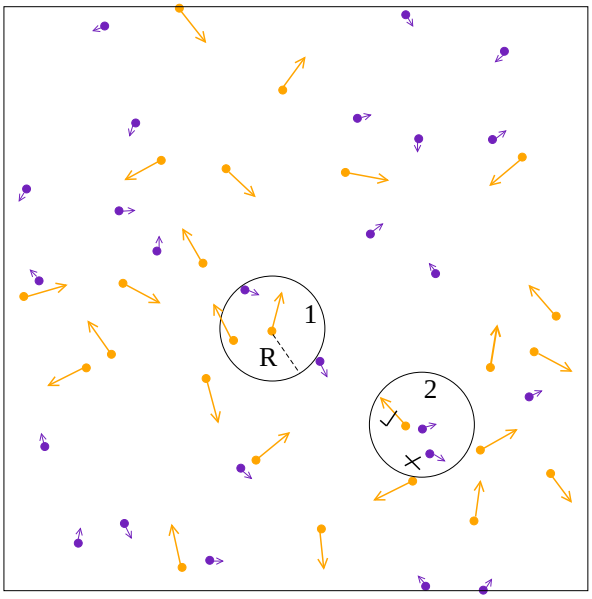

Figure 4.1: The distribution of the SPPs is shown on a square box of size $L = 10$ where $N_0 = N_a = 25$. The orange colour represents usual SPPs and the indigo colour represents the adapters. The arrow associated with an SPP indicates its orientation and here $v_0 > v_a$. An usual SPP present at the center of circle-1 interacts with both SPPs present within the circle of radius R. Whereas, an adapter SPP at the center of circle-2 interacts only with usual SPPs present within the circle of radius R.

chosen with a uniform probability from the interval $[-\eta\pi, +\eta\pi]$. The strength of the angular noise η varies from 0 to 1 and act as a control parameter. After averaging, an SPP of type-p ($p \in \{0, a\}$) at the position $\vec{r}_{p,i}$ is thus moving with a speed v_p in the direction $\theta_{p,i}$. Knowing the velocity $\vec{v}_{p,i}(t)$ at every time step, the position of the ith SPP $\vec{r}_{p,i}$ is updated following the forward update rules as given below

$$\vec{r}_{0,i}(t + \Delta t) = \vec{r}_{0,i}(t) + \vec{v}_{0,i}(t)\Delta t \tag{4.3}$$

$$\vec{r}_{a,i}(t + \Delta t) = \vec{r}_{a,i}(t) + \vec{v}_{a,i}(t)\Delta t \tag{4.4}$$

where Δt is the time between two successive updates, and it is chosen as $\Delta t = 1$. The linked cell-list algorithm as discussed in chapter-2 is used to keep track of time varying neighbour list. Eqs.4.1, 4.2, 4.3 and 4.4 are then evolved with time and dynamical properties of the model are studied varying η for different velocity ranges.

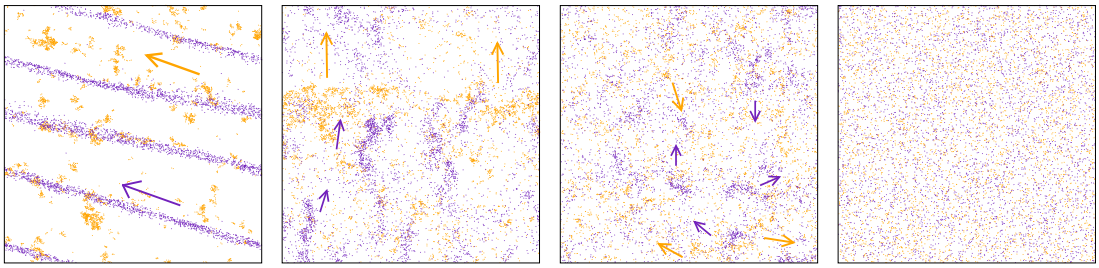

(a) $\eta = 0.01$ (b) $\eta = 0.20$ (c) $\eta = 0.32$ (d) $\eta = 0.60$

Figure 4.2: $v_0 \gg v_a$: Morphologies of the system of SPPs with $v_0 = 50v_a$ and $v_a = 0.01$ for different angular noise (a) $\eta = 0.01$, (b) $\eta = 0.20$, (c) $\eta = 0.32$ and (d) $\eta = 0.60$ for a system of size L = 128. Orange colour represents usual SPPs and indigo colour represents the adapters.

4.2 Results and Discussion

Throughout the simulation, both types of SPPs are kept in the same proportion as $N_0 = N_a = N/2$. The overall particle density is fixed as $\rho = N/L^2 = 0.5$ for all the observations. One Monte Carlo (MC) time step corresponds to the up-gradation of position and orientation of all the particles. Initial 7×10^5 MC steps are neglected to achieve the steady-state. An ensemble of size 48×10^5 is taken for statistical averages (2×10^5 samples at different times for 24 different initial configurations). First, the results are shown with the velocity of the usual SPPs as $v_0 = 50v_a$ for a fixed velocity of adaptors $v_a = 0.01$.

4.2.1 Results with $v_0 = 50v_a$ and $v_a = 0.01$

First, we present the morphologies of the system with $v_0 = 50v_a$ and $v_a = 0.01$ at different angular noise η on a system of size $L = 128$ in Fig.4.2. SPPs are represented by two different colours: orange for the fast-moving usual SPPs ($v_0 = 50v_b$) and indigo for the slow-moving adapters ($v_a = 0.01$). A variety of patterns appear as the noise parameter η changes from a smaller value to a larger one. For a low angular noise $\eta = 0.01$, it is observed in Fig.4.2(a) that the usual SPPs form clusters and they move in a particular direction (indicated by the orange arrow). On the other hand, the adapters are moving on a narrow lane in the same direction (indicated by the indigo arrow) as the clusters of the usual SPPs. These directed lanes (DL) and directed clusters (DS) are similar to the BM studied in the last chapter. It seems that the motion of the usual SPPs guides the motion of the adapters. Dense band

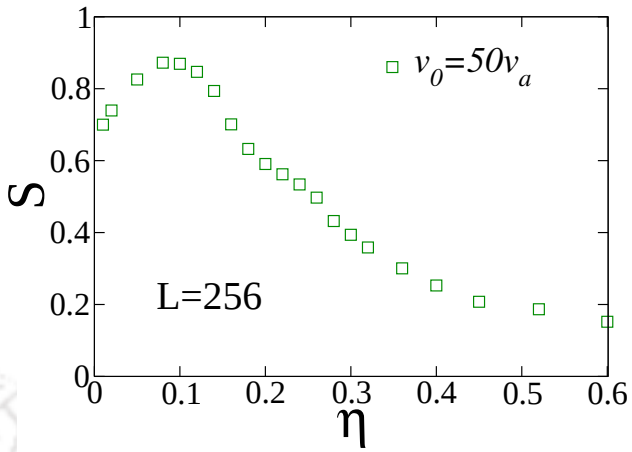

Figure 4.3: $v_0 \gg v_a$: Plot of the segregation coefficient S versus η for $v_0 = 50v_a$ with $v_a = 0.01$ for a system of size $L = 256$.

patterns by the usual SPPs are formed near $\eta = 0.20$. Density bands are known to occur in the VM for this velocity of the usual SPPs [104, 172]. Whereas adapters form elongated clusters which are scattered in the space. The system morphology is shown in Fig.4.2(b) for $\eta = 0.20$. Both the SPPs are moving in the same direction as the inter-particle interaction is present. Further increase of noise to $\eta = 0.32$ induces random motion to both the SPPs shown in Fig.4.2(c). Between these two phases shown in Fig.4.2(b) and (c) an orientational order-disorder transition occurs. For relatively high $\eta = 0.60$ shown in Fig.4.2(d), a homogeneous gas-like mixture is observed.

With different values of angular noise η, phase-separated collective patterns are observed in this system. Segregation coefficient [77, 170] is calculated to measure the demixing. The square box of area L^2 is divided into Q square sub-regions of linear size l and area L^2/Q each. The segregation coefficient is defined as

$$S = \frac{1}{N} \sum_{j=1}^{Q} |n_{0j} - n_{aj}| \tag{4.5}$$

where j is the index for the sub-regions, n_0 and n_a are the number of the usual SPPs and adapters respectively in the sub-region area. The coefficient S is measured taking $l = 8$, similar to the length scale of the average cluster size near the transition. The value $S = 1$ represents a fully demixed or phase-separated pattern, whereas it is low for mixed structures. The variation of the coefficient S at different η values are shown in Fig.4.3. The coefficient S is higher at the low η region, whereas decreases

with the increase of η, as expected. Such phase separation was also observed in the last chapter. It seems that as the species have widely different velocities, according to their position update rules, they cannot be synchronised to the other types to be part of the common flocks, and hence they show segregated patterns.

Now, we present the results of the orientational order-disorder phase transition for this model. Variations of order parameter ϕ, Binder cumulant U, susceptibility χ and order parameter distribution $P(\phi)$ are presented in Fig.4.4 for velocities $v_0 = 50v_a$ and $v_a = 0.01$ for a system of size $L = 256$. We analyze the data for the whole system, considering both types of SPPs together as well as the partial systems involving only one type of SPPs. The order parameter of the transition ϕ for the whole system is defined as

$$\phi(\eta, L) = \frac{1}{N}\left|\sum_{p}\sum_{i=1}^{N_p}\frac{\vec{v}_{p,i}}{|\vec{v}_{p,i}|}\right| \tag{4.6}$$

where N is the total number of SPPs. The partial order-parameter of the transition ϕ_p for the p-type SPPs is defined as

$$\phi_p(\eta, L) = \frac{1}{N_p}\left|\sum_{i=1}^{N_p}\frac{\vec{v}_{p,i}}{|\vec{v}_{p,i}|}\right| \tag{4.7}$$

where N_p is the number of p-type ($p \in \{0, a\}$) SPPs. The order parameter ϕ of the whole system and that of the partial systems ϕ_p are plotted against η in Fig.4.4(a). The system undergoes an order-disorder transition with the variation of η. In this model, the value of the order parameter of the usual SPPs (ϕ_0) is higher than the order parameter of the adapters (ϕ_a). It is expected as the adapters do not interact among themselves and have low-velocity [145]. The derivatives of ϕ and ϕ_p with respect to η are plotted in the inset of Fig.4.4(a) and minima of the plots at the transition noise $\eta_c \approx 0.27$ are observed for systems with the usual SPPs as well as for the whole system. Whereas, for the adapters, minima observed at $\eta \approx 0.16$.

The susceptibility χ for the whole system and that of the partial systems χ_p can be estimated from the fluctuation in their respective order parameters ϕ and ϕ_p as

$$\chi = L^2\left[\langle\phi^2\rangle - \langle\phi\rangle^2\right], \quad \chi_p = L^2\left[\langle\phi_p^2\rangle - \langle\phi_p\rangle^2\right] \tag{4.8}$$

where $\langle\phi^n\rangle = \int \phi^n P(\phi)d\phi$, $\langle\phi_p^n\rangle = \int \phi_p^n P(\phi_p)d\phi_p$, $P(\phi)$ and $P(\phi_p)$ are the distribution functions of ϕ and ϕ_p respectively. The respective fluctuations in order

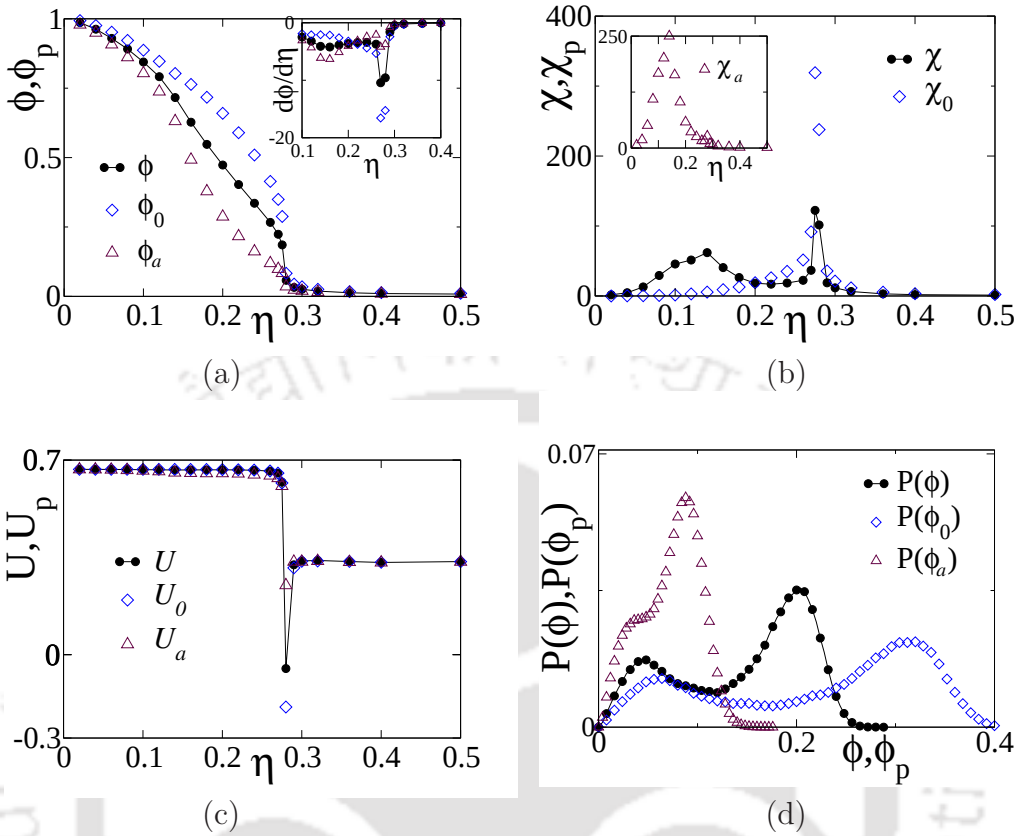

Figure 4.4: For $v_0 = 50v_a$, $v_a = 0.01$: (a) Plot of ϕ and ϕ_p versus η. Derivatives of ϕ and ϕ_p with respect to η are shown in the inset. (b) Plot of χ and χ_p versus η. In the inset χ_a versus η is shown. (c) Plot of U and U_p versus η. (d) Plot of $P(\phi)$ and $P(\phi_p)$ at $\eta = \eta_c$. System size is $L = 256$.

parameter, χ and χ_p are plotted against η in Fig.4.4(b). They diverge at $\eta_c \approx 0.27$ for the usual SPPs as well as for the whole system. Whereas, χ_a has a higher peak near $\eta \approx 0.16$ and comparatively lower peak at $\eta \approx 0.27$. In the inset, χ_a versus η is shown. There is an increase of χ also, near $\eta \approx 0.16$ region, which seems to be affected by χ_a. Similarly, the fourth-order Binder cumulant for the whole system and that of the partial systems are defined as,

$$U = 1 - \frac{\langle \phi^4 \rangle}{3\langle \phi^2 \rangle^2}, \quad U_p = 1 - \frac{\langle \phi_p^4 \rangle}{3\langle \phi_p^2 \rangle^2} \tag{4.9}$$

where the higher order averages are obtained following the definitions of $\langle \phi^n \rangle$ and $\langle \phi_p^n \rangle$ given above. In Fig.4.4(c), the Binder cumulants U and U_p are plotted against the angular noise η. Both U and U_0 is negative at transition, which implies a first-order phase transition. However, the cumulant U_a has a dip at the transition

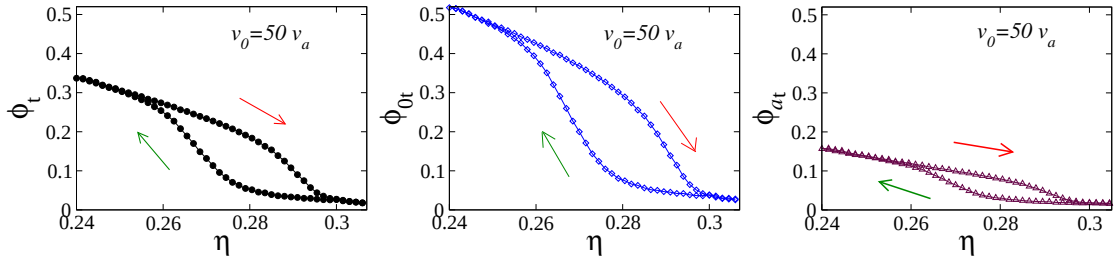

Figure 4.5: For $v_0 = 50v_a$, $v_a = 0.01$: Hysteresis plot (a) for the whole system, (b) for usual SPPs and (c) for adapters, in the variation of the respective instantaneous order parameters with η. Results obtained by implementing ramp-up or forward (red arrow) and ramp-down or backward (green arrow) simulation schemes, respectively.

point but with a positive value. In Fig.4.4(d), the distribution of order parameters $P(\phi)$ and $P(\phi_p)$ are plotted at $\eta_c = 0.27$. The distributions are bimodal for $P(\phi_0)$ and $P(\phi)$ as expected in a discontinuous phase transition. These are characteristic features of a discontinuous transition. Discontinuous transition is known to occur in the VM at high velocities [104]. Whereas, $P(\phi_a)$ also shows bimodal nature; however, the peaks are close to each other. It seems that the usual SPPs has a strong effect on the adapters.

Hysteresis study: It is well known that the hysteresis phenomena usually accompany the first-order phase transition [104, 174, 175] which occurs near the transition. New simulations are carried out to measure the instantaneous order parameter (ϕ_t) by either gradually increasing or decreasing the angular noise η with a fixed ramp rate, where each previous state will be implemented as the initial state of the next simulation process with new η. The ramp rate used here is 1.27×10^{-6} in radians/unit time. Each hysteresis loop is obtained by averaging over 800 independent realizations. On ramping the angular noise parameter η at the same ramping rate up and down through the transition point, a hysteresis loop is formed in the case of the first-order phase transition, and the loop area implies the phase coexistence. Hysteresis plot for the whole system, as well as for the usual SPPs and adapters, are shown in Fig.4.5(a), (b) and (c) respectively. There arise abrupt jump in the ϕ_t (or ϕ_{pt}) and the positions of the jump by the implementation of the forward and backward simulations schemes are different. So the emergence of a hysteresis loop indicates the irreversibility of transition. It is observed that the hysteresis is relatively prominent for the usual SPPs (Fig.4.5(b)). Moreover, hysteresis is also seen for the adapters (Fig.4.5(c)) and as well as the whole system (Fig.4.5(a)) in this

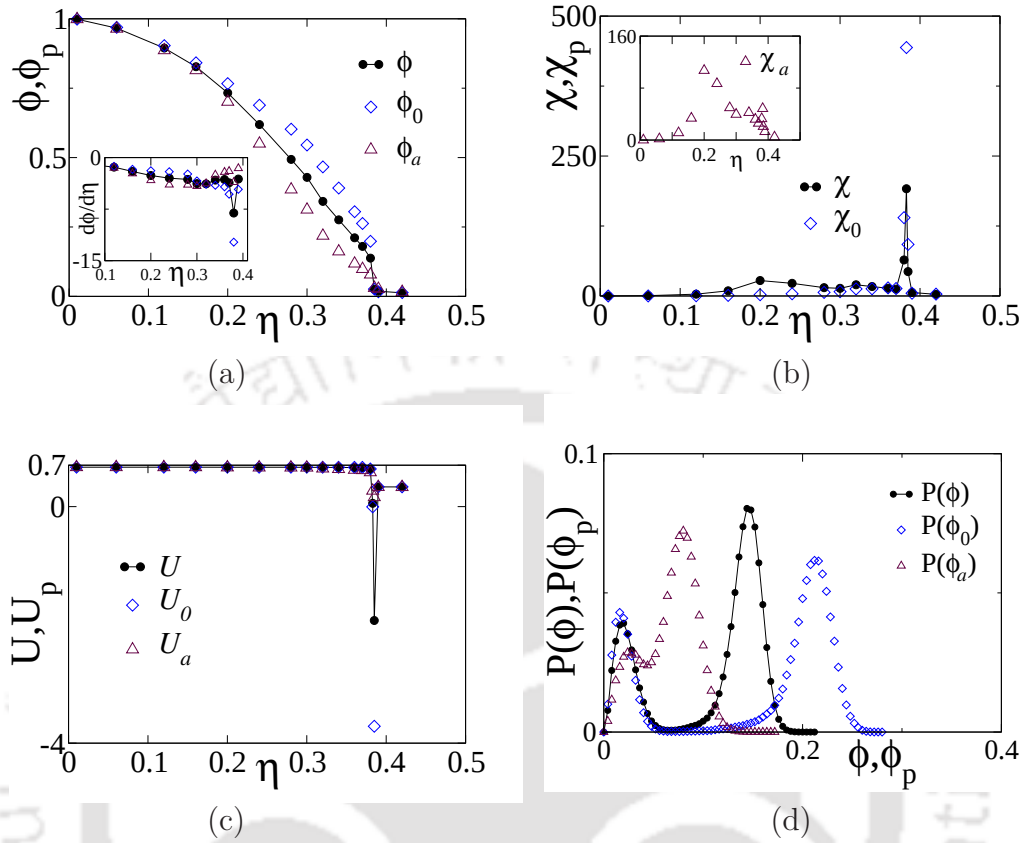

Figure 4.6: For $v_0 = 150v_a$, $v_a = 0.01$: (a) Plot of ϕ and ϕ_p versus η. Derivatives of ϕ and ϕ_p with respect to η are shown in the inset. (b) Plot of χ and χ_p versus η. In the inset, χ_a versus η is shown. (c) Plot of U and U_p versus η. (d) Plot of $P(\phi)$ and $P(\phi_p)$ at $\eta = \eta_c$. System size is $L = 256$.

case. Most of the active systems, which exhibit discontinuous transition, display a hysteresis loop. For example, model of SPPs with scalar and vector noise [104], model of SPPs with a variable angular range of interaction [174] and many others.

4.2.2 Results with $v_0 = 150v_a$ and $v_a = 0.01$

The situation will be more dramatic if the value of v_0 is increased further. We now present simulation results obtained for a much higher velocity of the usual SPPs $v_0 = 150v_a$ keeping the velocity of the adapters as $v_a = 0.01$ for a system of size $L = 256$. The order parameter of the whole system and the partial systems, ϕ and ϕ_p are plotted against η in Fig.4.6(a). There are jumps in the values of ϕ and ϕ_p near the transition. The derivatives of ϕ and ϕ_p with respect to η are plotted in the inset of Fig.4.6(a) and sharp minima are observed at $\eta_c \approx 0.38$ for the usual

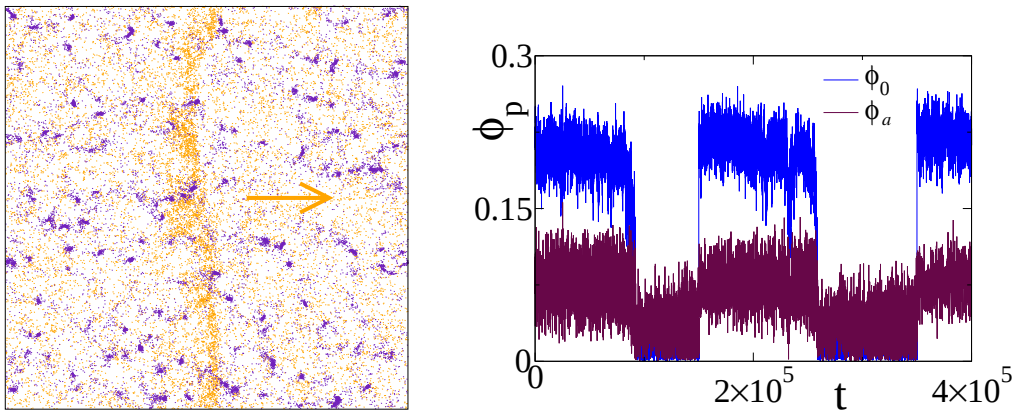

(a) (b)

Figure 4.7: For $v_0 = 150v_a, v_a = 0.01$: (a) morphology for η_c for system of size $L = 256$. Orange and indigo colour represent the usual SPPs and adapters respectively. (b) Order-parameter dynamics at η_c.

SPPs and whole system. The respective fluctuations in order parameter, χ and χ_p are plotted against η in Fig.4.6(b). There is a sharp peak in the fluctuations at $\eta_c \approx 0.38$ for all the order parameters. Whereas χ_a has two peaks at $\eta \approx 0.38$ and $\eta \approx 0.20$ as shown in the inset. However, the peak heights are not very different in this case, and the peat at $\eta \approx 0.20$ is not prominent as the $v_a = 50v_b$ case. The Binder cumulants U and U_p versus η plots are shown in Fig.4.6(c). The cumulant U_0 and U have sharp negative dips at the transition. However, the cumulant U_a has a dip at the transition point but has yet to achieve a negative value. The distributions of order parameters $P(\phi)$ and $P(\phi_p)$ at $\eta_c = 0.38$ are shown in Fig.4.6(d). In this case, all three distributions $P(\phi)$, $P(\phi_0)$ and $P(\phi_a)$ exhibit bimodal distributions which implies the two-phase co-existence in the system. These are characteristic features of a discontinuous transition. Discontinuous transition is known to occur in the VM at high velocities [104]. At the transition region, dense travelling bands of SPPs form and disappear, resulting in the coexistence of two phases in the system. A similar density band of fast-moving SPPs was observed in the BM for high v_f (Fig.3.16) in the last chapter. Below we explain the situation by studying the time evolution of the system morphology at the transition region.

The morphology of a system of size $L = 256$ are shown in Fig.4.7(a) for $\eta = \eta_c$. A dense travelling band of the usual SPPs and small clusters of adapters are seen. The density band of the usual SPPs are moving in a particular direction (shown by the orange arrow). Whereas small clusters of adapters try to follow the moving

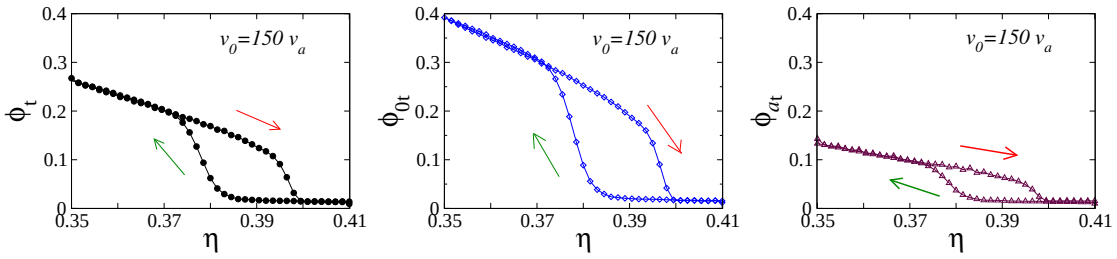

(a) (b) (c)

Figure 4.8: $v_0 \gg v_a$ and $v_0 = 150v_a$, $v_a = 0.01$: Hysteresis plot (a) for the whole system, (b) for usual SPPs and (c) for adapters, in the variation of the respective instantaneous order parameters with η. Results obtained by implementing ramp-up or forward (red arrow) and ramp-down or backward (green arrow) simulation schemes, respectively.

direction of the band. The steady-state dynamics at $\eta = \eta_c$ of the order parameters are given in Fig.4.7(b) where the values of both ϕ_0 (blue) and ϕ_a (maroon) oscillate between two phases in a synchronized manner. The higher value of ϕ_0 corresponds to the presence of the travelling band (an ordered phase) and the lower value of ϕ_0 corresponds to the disappearance of the travelling band (disordered phase). On the other hand, the higher value of ϕ_a corresponds to the ordered phase of directed clusters of the adapters, and the lower value of ϕ_a corresponds to a disordered phase of randomly moving clusters. The order is less for the adapters for the absence of interaction among them. As a result, the difference between the two phases is less. This type of phase synchronization is similar to the BM (Fig.3.16), discussed in the last chapter, for velocity range $v_f = 150v_s$, $v_s = 0.01$. It seems that the mutual alignment interaction among the different species is responsible for this type of behaviour.

Hysteresis study: Now, we will study hysteresis for this velocity range with $v_0 = 150v_a$ and $v_a = 0.01$. On ramping the angular noise η at the same ramping rate up and down through the transition point, a hysteresis loop forms in the case of first-order phase transition [104, 175]. The hysteresis plot for the whole system as well as for the usual SPPs and adapters are shown in Fig.4.8(a), (b) and (c) respectively. It is observed that the hysteresis is relatively prominent for usual SPPs (Fig.4.8(b)). However, hysteresis can be also seen for the adapters (Fig.4.8(c)) and as well as the whole system (Fig.4.8(a)). These results confirm the first-order nature of the phase transition.

Part-II

It is well known that a discontinuous phase transition [104] occurs with the appearance of density bands in the VM at high velocities (v_0). It is then interesting to explore the high-velocity regime of this adapter model. In this part, we consider a situation where the orientation adapters move with higher velocities than the usual SPPs. Thus, the velocity of the usual SPPs v_0 and that of the adapter v_a both are kept high and further, $v_a > v_0$. Apart from the velocities, all other characteristics of the adapters and usual SPPs remain the same, as mentioned in part-I.

4.3 The Model

The same update equations for the orientation and positions of the adapter model described in part-I are used. We mention here once more for the ready reference. The time evolution of the orientations of an usual SPP $\theta_{0,i}$ and that of an adapter SPP $\theta_{a,i}$ are determined by

$$\theta_{0,i}(t+\Delta t) = \langle\theta(t)\rangle_{R\in\{0,a\}} + \Delta\theta \tag{4.10}$$

$$\theta_{a,i}(t+\Delta t) = \langle\theta(t)\rangle_{R\in\{0\}} + \Delta\theta \tag{4.11}$$

Similarly, the position of the usual SPPs $\vec{r}_{0,i}$ and for the adapter SPP $\vec{r}_{a,i}$ are updated following the forward update rules as given below

$$\vec{r}_{0,i}(t+\Delta t) = \vec{r}_{0,i}(t) + \vec{v}_{0,i}(t)\Delta t \tag{4.12}$$

$$\vec{r}_{a,i}(t+\Delta t) = \vec{r}_{a,i}(t) + \vec{v}_{a,i}(t)\Delta t \tag{4.13}$$

where Δt is the time between two successive updates, and it is chosen as $\Delta t = 1$.

The distribution of randomly oriented 25 usual SPPs (in orange) and 25 adapters (in indigo) are shown in Fig.4.9. Longer and shorter arrows show the velocities v_a and v_0, respectively as in this case $v_a > v_0$. The circular region of radius R indicates the region of interaction.

4.4 Results and Discussion

Throughout the simulation, both the SPPs are kept in the same proportion as $N_0 = N_a = N/2$. The overall particle density $\rho = N/L^2$ is fixed as $\rho = 0.5$ for all the

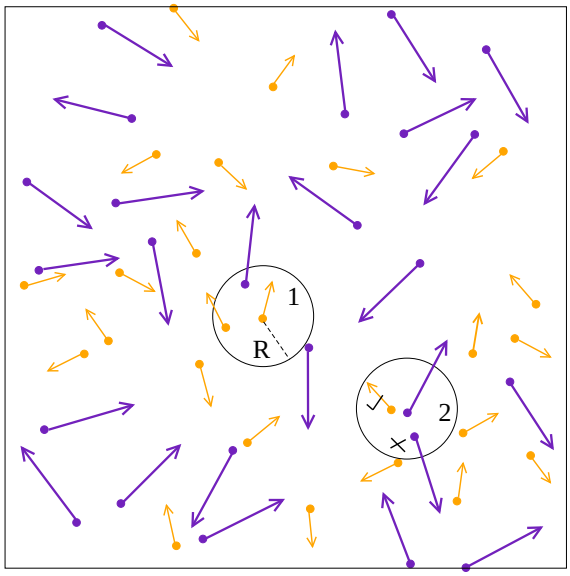

Figure 4.9: The distribution of the SPPs is shown on a square box of size $L = 10$ where $N_0 = N_a = 25$. The orange colour represents usual SPPs and the indigo colour represents the adapters. The arrow associated with an SPP indicates its orientation and here $v_a > v_0$. An usual SPP present at the center of circle-1 interacts with both SPPs present within the circle of radius R. Whereas, an adapter SPP at the center of circle-2 interacts only with usual SPPs present within the circle of radius R.

observations. One Monte Carlo (MC) time step corresponds to the up-gradation of position and orientation of all the particles. Initial 3×10^5 MC steps are neglected to achieve the steady-state. An ensemble of size 48×10^5 is taken for statistical averages (2×10^5 samples at different times for 24 different initial configurations). The results are shown with the velocity of the adapters as $v_a > v_0$ for a fixed velocity of the usual SPPs $v_0 = 1.0$. Variations of the order parameter ϕ, Binder cumulant U, and order parameter distribution $P(\phi)$ are presented in Fig.4.10, varying the angular noise η for two different velocity of adapters as $v_a = 1.2v_0$ and $v_a = 7.0v_0$.

4.4.1 Results with $v_a = 1.2v_0$ and $v_0 = 1.0$

First, we present data for ϕ (and ϕ_p), U (and U_p), and $P(\phi)$ (and $P(\phi_p)$) respectively in Fig.4.10(a), (b) and (c) on a system of size $L = 256$ for $v_a = 1.2v_0$, $v_0 = 1.0$. In this case, the velocity v_a of adapters is almost similar as the usual SPPs. The order parameter ϕ of the whole system and ϕ_p, that of the partial systems, are plotted against η in Fig.4.10(a). There are jumps in the values of ϕ and ϕ_p near the transition. The values of ϕ, ϕ_0 and ϕ_a are almost similar for a given η in this case.

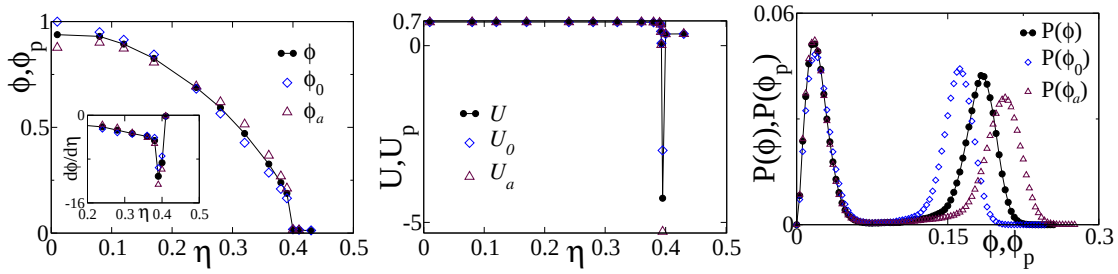

(a) (b) (c)

Figure 4.10: For $v_0 = 1.0$, $v_a = 1.2v_0$: (a) Plot of ϕ and ϕ_p versus η. Derivatives of ϕ and ϕ_p with respect to η are shown in the inset. (b) Plot of U and U_p versus η. (c) Plot of $P(\phi)$ and $P(\phi_p)$ at $\eta = \eta_c$. System size is $L = 256$.

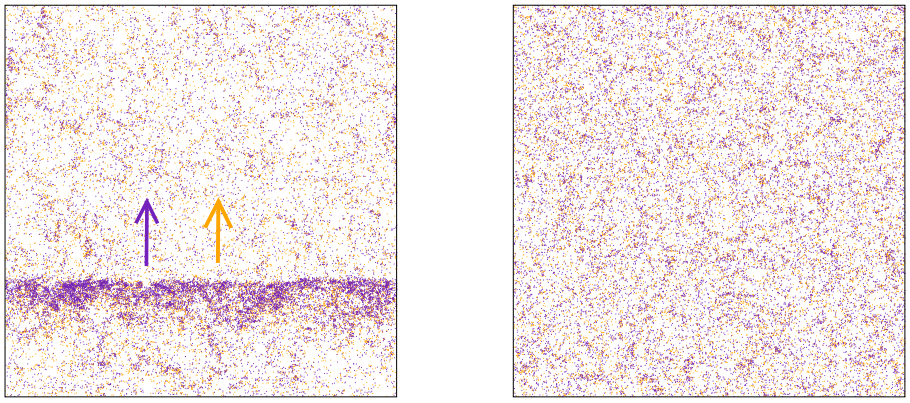

(a) (b)

Figure 4.11: For $v_0 = 1.0$, $v_a = 1.2v_0$: System morphology for $\eta \approx \eta_c$ with (a) ordered phase (density band) and (b) disorderd phase. Orange colour represents usual SPPs and indigo colour represents the adapters.

The derivatives of ϕ and ϕ_p with respect to η are plotted in the inset of Fig.4.10(a) and sharp minima are observed at $\eta_c \approx 0.39$ (same for the whole and the partial systems). The Binder cumulants U and U_p versus η plots are shown in Fig.4.10(b). The cumulant for the usual SPPs (U_0), for adapters (U_a) and for the whole system (U) all shows a sharp negative dip at the transition. It implies the discontinuous transition for the whole as well as for the partial systems. Then, the distributions of order parameters $P(\phi)$ and $P(\phi_p)$ at $\eta = \eta_c$ are shown in Fig.4.10(c). In this case, all three distributions $P(\phi)$, $P(\phi_0)$ and $P(\phi_a)$ exhibit bimodal distributions which implies the two-phase co-existence in the system [104, 174]. It seems that at the transition point, dense travelling bands of SPPs form and disappear, resulting in the coexistence of two phases in the system, which is shown in Fig.4.11(a) and (b) respectively. Both the adapters and usual SPPs are observed in the density

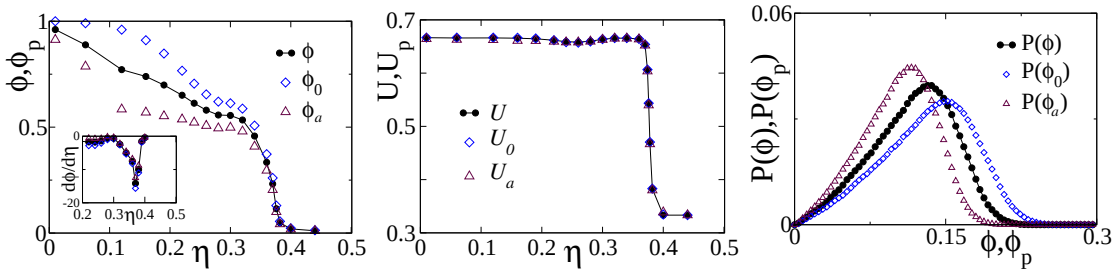

Figure 4.12: For $v_0 = 1.0$, $v_a = 7.0v_0$: (a) Plot of ϕ and ϕ_p versus η. Derivatives of ϕ and ϕ_p with respect to η are shown in the inset. (b) Plot of U and U_p versus η. (c) Plot of $P(\phi)$ and $P(\phi_p)$ at $\eta = \eta_c$. System size is $L = 256$.

band, and they move together in a particular direction (shown by arrows). This is expected as the adapters follow the usual SPPs; they move in the density band's direction. Moreover, their velocity is similar to the usual SPPs; they also form a dense band pattern near the usual SPPs. The situation will be different for a much higher velocity of the adapters with the same velocity of the usual SPPs.

4.4.2 Results with $v_a = 7.0v_0$ and $v_0 = 1.0$

Next, the situation is going to be drastic if the velocity v_a of adapters is much higher than the usual SPPs. We present the data ϕ (and ϕ_p), U (and U_p), and $P(\phi)$ (and $P(\phi_p)$) respectively on a system of size $L = 256$ for $v_a = 7.0v_0$, $v_0 = 1.0$ in Fig.4.12(a), (b) and (c) respectively. The order parameters ϕ and ϕ_p, are plotted against η in Fig.4.12(a). The order of the usual SPPs (ϕ_0) is higher than the order of adpters (ϕ_a) in the low η region in this case. However, near the transition their values are similar. The values of ϕ and ϕ_p are decreasing smoothly to zero as η increases. The derivatives of ϕ and ϕ_p with respect to η are plotted in the inset of Fig.4.12(a) and minima of the plots at the transition noise $\eta_c \approx 0.37$ (same for the whole and partial systems) are observed. In Fig.4.12(b), U and U_p are plotted against η. Both U and U_p remain positive over the whole range of η. In Fig.4.12(c), the distribution of order parameters $P(\phi)$ and $P(\phi_p)$ are plotted at $\eta = \eta_c$. All the distributions are unimodal. The positive Binder cumulants and unimodal distributions of order parameters indicate a continuous transition in the whole system as well as in the partial systems for the case of $v_a = 7.0v_0$ and $v_0 = 1.0$.

The system morphologies for the ordered phase with $\eta = 0.30$ and for disordered phase with $\eta = 0.42$ are shown in Fig.4.13(a) and (b) respectively for the case of

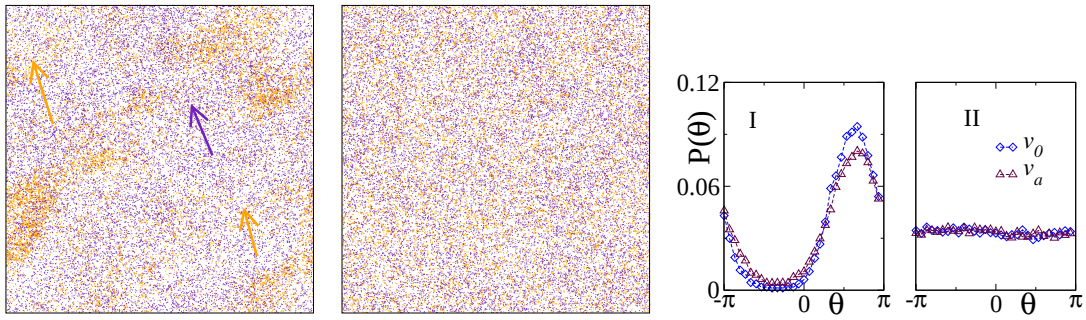

(a) $\eta = 0.30$ (b) $\eta = 0.42$ (c) θ-distribution

Figure 4.13: For $v_0 = 1.0$, $v_a = 7.0v_0$: System morphology for (a) ordered phase $\eta = 0.30$ and (b) disorderd phase $\eta = 0.42$ for the system of size $L = 256$. (c) $P(\theta)$ of the morphology (a) and (b) are plotted in I and II. Orange colour represents usual SPPs and indigo colour represents the adapters.

$v_a = 7.0v_0$ and $v_0 = 1.0$. Below the transition, at $\eta = 0.30$ shown in Fig.4.13(a), less dense large clusters of usual SPPs are observed with small clusters of adapters, and they are directed in the same direction (shown by arrow). Whereas, above the transition, at $\eta = 0.42$ shown in Fig.4.13(b) they move randomly. The orientation distribution of these two morphologies are shown in Fig.4.13(c)I and II, respectively. In this case, adapters move with much higher velocity and cannot flock with the usual SPPs. Moreover, they adopt the alignment information from usual SPPs, which are distant. It seems that as the usual SPPs interact with the adapters, randomness enters in the alignment of the usual SPPs. Hence, the correlation between the usual SPPs gets destroyed to form a dense band structure.

Hysteresis study: Simulations are carried out to measure the instantaneous order parameter (ϕ_t) by either gradually increasing or decreasing η with a fixed ramp rate as discussed earlier. The simulation results of hysteresis for the whole system with different values of adapter's velocity as $v_a = 1.2v_0$, $4.0v_0$ and $7.0v_0$ for a fixed $v_0 = 1.0$, are presented in Fig.4.14(a),(b) and (c) respectively. Observations show that when v_a is relatively less as $v_a = 1.2v_0$ with $v_0 = 1.0$, there arise an abrupt jump in the ϕ_t and the positions of the jump by the implementation of the forward and backward simulations schemes are different. So the emergence of a hysteresis loop indicates the irreversibility of transition [104], shown in Fig.4.14(a). Hysteresis loop is still exist for a moderately high value of $v_a = 4.0v_0$ shown in Fig.4.14(b), however, it is less prominent than the $v_a = 1.2v_0$ case. Then, for a large enough value of $v_a = 7.0v_0$, the change of the order parameter versus η becomes reversible,

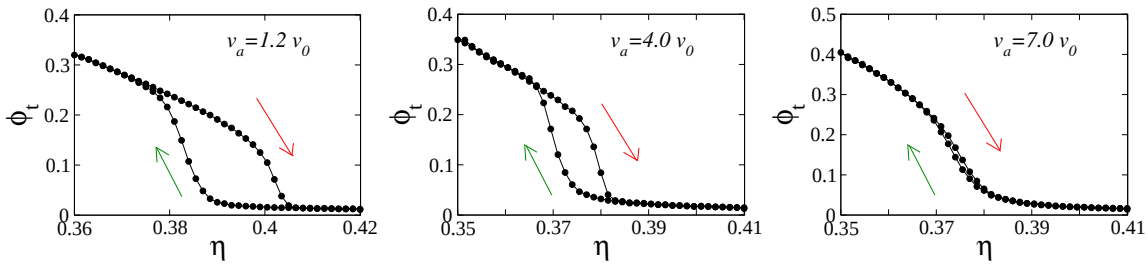

(a) $v_a = 1.2v_0$ (b) $v_a = 4.0v_0$ (c) $v_a = 7.0v_0$

Figure 4.14: For $v_a > v_0$: Hysteresis plot of the whole system for different values of adapter velocity as (a) $v_a = 1.2v_0$, (b) $v_a = 4.0v_0$ and (c) $v_a = 7.0v_0$ with the fixed $v_0 = 1.0$. Results obtained by implementing ramp-up or forward (red arrow) and ramp-down or backward (green arrow) simulation schemes, respectively.

which indicates continuous phase transition, shown in Fig.4.14(c). It needs to be noted that similar behaviour of hysteresis plots for the different values of v_a is also observed for the partial systems, i.e., with usual SPPs as well as the adapters.

4.5 Summary and Discussion

In this work, the collective motion of a mixture of usual SPPs and orientation adapters has been modelled. The usual SPPs and the adapters have very different velocities. There are two parts to this chapter. In the first part, the adapter has a much lower velocity than the usual SPPs, whereas in the second part, the adapter has a higher velocity than the usual SPPs. Pattern formation and dynamical phase transition in these systems are studied. Below we summarise the results of each part.

Part-I: Different pattern formation is studied for adapter velocity $v_a = 0.01$ and usual SPPs' velocity $v_0 = 50v_a$. Directed lanes, directed clusters, density band, elongated clusters etc., are observed at different values of the angular noise η. Phase separation or demixing between the two types have been observed in the ordered region as expected. The dense travelling band structures of the usual SPPs near the transition ($\eta \approx \eta_c$) for velocities $v_0 = 50v_a$ and $v_0 = 150v_a$ are observed. As a consequence of the formation of travelling bands, the dynamical transition of the usual SPPs is found discontinuous. The dense band of usual SPPs appears and disappears with time at the transition point. As a result, co-existence of two phases occurs. The discontinuous transition is further characterized by a negative dip in

the Binder cumulant U_0 and bimodal distribution of the order parameter ϕ_0. This is excepted as similar behaviour occurs in the VM. However, more dramatic events happened for the adapters. Though the adapters do not interact with another adapter, they get oriented in the same direction as the usual SPPs as they only interact with them. Once they are aligned, they also form flocks over time in the form of lanes and clusters. At $\eta \approx \eta_c$, the flocks of adapters appear as directed clusters and disappear as random clusters in synchronization with the appearance of travelling bands of the usual SPPs and their disappearance. Thus, there is also the co-existence of two phases of the adapters at the transition point. Though the dip in the Binder cumulant is not negative, the order parameter distribution is not fully resolved into two peaks, a weak hysteresis effect is observed for the adapter. It seems that the transition is going to be discontinuous in the thermodynamic limit. However, that would be surprising as the dynamical transition at such a low velocity $v_a = 0.01$ should have been a continuous type. The whole system, collection of the usual SPPs and the adapters, clearly exhibits a discontinuous transition.

In part-II, the adapters have higher velocity than the usual SPPs, while the velocity of the usual SPPs is fixed at a high velocity $v_0 = 1.0$. For the adapter velocity $v_a = 1.2v_0$ and $v_0 = 1.0$, both adapters and the usual SPPs form dense travelling bands in the system. Both the travelling bands move in the same direction in accordance with the orientation rule. Near the transition point, such bands appear and disappear over time, giving rise to co-existence of two phases. The adapters and the usual SPPs both undergo a discontinuous transition characterized by a negative dip in Binder cumulant and bimodal distribution of order parameters. The nature of the transition is further confirmed by the existence of hysteresis in the order parameter under a continuously varying noise field. It is quite expected in the context of the VM.

However, more dramatic effects are revealed as the adapter velocity becomes much higher than the usual SPPs. Surprisingly, the formation of travelling bands disappears from the system. In the ordered phase, the flocks of usual SPPs form directed clusters, and the adapters form relatively smaller directed clusters. All these clusters move in the same direction as expected. In the disordered phase ($\eta > \eta_c$), these clusters melt into smaller clusters and move randomly. Consequently, continuous transitions occur for both the adapters and the usual SPPs, even at such high velocities. The continuous transitions are characterized by positive Binder cumulant and unimodal distribution of the order parameter. The hysteresis loops also disappear for these systems. The alignment of an adapter obtained from local inter-

action may be very different from the alignment of SPPs at a distant point where the adapter moves after position update due to its high velocity. Such misalignment in orientations between the adapters and the SPPs introduces extra fluctuations in the system. Such fluctuations grow predominantly in the transition region, and all long-range correlations get destroyed. The continuous nature of the transition is essentially a manifestation of such smooth crossover from correlated system to uncorrelated system.

Chapter 5

Summary and Conclusion

In this thesis, various models on active systems are explored in search of the emergence of collective motion in varied scenarios. We have studied dry active matter with polar interaction similar to the Vicsek model (VM). Besides exotic pattern formations, orientational phase transitions are observed in each model with the variation of an appropriate system variable. Though the transition nature depends on the values of system parameters, the properties exhibited at the transition point are characterised and understood rigorously. Below we summarise the thesis, which contains the effect of perturbation, mixing of different species and the effect of orientation adapters on the collective properties of SPPs as discussed in the previous chapters.

In the first chapter, after providing a general introduction to the topic, a thorough survey of the literature is made on the studies of collective behaviour of SPPs. A brief overview of the features of phase transitions is described. A small presentation on the spin models is also given. The Vicsek model (VM), its characteristic properties, orientational order-disorder transition, nature of transition, relevance to the spin models, etc., are discussed in this chapter. Finally, the problems which will be taken up in this thesis are proposed with sufficient motivation.

The second chapter presents the collective dynamics of SPPs with inherent perturbation in the system. A new model is developed incorporating a trapping perturbation in the VM. Due to the perturbation, the SPPs get trapped for a while with a position-dependent trapping probability as they pass through the trapping region and pick up a random direction of velocity on release. The trapping perturbation has two-fold effects on the system. It creates a temporal density fluctuation in the number of the moving particles as well as provides a short impulse on the average orientation besides the angular noise. The effect of the perturbation on

the VM is then studied, varying the scalar noise η and the perturbation strength α for a specific density ρ_0. A thorough FSS analysis has been performed whenever it was required. The system's response is obtained at low, intermediate and high velocities. In the low-velocity case, a continuous transition is observed with the same critical exponents as the VM. The perturbation in the VM gives rise to novel features on the formation of travelling density bands and the nature of phase transition for the higher velocities. There exists a crossover system size $L^*(\rho_0, v_0)$ for the VM ($\alpha = 0$) for $v_0 = 0.5$ and $\rho_0 = 0.5$ below which the model exhibits continuous transition and above which it exhibits discontinuous transition with dense travelling bands in the system. In the presence of trapping perturbation, the value of crossover system size $L^*_\alpha(\rho_0, v_0)$ increases and becomes greater than $L^*(\rho_0, v_0)$, that of without perturbation. Further, there exists an α^* for a given system of size L, $L^*(\rho_0, v_0) < L < L^*_\alpha(\rho_0, v_0)$, below which the transition is discontinuous and above which the transition is continuous. As the velocity v_0 increases, the value of $L^*_\alpha(\rho_0, v_0)$ decreases but remains greater than the corresponding $L^*(\rho_0, v_0)$. The perturbation in the VM can destroy the travelling band up to a certain system size beyond $L^*(\rho_0, v_0)$. Consequently, the value of the crossover size has increased to a higher value $L^*_\alpha(\rho_0, v_0)$, below which the transition is continuous with the same critical exponents of the VM and above which the transition is discontinuous. The perturbation in the form of fluctuations in local density and orientation can destroy the dense travelling band in the system up to a certain system size $L^*_\alpha(\rho_0, v_0)$ for a given ρ_0, v_0 and α. For the systems of size beyond $L^*_\alpha(\rho_0, v_0)$, the transition remains discontinuous even in the presence of perturbation.

In the third chapter, we have studied the collective behaviour of a binary mixture of SPPs with two different motile properties, such as slow-moving SPPs with velocity v_s and fast-moving SPPs with velocity v_f ($v_f \gg v_s$). Both inter and intra-particle interactions are considered in the BM. The model exhibits many different self-organised pattern formation and phase segregation. The mutual interaction among the two types of SPPs not only produce a variety of collective patterns such as directed lanes, clusters, and clumps; random clusters and clumps; micro-cluster and micro-clumps, etc., but also the flocks of two different SPPs move in the same direction in the ordered phase. The system exhibits a continuous order-disorder transition at a critical noise η_c for $v_f = 30v_s$ and $50v_s$ with $v_s = 0.01$ with a new set of critical exponents. The critical exponents are not only different from those of the VM but also depend on v_f. Though the continuous transition of the slow-moving SPPs is expected; it was quite unexpected for the fast-moving SPPs with

$v_f = 50v_s = 0.5$ as the VM exhibits a discontinuous transition at $v_0 = 0.5$ on a system of size $L = 256$. Thus the slow-moving SPPs induce the moderately fast-moving SPPs to manifest a similar behaviour. At a much higher velocity $v_f = 150v_s$, the dense travelling band of the fast-moving SPPs appears in the BM, and consequently, the fast-moving SPPs exhibit discontinuous transition. Interestingly, the slow-moving SPPs and the system as a whole also undergoes a discontinuous transition. At the high-velocity regime of v_f, discontinuous transitions occur not only for the fast-moving and the slow-moving SPPs but also for the whole system.

In the fourth chapter, the effect of orientation adapter on the collective behaviour of SPPs is studied. In this model, adapter SPPs exist besides the usual SPPs in equal proportion. The adapter SPPs do not interact among themselves but adopt the velocity orientation of the usual SPPs through local interactions. However, the usual SPPs do interact with themselves as well as with the adapters. In Part-I, different pattern formation is studied for adapter velocity $v_a = 0.01$ and usual SPPs' velocity $v_0 = 50v_a$. Directed lanes, directed clusters, density band, elongated clusters etc., are observed at different values of the angular noise η. Phase separation or demixing between the two types have been observed in the ordered region as expected. The dense travelling band structures of the usual SPPs near the transition ($\eta \approx \eta_c$) for velocities $v_0 = 50v_a$ and $v_0 = 150v_a$ are observed. As a consequence of the formation of travelling bands, the dynamical transition of the usual SPPs is found discontinuous. At the transition point, the dense band of usual SPPs appears and disappears with time. As a result, the co-existence of two phases occurs. Whereas the adapters get influenced by the other species' community and also obtain two-phase co-existence. Though the dip in the Binder cumulant is not negative, the order parameter distribution is not fully resolved into two peaks, a weak hysteresis effect is observed for the adapter. It seems that the transition is going to be discontinuous in the thermodynamic limit. However, that would be surprising as the dynamical transition at such a low velocity $v_a = 0.01$ should have been a continuous type. The whole system, collection of the usual SPPs and the adapters, clearly exhibits a discontinuous transition. In part-II, the adapters have higher velocity than the usual SPPs, while the velocity of the usual SPPs is fixed at a high velocity $v_0 = 1.0$. For the adapter velocity $v_a = 1.2v_0$ and $v_0 = 1.0$, both adapters and the usual SPPs form dense travelling bands and move in the same direction. Near the transition point, such bands appear and disappear over time, giving rise to the co-existence of two phases. The adapters and the usual SPPs both undergo a discontinuous transition. The nature of the transition is further confirmed by the existence of

hysteresis in the order parameter under a continuously varying noise field. However, when the adapter velocity becomes much higher than the usual SPPs, the formation of travelling bands disappears from the system. In the ordered phase, the flocks of usual SPPs form directed clusters, and the adapters form relatively smaller directed clusters. In the disordered phase, these clusters melt into smaller clusters and move randomly. Consequently, continuous transitions occur for both the adapters and the usual SPPs, even at such high velocities. Due to the high velocity of the adapters, extra fluctuations occurs in the system. Such fluctuations grow predominantly in the transition region, and all long-range correlations get destroyed. The continuous nature of the transition is essentially a manifestation of such smooth crossover from correlated system to uncorrelated system.

The thesis represents many novel results obtained from different models of collective motion of SPPs incorporating perturbation, mixing of species and including orientation adapters. Different mechanisms are developed to determine system properties. Several aspects of these models are explored by performing extensive numerical simulations. The models developed here are generic in nature however could be extended to various new problems by modifying the model's parameters suitably. It is worth mentioning that the methodologies used and results obtained in this thesis may be beneficial for further studies on these systems. For example, perturbations can also be imparted in the systems in many other forms and can be compared with the results obtained in the present model. One of the possible situations is: instead of imposing spatial trapping, randomly selected particles of a specified fraction can be trapped for a while and released with random orientation throughout the system. Study of the collective behaviour of such systems with different perturbations can be beneficial to control the dynamics and system properties of real-life SPPs such as swarms of insects or can be applied to traffic management, jamming etc. Furthermore, the presence of PBCs favours the formation of bands. Systems with or without perturbation can be studied in other types of boundary conditions, such as reflecting or open boundaries. In such cases, the position update rules at the boundary can be random or with some specifications. The binary model of different species can be studied further with different densities and proportions. Further, the magnitude of the velocity of individual SPPs can be taken into account in estimating the interaction. Similar aspects can also be explored in the model with orientation adapters. The study of such models can give interesting features into the physics of active matter, and nontrivial results can be found, which can help us to understand the subject more. These topics

of research encompass a variety of physical behaviours that have fundamental and applied significance. Research activities in Physics involving interdisciplinary areas such as active matter are growing. It has witnessed a large spectrum of physical systems, models and settings in which novel ideas can be predicted, verified and implemented. The knowledge of such systems will be beneficial to understand and apply in many related fields, such as swarm robotics, molecular biology, biomedical applications, security systems, traffic and crowd management and many more.

Abbreviations

SPPs: self-propelled particles
VM: Vicsek model
PBCs: periodic boundary conditions
MC steps: Monte-Carlo steps
FSS: finite-size scaling
BM: binary model
DS: directed clusters
DL: directed lanes
DC: directed clumps
RS: random clusters
RC: random clumps
MS: micro-cluster
MC: micro-clumps
HGM: homogeneous gas-like mixture

Bibliography

[1] T. Vicsek and A. Zafeiris, Phys. Rep. **517**, 71 (2012).
[2] S. Ramaswamy, Annu. Rev. Condens. Matter Phys. **1**, 323 (2010).
[3] M. R. Shaebani, A. Wysocki, R. G. Winkler, G. Gompper, and H. Rieger, Nat Rev Phys **2**, 181 (2020).
[4] C. Becco, N. Vandewalle, J. Delcourt, and P. Poncin, Physica A **367**, 487 (2006).
[5] N. C. Makris et al., Science **323**, 1734 (2009).
[6] A. Filella, F. Nadal, C. Sire, E. Kanso, and C. Eloy, Physical review letters **120**, 198101 (2018).
[7] M. Ballerini et al., Proc. Natl. Acad. Sci. U.S.A. **105**, 1232 (2008).
[8] A. Cavagna et al., Proc. Natl. Acad. Sci. U.S.A. **107**, 11865 (2010).
[9] F. Ginelli et al., Proceedings of the National Academy of Sciences **112**, 12729 (2015).
[10] D. Helbing, I. Farkas, and T. Vicsek, Nature **407**, 487 (2000).
[11] D. Helbing, A. Johansson, and H. Z. Al-Abideen, Physical review E **75**, 046109 (2007).
[12] D. H. Kelley and N. T. Ouellette, Scientific reports **3**, 1073 (2013).
[13] A. Okubo and H. Chiang, Population Ecology **16**, 1 (1974).
[14] J. Buhl et al., Science **312**, 1402 (2006).
[15] P. Romanczuk, I. D. Couzin, and L. Schimansky-Geier, Phys. Rev. Lett. **102**, 010602 (2009).
[16] S. Gueron and S. A. Levin, Journal of theoretical Biology **165**, 541 (1993).
[17] J. A. Shapiro, Annual review of microbiology **52**, 81 (1998).
[18] H. Zhang, A. Be'Er, R. S. Smith, E.-L. Florin, and H. L. Swinney, Europhys. Lett. **87**, 48011 (2009).
[19] H.-P. Zhang, A. Beer, E.-L. Florin, and H. L. Swinney, Proc. Natl. Acad. Sci. U.S.A. **107**, 13626 (2010).
[20] G. Malet-Engra et al., Current Biology **25**, 242 (2015).
[21] V. Schaller, C. Weber, C. Semmrich, E. Frey, and A. R. Bausch, Nature **467**, 73 (2010).
[22] T. Sanchez, D. T. Chen, S. J. DeCamp, M. Heymann, and Z. Dogic, Nature **491**, 431 (2012).
[23] C. Bechinger et al., Rev. Mod. Phys. **88**, 045006 (2016).
[24] J. Palacci, S. Sacanna, A. P. Steinberg, D. J. Pine, and P. M. Chaikin, Science **339**,

936 (2013).
[25] V. Narayan, S. Ramaswamy, and N. Menon, Science **317**, 105 (2007).
[26] J. Deseigne, O. Dauchot, and H. Chaté, Phys. Rev. Lett. **105**, 098001 (2010).
[27] O. Feinerman, I. Pinkoviezky, A. Gelblum, E. Fonio, and N. S. Gov, Nature Physics **14**, 683 (2018).
[28] A. Dussutour and S. C. Nicolis, Chaos, Solitons & Fractals **50**, 32 (2013).
[29] H. J. Charlesworth and M. S. Turner, Proceedings of the National Academy of Sciences **116**, 15362 (2019).
[30] I. D. Couzin, J. Krause, N. R. Franks, and S. A. Levin, Nature **433**, 513 (2005).
[31] B. J. Nelson, I. K. Kaliakatsos, and J. J. Abbott, Annual review of biomedical engineering **12**, 55 (2010).
[32] L. K. Abdelmohsen, F. Peng, Y. Tu, and D. A. Wilson, Journal of Materials Chemistry B **2**, 2395 (2014).
[33] J. Wang and W. Gao, ACS nano **6**, 5745 (2012).
[34] D. Patra et al., Nanoscale **5**, 1273 (2013).
[35] S. Ebbens, Current opinion in colloid & interface science **21**, 14 (2016).
[36] G. M. Viswanathan, M. G. Da Luz, E. P. Raposo, and H. E. Stanley, *The physics of foraging: an introduction to random searches and biological encounters*, Cambridge University Press, 2011.
[37] M. Brambilla, E. Ferrante, M. Birattari, and M. Dorigo, Swarm Intelligence **7**, 1 (2013).
[38] D. Helbing, Rev. Mod. Phys. **73**, 1067 (2001).
[39] M. C. Marchetti et al., Rev. Mod. Phys. **85**, 1143 (2013).
[40] M. E. Cates and J. Tailleur, Annu. Rev. Condens. Matter Phys. **6**, 219 (2015).
[41] A. Cavagna, I. Giardina, and T. S. Grigera, Physics Reports **728**, 1 (2018).
[42] Y. Fily and M. C. Marchetti, Physical review letters **108**, 235702 (2012).
[43] A. Wysocki, R. G. Winkler, and G. Gompper, EPL (Europhysics Letters) **105**, 48004 (2014).
[44] P. Digregorio et al., Physical review letters **121**, 098003 (2018).
[45] J. Bialké, H. Löwen, and T. Speck, EPL (Europhysics Letters) **103**, 30008 (2013).
[46] J. U. Klamser, S. C. Kapfer, and W. Krauth, Nature communications **9**, 1 (2018).
[47] N. de Macedo Biniossek, H. Löwen, T. Voigtmann, and F. Smallenburg, Journal of Physics: Condensed Matter **30**, 074001 (2018).
[48] A. P. Solon, H. Chaté, and J. Tailleur, Physical review letters **114**, 068101 (2015).
[49] T. Speck, J. Bialké, A. M. Menzel, and H. Löwen, Physical Review Letters **112**, 218304 (2014).
[50] I. Buttinoni et al., Physical review letters **110**, 238301 (2013).
[51] J. Stenhammar, A. Tiribocchi, R. J. Allen, D. Marenduzzo, and M. E. Cates, Physical review letters **111**, 145702 (2013).
[52] J. S. Bois, F. Jülicher, and S. W. Grill, Physical review letters **106**, 028103 (2011).
[53] J. Smrek and K. Kremer, Phys. Rev. Lett. **118**, 098002 (2017).
[54] S. N. Weber, C. A. Weber, and E. Frey, Phys. Rev. Lett. **116**, 058301 (2016).

[55] J. Stenhammar, R. Wittkowski, D. Marenduzzo, and M. E. Cates, Phys. Rev. Lett. **114**, 018301 (2015).
[56] N. W. Goehring and S. W. Grill, Trends in cell biology **23**, 72 (2013).
[57] D. St Johnston and J. Ahringer, Cell **141**, 757 (2010).
[58] B. Rubinstein, B. D. Slaughter, and R. Li, Physical biology **9**, 045006 (2012).
[59] P. K. Trong, E. M. Nicola, N. W. Goehring, K. V. Kumar, and S. W. Grill, New Journal of Physics **16**, 065009 (2014).
[60] S. Alonso and M. Baer, Physical biology **7**, 046012 (2010).
[61] N. W. Goehring et al., Science **334**, 1137 (2011).
[62] E. F. Keller and L. A. Segel, Journal of theoretical biology **26**, 399 (1970).
[63] T. Hillen and K. J. Painter, Journal of mathematical biology **58**, 183 (2009).
[64] M. Meyer, L. Schimansky-Geier, and P. Romanczuk, Physical Review E **89**, 022711 (2014).
[65] Q.-X. Liu et al., Proceedings of the National Academy of Sciences **110**, 11905 (2013).
[66] M. Cross and H. Greenside, *Pattern formation and dynamics in nonequilibrium systems*, Cambridge University Press, 2009.
[67] P. Ball and N. R. Borley, *The self-made tapestry: pattern formation in nature*, volume 198, Oxford University Press Oxford, 1999.
[68] P. M. Bendix et al., Biophysical journal **94**, 3126 (2008).
[69] C. Dombrowski, L. Cisneros, S. Chatkaew, R. E. Goldstein, and J. O. Kessler, Phys. Rev. Lett. **93**, 098103 (2004).
[70] T. Vicsek, A. Czirók, E. Ben-Jacob, I. Cohen, and O. Shochet, Phys. Rev. Lett. **75**, 1226 (1995).
[71] H. Gruler, U. Dewald, and M. Eberhardt, The European Physical Journal B-Condensed Matter and Complex Systems **11**, 187 (1999).
[72] F. Peruani, A. Deutsch, and M. Bär, Physical Review E **74**, 030904 (2006).
[73] A. Baskaran and M. C. Marchetti, Physical Review E **77**, 011920 (2008).
[74] U. Erdmann, W. Ebeling, L. Schimansky-Geier, and F. Schweitzer, The European Physical Journal B-Condensed Matter and Complex Systems **15**, 105 (2000).
[75] C. Reichhardt and C. O. Reichhardt, Physical Review E **90**, 012701 (2014).
[76] W. R. DiLuzio et al., Nature **435**, 1271 (2005).
[77] B.-q. Ai, Z.-g. Shao, and W.-r. Zhong, Soft Matter **14**, 4388 (2018).
[78] R. Di Leonardo, D. DellArciprete, L. Angelani, and V. Iebba, Physical review letters **106**, 038101 (2011).
[79] A. Cēbers, Journal of magnetism and magnetic materials **323**, 279 (2011).
[80] C. W. Reynolds, Flocks, herds and schools: A distributed behavioral model, in *Proceedings of the 14th annual conference on Computer graphics and interactive techniques*, pages 25–34, 1987.
[81] J. Toner and Y. Tu, Phys. Rev. E **58**, 4828 (1998).
[82] P. M. Chaikin, T. C. Lubensky, and T. A. Witten, *Principles of condensed matter physics*, volume 10, Cambridge university press Cambridge, 1995.

[83] S. Mishra, A. Baskaran, and M. C. Marchetti, Physical Review E **81**, 061916 (2010).
[84] A. P. Solon and J. Tailleur, Phys. Rev. E **92**, 042119 (2015).
[85] C. Huepe and M. Aldana, Physica A: Statistical Mechanics and its Applications **387**, 2809 (2008).
[86] G. Grégoire and H. Chaté, Phys. Rev. Lett. **92**, 025702 (2004).
[87] M. Nagy, I. Daruka, and T. Vicsek, Physica A **373**, 445 (2007).
[88] H. Chaté, F. Ginelli, G. Grégoire, and F. Raynaud, Phys. Rev. E **77**, 046113 (2008).
[89] C. Huepe and M. Aldana, Physical review letters **92**, 168701 (2004).
[90] F. Ginelli, F. Peruani, M. Bär, and H. Chaté, Physical review letters **104**, 184502 (2010).
[91] H. Chaté, F. Ginelli, G. Grégoire, F. Peruani, and F. Raynaud, The European Physical Journal B **64**, 451 (2008).
[92] D. Strömbom, Journal of theoretical biology **283**, 145 (2011).
[93] A. Costanzo, EPL (Europhysics Letters) **125**, 20008 (2019).
[94] Z. Cheng, Z. Chen, T. Vicsek, D. Chen, and H.-T. Zhang, New Journal of Physics **18**, 103005 (2016).
[95] B. Li, Z.-X. Wu, and J.-Y. Guan, Phys. Rev. E **99**, 022609 (2019).
[96] F. Peruani, T. Klauss, A. Deutsch, and A. Voss-Boehme, Phys. Rev. Lett. **106**, 128101 (2011).
[97] F. Ginelli and H. Chaté, Phys. Rev. Lett. **105**, 168103 (2010).
[98] G. Grégoire, H. Chaté, and Y. Tu, Physica D: Nonlinear Phenomena **181**, 157 (2003).
[99] M. Aldana, V. Dossetti, C. Huepe, V. Kenkre, and H. Larralde, Physical review letters **98**, 095702 (2007).
[100] F. Peruani and I. S. Aranson, Physical Review Letters **120**, 238101 (2018).
[101] D. Grossman, I. Aranson, and E. B. Jacob, New Journal of Physics **10**, 023036 (2008).
[102] M. Zumaya, H. Larralde, and M. Aldana, Scientific reports **8**, 1 (2018).
[103] G. Baglietto and E. V. Albano, Phys. Rev. E **78**, 021125 (2008).
[104] H. Chaté, F. Ginelli, G. Grégoire, and F. Raynaud, Phys. Rev. E **77**, 046113 (2008).
[105] J. A. Pimentel, M. Aldana, C. Huepe, and H. Larralde, Phys. Rev. E **77**, 061138 (2008).
[106] M. Aldana, V. Dossetti, C. Huepe, K. V. M, and H. Larralde, Phys. Rev. Lett. **98**, 095702 (2007).
[107] M. Aldana and C. Huepe, J. Stat. Phys. **112**, 135 (2003).
[108] M. Romensky, V. Lobaskin, and T. Ihle, Phys. Rev. E **90**, 063315 (2014).
[109] M. Durve and A. Sayeed, Phys. Rev. E **93**, 052115 (2016).
[110] O. Chepizhko, E. G. Altmann, and F. Peruani, Phys. Rev. Lett. **110**, 238101 (2013).
[111] O. Chepizhko and F. Peruani, Eur. Phys. J. Spec. Top. **224**, 1287 (2015).
[112] D. A. Quint and A. Gopinathan, Phys. Biol. **12**, 046008 (2015).
[113] C. J. O. Reichhardt and C. Reichhardt, New J. Phys. **20**, 025002 (2018).
[114] J.-B. C. D. B. Alexandre Morin, Nicolas Desreumaux, Nat. Phys. **13**, 63 (2016).
[115] R.-C. Reichhardt, C. J. Olson, Nat. Phys. **13**, 10 (2016).

[116] R. Das, M. Kumar, and S. Mishra, Phys. Rev. E **98**, 060602 (2018).
[117] S. Köhler, V. Schaller, and A. R. Bausch, Nature materials **10**, 462 (2011).
[118] L. Huber, R. Suzuki, T. Krüger, E. Frey, and A. Bausch, Science **361**, 255 (2018).
[119] I. Theurkauff, C. Cottin-Bizonne, J. Palacci, C. Ybert, and L. Bocquet, Physical review letters **108**, 268303 (2012).
[120] F. Peruani and M. Baer, New Journal of Physics **15**, 065009 (2013).
[121] N. Kyriakopoulos, H. Chaté, and F. Ginelli, Phys. Rev. E **100**, 022606 (2019).
[122] J. Toner and Y. Tu, Physical review letters **75**, 4326 (1995).
[123] I. D. Couzin, J. Krause, R. James, G. D. Ruxton, and N. R. Franks, Journal of theoretical biology **218**, 1 (2002).
[124] G. F. Young, L. Scardovi, A. Cavagna, I. Giardina, and N. E. Leonard, PLoS Comput Biol **9**, e1002894 (2013).
[125] D. L. Blair, T. Neicu, and A. Kudrolli, Physical Review E **67**, 031303 (2003).
[126] A. Kudrolli, G. Lumay, D. Volfson, and L. S. Tsimring, Physical review letters **100**, 058001 (2008).
[127] V. Narayan, N. Menon, and S. Ramaswamy, Journal of Statistical Mechanics: Theory and Experiment **2006**, P01005 (2006).
[128] H. E. Stanley, *Introduction to Phase Transitions and Critical Phenomena*, Oxford University Press, New York, 1971.
[129] L. Verlet, Physical review **159**, 98 (1967).
[130] W. Mattson and B. M. Rice, Computer Physics Communications **119**, 135 (1999).
[131] M. P. Allen and D. J. Tildesley, *Computer simulation of liquids*, Oxford university press, 2017.
[132] G. Baglietto and E. V. Albano, Comput. Phys. Commun. **180**, 527 (2009).
[133] B. Gönci, M. Nagy, and T. Vicsek, Eur. Phys. J. Spec. Top. **157**, 53 (2008).
[134] G. Grégoire and H. Chaté, Phys. Rev. Lett. **92**, 025702 (2004).
[135] M. Aldana, H. Larralde, and B. Vázquez, Int. J. Mod. Phys. B **23**, 3661 (2009).
[136] H. Chaté, F. Ginelli, and G. Grégoire, Phys. Rev. Lett. **99**, 229601 (2007).
[137] F. Ginelli, Eur. Phys. J. Special Topics **225**, 2099 (2016).
[138] R. M. Holdo, J. M. Fryxell, A. R. Sinclair, A. Dobson, and R. D. Holt, PloS one **6**, e16370 (2011).
[139] F. J. Pérez-Reche et al., Phys. Rev. Lett. **109**, 098102 (2012).
[140] E. Bertin, M. Droz, and G. Grégoire, J. Phys A: Math. Theor. **42**, 445001 (2009).
[141] T. Ihle, Phys. Rev. E **83**, 030901 (2011).
[142] G. Baglietto and E. V. Albano, Phys. Rev. E **80**, 050103 (2009).
[143] K. Binder, Reports on progress in physics **50**, 783 (1987).
[144] K. Christensen and N. R. Moloney, *Complexity and criticality*, volume 1, World Scientific Publishing Company, 2005.
[145] D. S. Cambui, A. S. de Arruda, and M. Godoy, Physica A **444**, 582 (2016).
[146] W. Janke, First-order phase transitions, in *Computer Simulations of Surfaces and Interfaces*, pages 111–135, Springer, 2003.
[147] S. Adhikary and S. Santra, in *AIP Conference Proceedings*, volume 2220, page

140006, AIP Publishing LLC, 2020.
[148] J. D. Murray, *Mathematical biology II: spatial models and biomedical applications*, volume 3, Springer, 2001.
[149] R. Thar and M. Kühl, FEMS microbiology letters **246**, 75 (2005).
[150] A. Sokolov, I. S. Aranson, J. O. Kessler, and R. E. Goldstein, Phys. Rev. Lett. **98**, 158102 (2007).
[151] I. D. Couzin and N. R. Franks, Proceedings of the Royal Society of London. Series B: Biological Sciences **270**, 139 (2003).
[152] W. Herrnkind, Science **164**, 1425 (1969).
[153] R. G. Bill and W. F. Herrnkind, Science **193**, 1146 (1976).
[154] N. C. Makris et al., Science **311**, 660 (2006).
[155] D. Helbing and P. Molnar, Phys. Rev. E **51**, 4282 (1995).
[156] Y.-Q. Jiang, B.-K. Chen, B.-H. Wang, W.-F. Wong, and B.-Y. Cao, Frontiers of Physics **12**, 124502 (2017).
[157] C. Bechinger et al., Rev. Mod. Phys. **88**, 045006 (2016).
[158] S. Kumari, A. S. Nunes, N. A. Araújo, and M. M. Telo da Gama, The Journal of chemical physics **147**, 174702 (2017).
[159] P. Dolai, A. Simha, and S. Mishra, Soft Matter **14**, 6137 (2018).
[160] R. C. Maloney and C. K. Hall, Langmuir **36**, 6378 (2020).
[161] S. R. McCandlish, A. Baskaran, and M. F. Hagan, Soft Matter **8**, 2527 (2012).
[162] A. M. Menzel, Phys. Rev. E **85**, 021912 (2012).
[163] C. Reichhardt, J. Thibault, S. Papanikolaou, and C. Reichhardt, Phys. Rev. E **98**, 022603 (2018).
[164] M. Ikeda, H. Wada, and H. Hayakawa, Europhys. Lett. **99**, 68005 (2012).
[165] N. Bain and D. Bartolo, Nature communications **8**, 1 (2017).
[166] B. Liebchen and D. Levis, Phys. Rev. Lett. **119**, 058002 (2017).
[167] P. B. Sampat and S. Mishra, Phys. Rev. E **104**, 024130 (2021).
[168] F. Farrell, M. Marchetti, D. Marenduzzo, and J. Tailleur, Phys. Rev. Lett. **108**, 248101 (2012).
[169] D. Stauffer and A. Aharony, *Introduction to percolation theory*, CRC press, 2018.
[170] X. Yang, M. L. Manning, and M. C. Marchetti, Soft matter **10**, 6477 (2014).
[171] M. Romenskyy and V. Lobaskin, Eur. Phys. J. B **86**, 91 (2013).
[172] S. Adhikary and S. B. Santra, Europhys. Lett. **135**, 48003 (2021).
[173] J. P. Singh and S. Mishra, arXiv preprint arXiv:1902.00296 (2019).
[174] M. Durve and A. Sayeed, Phys. Rev. E **93**, 052115 (2016).
[175] B. Li, Z.-X. Wu, and J.-Y. Guan, Phys. Rev. E **99**, 022609 (2019).

List of publications

1. *Effect of trapping perturbation on the collective dynamics of self-propelled particles*, Sagarika Adhikary and S. B. Santra, Europhys. Lett. **135**, 48003 (2021).
2. *Collective Behavior of Self-Propelled Particles in a Trapping Environment*, Sagarika Adhikary and S. B. Santra, AIP. Conf. Proc. **2220**, 140006 (2020).
3. *Collective pattern formation in a binary mixture of self-propelled particles*, Sagarika Adhikary and S. B. Santra, Journal of Physics: Conference Series (in press) (2022).
4. *Pattern formation and phase transition in the collective dynamics of a binary mixture of polar self-propelled particles*, Sagarika Adhikary and S. B. Santra, Manuscript under review.
5. *Effect of orientation adapters on the collective behavior of self-propelled particles*, Sagarika Adhikary and S. B. Santra, Manuscript under preparation.

Conference attended

1. *Collective Motion of Active Particles in a Specific Environment*, Sagarika Adhikary and S. B. Santra, **Complex Dynamical Systems and Applications 2017**, IIT Guwahati, Assam, India.
2. *Collective Behavior of Self-Propelled Particles in a Trapping Environment*, Sagarika Adhikary and S. B. Santra, **International Conference on Condensed Matter and Applied Physics 2019**, Bikaner, Rajasthan, India.

3. *Collective Pattern Formation in a Binary Mixture of Self-Propelled Particles*, Sagarika Adhikary and S. B. Santra, **XXXII Conference on Computational Physics 2021 (CCP2021)**, Coventry University, England.

Vita

Sagarika Adhikary was born in the year of 1992, in Coochbehar, West Bengal, India. She did her B.Sc. with Physics Honours in 2012 from A. B. N. Seal College under North Bengal University and M.Sc. in Physics from Jawaharlal Nehru University in 2014. She had enrolled in the PhD programme at the Indian Institute of Technology Guwahati in 2014. She had qualified Graduate Aptitude Test in Engineering (GATE) in 2014. She earned the Senior Research Fellowship in 2016 from the Indian Institute of Technology Guwahati.